

MINIMIZATION OF BANDED STRUCTURE IN SPRING STEELS BY THE
OPTIMIZATION OF CONTINUOUS CASTING MACHINE PARAMETERS

A THESIS SUBMITTED TO
THE GRADUATE SCHOOL OF NATURAL AND APPLIED SCIENCES
OF
MIDDLE EAST TECHNICAL UNIVERSITY

BY

MEHMET AKPINAR

IN PARTIAL FULFILLMENT OF THE REQUIREMENTS
FOR
THE DEGREE OF MASTER OF SCIENCE
IN
METALLURGICAL AND MATERIALS ENGINEERING

JUNE 2019

Approval of the thesis:

**MINIMIZATION OF BANDED STRUCTURE IN SPRING STEELS BY THE
OPTIMIZATION OF CONTINUOUS CASTING MACHINE PARAMETERS**

submitted by **MEHMET AKPINAR** in partial fulfillment of the requirements for the degree of **Master of Science in Metallurgical and Materials Engineering Department, Middle East Technical University** by,

Prof. Dr. Halil Kalıpçılar
Dean, Graduate School of **Natural and Applied Sciences**

Prof. Dr. C. Hakan Gür
Head of Department, **Met. and Mat. Eng.**

Prof. Dr. Ali Kalkanlı
Supervisor, **Met. and Mat. Eng., METU**

Examining Committee Members:

Prof. Dr. Bilgehan Ögel
Met. and Mat. Eng., METU

Prof. Dr. Ali Kalkanlı
Met. and Mat. Eng., METU

Prof. Dr. C. Hakan Gür
Met. and Mat. Eng., METU

Prof. Dr. Rıza Gürbüz
Met. and Mat. Eng., METU

Prof. Dr. Mehmet Erdoğan
Met. and Mat. Eng., Gazi University

Date: 20.06.2019

I hereby declare that all information in this document has been obtained and presented in accordance with academic rules and ethical conduct. I also declare that, as required by these rules and conduct, I have fully cited and referenced all material and results that are not original to this work.

Name, Surname: Mehmet Akpınar

Signature:

ABSTRACT

MINIMIZATION OF BANDED STRUCTURE IN SPRING STEELS BY THE OPTIMIZATION OF CONTINUOUS CASTING MACHINE PARAMETERS

Akpınar, Mehmet
Master of Science, Metallurgical and Materials Engineering
Supervisor: Prof. Dr. Ali Kalkanlı

June 2019, 95 pages

Leaf springs are one of the important components of suspension systems especially of light and heavy commercial vehicles. The plate products produced by spring steel qualities such as 51CrV4, 55Cr3, and 52CrMoV4 are often preferred by the leaf spring manufacturers. In continuous casting steelmaking, the segregation of the alloying elements such as C, Mn, Si into inter-dendritic regions during solidification causes different chemical composition in these regions compared to others. Depending on the chemical composition of the steel, different phases may form in these regions which are elongated parallel to the rolling direction after hot rolling. This phenomenon is called microstructural banding. The martensite bands with high hardness in 52CrMoV4 steel negatively impact the cold sawing and drilling of materials. Consequently, production rate and tool life decrease during cutting and hole-making operations in the leaf spring manufacturing process. This thesis investigates the effects of secondary cooling intensity and electro-magnetic stirring on the distribution of alloying elements in billet, and the martensite band intensity in the hot rolled product. As a result, by the optimization of continuous casting parameters, the area ratio of martensite bands was reduced to about 15% from 40% without any additional operation and cost. Accordingly, the center hardness of the products was decreased by 15 HRC. Also, it was provided that the tool life of band saws used in cutting operation

was increased by about 2.5 times and that of drilling heads used in the hole-making operation was doubled.

Keywords: Continuous Casting, Segregation, Microstructural Banding, Electro-Magnetic Stirring, Secondary Cooling

ÖZ

SÜREKLİ DÖKÜM MAKİNESİ PARAMETRELERİNİN OPTİMİZASYONU İLE YAY ÇELİKLERİNDE GÖRÜLEN BANTLAŞMANIN AZALTILMASI

Akpınar, Mehmet
Yüksek Lisans, Metalurji ve Malzeme Mühendisliği
Tez Danışmanı: Prof. Dr. Ali Kalkanlı

Haziran 2019, 95 sayfa

Makas yayları özellikle hafif ve ağır ticari araçların süspansiyon sistemlerinin en önemli parçalarının başında gelmektedir. 51CrV4, 55Cr3 ve 52CrMoV4 gibi standart yay çelik kalitelerinden üretilen lama malzemeler makas yayı üreten birçok firma tarafından yaygın olarak tercih edilmektedir. Sürekli döküm ile çelik üretiminde C, Mn, Si gibi alaşım elementlerinin katılma esnasında dendritler arası bölgelere segregasyonu, bu bölgelerde diğer bölgelere göre farklı bir kimyasal kompozisyon oluşmasına neden olmaktadır. Haddeme sonrasında, deformasyon yönüne paralel olarak uzayan bu bölgelerde çeliğin kimyasal kompozisyonuna bağlı olarak farklı fazlar oluşabilmektedir. Bu olay çelikte mikro yapısal bantlaşma olarak adlandırılmaktadır. 52CrMoV4 çelik kalitesinde görülen yüksek sertliğe sahip martenzit bantları malzemelerin soğuk kesilebilirliğini ve işlenebilirliğini oldukça olumsuz etkilemektedir. Bu durum, malzemelerin makas yayı üretim prosesine göre belirlenen boylara kesilmesi ve merkez deliklerinin işlenmesi sırasında hem üretim hızını düşürmekte hem de kullanılan ekipman sarfiyatını oldukça arttırmaktadır. Bu çalışmada; sürekli dökümde ikincil soğutma yoğunluğu ile elektro-manyetik karıştırıcı parametrelerinin kütük içerisinde alaşım elementlerinin dağılımına ve sıcak haddelenmiş ürünlerdeki martenzit bantlarının miktarına olan etkisi araştırılmıştır. Sonuç olarak, sürekli döküm parametrelerinin optimizasyonu ile mikro yapıda görülen

martensit bantlarının miktarı hiçbir ek işlem ve maliyet olmadan %40 seviyesinden %15 civarına düşürülmüştür. Buna paralel olarak, malzemelerin merkez sertliği yaklaşık olarak 15 HRC azaltılmıştır. Aynı zamanda, malzemelerin boy katlarına kesim işlemlerinde kullanılan şerit testere ömürlerinde yaklaşık 3.5, merkez deliklerinin işlenmesinde kullanılan delme takım uç ömürlerinde ise yaklaşık 2 kat artış sağlanmıştır.

Anahtar Kelimeler: Sürekli Döküm, Segregasyon, Mikroyapısal Bantlaşma, Elektro-Manyetik Karıştırma, İkincil Soğutma

To my family

ACKNOWLEDGMENTS

Primarily, I would like to express my sincere gratitude to my advisor Prof. Dr. Ali Kalkanlı who has supported me continuously with his immense knowledge throughout the research.

Besides my advisor, I would like to thank ÇEMTAŞ for giving me a valuable opportunity to carry out my experimental works and publish this thesis.

Throughout the development of the thesis topic, there are many people whose inputs are inevitable to mention. Especially, I would like to thank Bertan Parmaksızođlu who has provided the greatest mentorship at the beginning of the study. Moreover, I am also grateful to İ. İrfan Ayhan, Caner Güney, N. Başak Dürger, Berkay Şahin, Ali Fuat Aytemiz and Murat Güven for their technical contributions. I also thank laboratory, steel mill and rolling mill staff for their great support.

I am grateful to my friends Hasan Güdük, Ođuzhan Eren, Anıl İpek and Görkem Ak for their precious friendship for many years.

I would like to thank very much to my mother, Nezahat Akpınar, my father, Ahmet Akpınar and my brother, Murat Akpınar for their continuous and heart-warming support in all my life. It is really valuable and encouraging to have their support by my side. Also, I would like to thank my future sister-in-law Gizem Sönmez who is about to join Akpınar family for her valuable help in revising my thesis.

Above all, I thank Huriye Cantok for her peerless support and I am grateful every moment she stands by me.

TABLE OF CONTENTS

ABSTRACT	v
ÖZ	vii
ACKNOWLEDGMENTS	x
TABLE OF CONTENTS	xi
LIST OF TABLES	xiii
LIST OF FIGURES	xv
CHAPTERS	1
1. INTRODUCTION	1
2. LITERATURE REVIEW	5
2.1. Mechanism of Microstructural Banding Formation	7
2.2. Factors Affecting Formation of Microstructural Banding.....	10
2.2.1. Micro Alloying Elements.....	14
2.2.2. Continuous Casting Parameters	15
2.2.2.1. Primary and secondary cooling intensity	15
2.2.2.2. Strand Velocity.....	18
2.2.2.3. Casting Superheat.....	18
2.2.2.4. Electro-Magnetic Stirring.....	20
2.2.3. Hot Rolling Parameters.....	24
3. EXPERIMENTAL PROCEDURE	27
3.1. Production of the Experimental Castings	27
3.2. Sampling and Investigations	29

4. RESULTS AND DISCUSSION	33
4.1. Characterization of the Microstructural Banding in 52CrMoV4 Steel	33
4.2. The Amount of Heat Extracted by Primary Cooling in Mould.....	37
4.3. Carbon Segregation Pattern in Transverse Billet Slices	41
4.4. Microstructure Examination Results.....	51
4.5. Micro and Macro Hardness Measurements	58
4.6. The Effect of Banding Intensity on the Cutting and Drilling Operations	62
5. CONCLUSION	65
6. SUGGESTIONS FOR FUTURE WORK	69
REFERENCES	71
APPENDICES	77
APPENDIX A. SMS Concast Mould Flow Graph.....	77
APPENDIX B. Calculations of Center Carbon Segregation Indexes	78
APPENDIX C. Microstructures and Area Ratio Analyses	87

LIST OF TABLES

TABLES

Table 2-1. Results of EDS analysis (wt%) of Site 1 and Site 2	9
Table 3-1. Nominal composition of 52CrMoV4 steel and target analysis of experimental castings	27
Table 3-2. Experimental matrix	28
Table 4-1. Results of EDS analysis (wt%) of different phases in 52CrMoV4 steel ..	35
Table 4-2. Carbon distribution through vertical and horizontal centerline for Experiment 8	44
Table 4-3. Center carbon distributions of experimental billets and center carbon segregation indexes	45
Table 4-4. Secondary cooling rate and theoretical SDAS values for mild, medium and intense secondary cooling regimes	50
Table 4-5. Hardness values (in HRC) at the center, 2 mm, 4 mm, 6 mm below the center	61
Table 4-6. Tool life in cutting and hole-making operations of Experiment 14 and Experiment 8	63
Table B-1. Carbon distribution through vertical and horizontal centerline for Experiment 1	78
Table B-2. Carbon distribution through vertical and horizontal centerline for Experiment 2	78
Table B-3. Carbon distribution through vertical and horizontal centerline for Experiment 3	79
Table B-4. Carbon distribution through vertical and horizontal centerline for Experiment 4	79
Table B-5. Carbon distribution through vertical and horizontal centerline for Experiment 5	80

Table B-6. Carbon distribution through vertical and horizontal centerline for Experiment 6.....	80
Table B-7. Carbon distribution through vertical and horizontal centerline for Experiment 7.....	81
Table B-8. Carbon distribution through vertical and horizontal centerline for Experiment 8.....	81
Table B-9. Carbon distribution through vertical and horizontal centerline for Experiment 9.....	82
Table B-10. Carbon distribution through vertical and horizontal centerline for Experiment 10.....	82
Table B-11. Carbon distribution through vertical and horizontal centerline for Experiment 11.....	83
Table B-12. Carbon distribution through vertical and horizontal centerline for Experiment 12.....	83
Table B-13. Carbon distribution through vertical and horizontal centerline for Experiment 13.....	84
Table B-14. Carbon distribution through vertical and horizontal centerline for Experiment 14.....	84
Table B-15. Carbon distribution through vertical and horizontal centerline for Experiment 15.....	85
Table B-16. Carbon distribution through vertical and horizontal centerline for Experiment 16.....	85
Table B-17. Carbon distribution through vertical and horizontal centerline for Experiment 17.....	86
Table B-18. Carbon distribution through vertical and horizontal centerline for Experiment 18.....	86

LIST OF FIGURES

FIGURES

Figure 1-1. Uneven cutting surface of the plate products after cold sawing, 52CrMoV4, 90x45 mm	2
Figure 1-2. Microstructure of the sample taken from center of the product (LM, Nital, 15 seconds, 100X) and micro hardness measurement on white band (737 HV 0.1) ...	3
Figure 2-1. Ferrite-pearlite banding in a wrought 1018 steels (Nital, LM, 100X)	5
Figure 2-2. Microstructures of 52CrMoV4 steel for different cooling rates a) 0.05 °C/sec b) 0.2 °C/sec c) 0.5 °C/sec d) 0.8 °C/sec e) 1 °C/sec f) 1.5 °C/sec g) 2 °C/sec h) 3 °C/sec i) 5 °C/sec	6
Figure 2-3. The Fe-Mn phase diagram.....	8
Figure 2-4. Banded microstructure in 34CrNiMo6 steel a) LM and b) SEM.....	9
Figure 2-5. CCT diagrams of a) Site 1 and b) Site 2	10
Figure 2-6. Sketch of continuous casting billet structure.....	10
Figure 2-7. Variation of maximum degree of center carbon segregation index with equiaxed zone ratio	11
Figure 2-8. Degree of homogenization versus time at 1200 °C for nickel and carbon for different dendrite arm spacings	13
Figure 2-9. EST (sec) with different mass fractions of Nb (%).....	14
Figure 2-10. Average SDAS (μm) with different mass fractions of Nb (%).....	15
Figure 2-11. Schematic cooling process for continuous casting of steel.....	16
Figure 2-12. Different cooling mechanisms in the secondary cooling region.....	17
Figure 2-13. The effect of casting speed (strand velocity) on the degree of center segregation for carbon.....	18
Figure 2-14. SDAS (μm) with different superheat	19
Figure 2-15. Variation of equiaxed zone ratio with the casting superheat.....	19
Figure 2-16. Mechanical properties of dendrites in mushy zone.....	20

Figure 2-17. Position of M-EMS and F-EMS on a CCM.....	21
Figure 2-18. Carbon distribution in 120x120 mm billets with and without EMS.....	22
Figure 2-19. Sketch of inner structure of continuously casted billet.....	23
Figure 2-20. The relationship between center segregation indexes of carbon, chromium and manganese	25
Figure 3-1. Test Master Pro mobile spectrometer and chemical composition measurements on transverse billet slice.....	29
Figure 3-2. Sampling for micro examinations	30
Figure 3-3. Emco Test Durascan 20 micro hardness test device and Emco Test M5C hardness test device	31
Figure 3-4. Hardness measurement points.....	31
Figure 4-1. Microstructure of the sample taken from center of the plate product, 52CrMoV4, 90x45 mm (LM, LePera, 4 minutes, 100X)	34
Figure 4-2. SEM micrograph of banded microstructure of 52CrMoV4 steel.....	34
Figure 4-3. CCT of Site 1 calculated by JMatPro software.....	35
Figure 4-4. CCT of Site 2 calculated by JMatPro software.....	36
Figure 4-5. CCT of Site 3 calculated by JMatPro software.....	36
Figure 4-6. Specific heat of 52CrMoV4 steel at various temperatures	37
Figure 4-7. Rate of heat removal by mould cooling water versus mould length.....	39
Figure 4-8. Thickness solidified, M, versus distance down the mould	40
Figure 4-9. Carbon distribution of Experiment 8	43
Figure 4-10. Center carbon segregation indexes for experiments with medium secondary cooling	46
Figure 4-11. Center carbon segregation indexes for experiments with intense secondary cooling	47
Figure 4-12. Average billet exit temperatures for different flow rate of secondary cooling water	48
Figure 4-13. The effect of cooling intensity on center carbon segregation index	49
Figure 4-14. Center carbon segregation indexes for all experiments	51

Figure 4-15. Microstructure of Experiment 1 having the highest banding intensity among the mild cooling experiments (200X, 4% Picral, 60 sec.).....	52
Figure 4-16. Microstructure of Experiment 2 having the lowest banding intensity among the mild cooling experiments (200X, 4% Picral, 60 sec.).....	52
Figure 4-17. Microstructure of Experiment 10 having the highest banding intensity among the medium cooling experiments (200X, 4% Picral, 60 sec.).....	53
Figure 4-18. Microstructure of Experiment 8 having the lowest banding intensity among the medium cooling experiments (200X, 4% Picral, 60 sec.).....	53
Figure 4-19. Microstructure of Experiment 13 having the highest banding intensity among the intense cooling experiments (200X, 4% Picral, 60 sec.).....	54
Figure 4-20. Microstructure of Experiment 14 having the lowest banding intensity among the intense cooling experiments (200X, 4% Picral, 60 sec.).....	54
Figure 4-21. The area ratio of the phases for mild cooling experiments	55
Figure 4-22. The area ratio of the phases for medium cooling experiments.....	56
Figure 4-23. The area ratio of the phases for intense cooling experiments	57
Figure 4-24. The effect of flow rate of secondary cooling water on microstructural banding intensity	58
Figure 4-25. Micro hardness measurements on martensite bands (843 HV 0.1 and 788 HV 0.1).....	59
Figure 4-26. Micro hardness measurements on bainite (470 HV 0.05 and 464 HV 0.1)	59
Figure 4-27. Micro hardness measurements on pearlite (353 HV 0.1 and 361 HV 0.05)	60
Figure 4-28. Comparison of cutting surfaces of the Experiment 14 (smooth) and Experiment 8 (uneven).....	62
Figure A-1. Actual flow rate of mould cooling water.....	77
Figure C-1. Microstructure of Experiment 1 (200X, 4% Picral, 60 sec.) and area ratio analysis.....	87
Figure C-2. Microstructure of Experiment 2 (200X, 4% Picral, 60 sec.) and area ratio analysis.....	87

Figure C-3. Microstructure of Experiment 3 (200X, 4% Picral, 60 sec.) and area ratio analysis	88
Figure C-4. Microstructure of Experiment 4 (200X, 4% Picral, 60 sec.) and area ratio analysis	88
Figure C-5. Microstructure of Experiment 5 (200X, 4% Picral, 60 sec.) and area ratio analysis	89
Figure C-6. Microstructure of Experiment 6 (200X, 4% Picral, 60 sec.) and area ratio analysis	89
Figure C-7. Microstructure of Experiment 7 (200X, 4% Picral, 60 sec.) and area ratio analysis	90
Figure C-8. Microstructure of Experiment 8 (200X, 4% Picral, 60 sec.) and area ratio analysis	90
Figure C-9. Microstructure of Experiment 9 (200X, 4% Picral, 60 sec.) and area ratio analysis	91
Figure C-10. Microstructure of Experiment 10 (200X, 4% Picral, 60 sec.) and area ratio analysis	91
Figure C-11. Microstructure of Experiment 11 (200X, 4% Picral, 60 sec.) and area ratio analysis	92
Figure C-12. Microstructure of Experiment 12 (200X, 4% Picral, 60 sec.) and area ratio analysis	92
Figure C-13. Microstructure of Experiment 13 (200X, 4% Picral, 60 sec.) and area ratio analysis	93
Figure C-14. Microstructure of Experiment 14 (200X, 4% Picral, 60 sec.) and area ratio analysis	93
Figure C-15. Microstructure of Experiment 15 (200X, 4% Picral, 60 sec.) and area ratio analysis	94
Figure C-16. Microstructure of Experiment 16 (200X, 4% Picral, 60 sec.) and area ratio analysis	94
Figure C-17. Microstructure of Experiment 17 (200X, 4% Picral, 60 sec.) and area ratio analysis	95

Figure C-18. Microstructure of Experiment 18 (200X, 4% Picral, 60 sec.) and area ratio analysis.....95

CHAPTER 1

INTRODUCTION

Leaf springs are one of the important components in suspension systems of heavy and light commercial vehicles. By absorbing energy due to road irregularities, leaf springs make driving more comfortable and safer. Monoleafs and multileafs are two main groups of leaf springs. Monoleafs are composed of only one plate product whereas multileafs are produced by assembling several plate products to a master plate. Depending on the required strength, different grades of steel can be used in leaf spring manufacturing. However, the most used steel grades are 55Cr3, 51CrV4 and 52CrMoV4 according to DIN EN 10089 steel standard. In general, continuously cast billets are hot rolled to plate products with various dimensions to produce raw materials of leaf springs. Afterwards, these products are cut into specified length by band saws according to the drawing of the part. Then, center holes are drilled for multileafs to stick the plate products together. After these operations, eye-rolling of the master plate is performed and leaf springs are quenched and tempered to achieve required strength and toughness.

Cold sawing of hot rolled materials is very important because the first step of the leaf spring production is cutting them to product length by band saws. In conjunction with this, machinability is also one of the essential properties for the raw materials of leaf springs since the next step is center hole-making. Therefore, it can be deduced that if raw materials cannot be easily machined, production time and loss increases, which reduces total efficiency.

When the cutting operation of plate products produced with 52CrMoV4 steel was examined, it was seen that center regions of the cutting surfaces of the products were

uneven as seen in Figure 1.1. In other words, it was not smooth and proper unlike that of other steel grades.

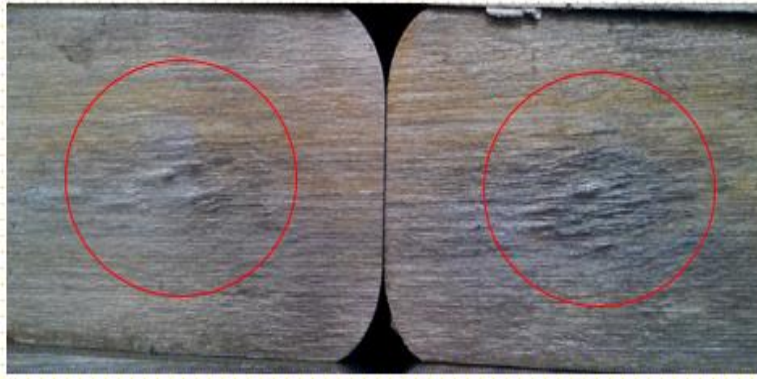


Figure 1-1. Uneven cutting surface of the plate products after cold sawing, 52CrMoV4, 90x45 mm

In addition to this, production records showed that cutting and drilling operations were too long, tool life was very short, and production losses due to improper cutting and drilling were very high for 52CrMoV4 steel comparing to the other steel grades.

Micro examinations of the samples taken from the products were carried out to find out the origin of the problem. These examinations showed that banded phases exist in the microstructures of hot rolled products of 52CrMoV4 steel and this banded structure becomes more intense at the centers of the products. Also, micro hardness measurements on the phases were conducted. The micro hardness of the white bands in Figure 1.2 was measured as 737 HV (~61.7 HRC) which is a very high value for cutting and drilling tools. On the other hand, micro hardness value of the matrix was measured as 350 HV (~35.5 HRC).

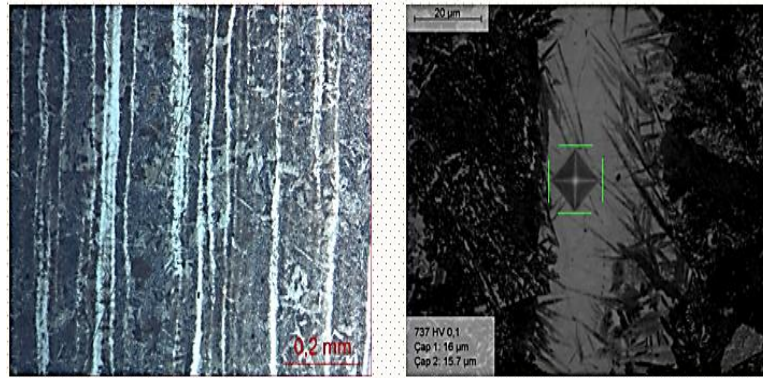


Figure 1-2. Microstructure of the sample taken from center of the product (LM, Nital, 15 seconds, 100X) and micro hardness measurement on white band (737 HV 0.1)

Characterization studies showed that these white bands are martensitic and the matrix is pearlite with dispersed bainite. Therefore, it was understood that the origin of the problem in cutting and center hole-making operations of the 52CrMoV4 steel is the high hardness of the martensite bands. The banded martensite phase also causes heterogeneous hardness distribution, which can affect the mechanical properties of the products.

This study was carried out to reduce the amount of these bands, and therefore, to provide improvement in the performance of plate products produced with 52CrMoV4 steel in cutting and drilling operations. By this way, it is possible to increase the production rate and to decrease the production losses, which increases the efficiency of total production.

Microstructural banding results from micro segregation of alloying elements during solidification. Hence, the main purpose of this study is to minimize segregation of alloying elements by the optimization of continuous casting machine (CCM) parameters. In this thesis, the flow rate of secondary cooling water, final electromagnetic stirring (F-EMS) frequency and current were tried to optimize for reducing segregation of alloying elements in billets, and this way, decreasing the banding intensity in the hot rolled products. For this purpose, 18 experimental castings with

different parameters were produced, and then, these were hot rolled to plate products with the dimensions of 90x45 mm. Firstly, chemical composition measurements were conducted in billets to see how the parameters affect the homogeneity of the billets in terms of the distribution of alloying elements. Then, the effect of rolling more homogenous billets on the banding intensity of the hot rolled products was researched by microstructural examinations. Also, center hardness measurements were done to see the changing of hardness with a decreasing amount of martensite bands. Finally, how the cutting and drilling performances of the products are improved by producing more homogenous products with lower martensitic band intensity was investigated.

CHAPTER 2

LITERATURE REVIEW

Microstructural banding is simply defined as a microstructural condition in which alternating bands of quite different phases are aligned parallel to each other and rolling direction. This type of banded structure consists of two or more different phases in hot rolled steels depending on the chemical composition of the steel. Although ferrite-pearlite banding is the most common, ferrite-martensite, ferrite-bainite, pearlite-martensite and carbide banding are well-known types of this structure [1-5].

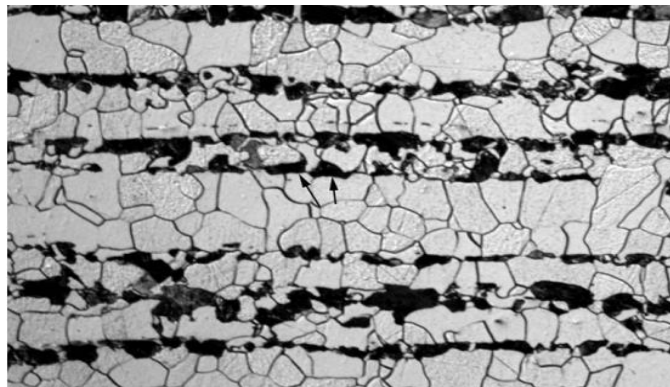


Figure 2-1. Ferrite-pearlite banding in a wrought 1018 steels (Nital, LM, 100X) [1]

Naturally, different phases are formed in hot rolled 52CrMoV4 steel which is the subject of this thesis. For microstructural characterization of 52CrMoV4 steel, Hou et al. [6] have carried out a study. In their study, the microstructures of 52CrMoV4 steel austenitized at 950 °C and then cooled at different cooling rates between 0.05 °C/sec and 5 °C/sec were examined. The results showed that the martensite phase can exist together with bainite and pearlite for the cooling rates from 0.5 °C/sec to 1.5 °C/sec. As the cooling rate increases, microstructure becomes finer, and only the martensite phase exists for cooling rate higher than 5 °C/sec. It is known that industrial cooling

rate after hot rolling is about 1 °C/sec. Therefore, it can be said that martensite, bainite, and pearlite can be found at room temperature in the microstructure of 52CrMoV4 steel according to this study.

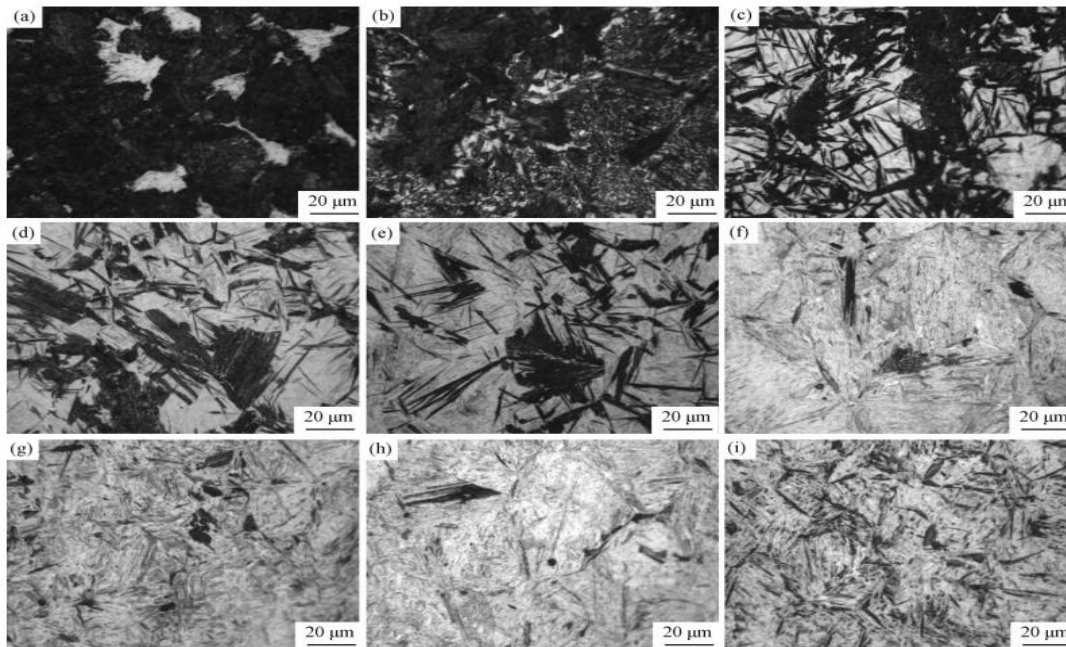


Figure 2-2. Microstructures of 52CrMoV4 steel for different cooling rates a) 0.05 °C/sec b) 0.2 °C/sec c) 0.5 °C/sec d) 0.8 °C/sec e) 1 °C/sec f) 1.5 °C/sec g) 2 °C/sec h) 3 °C/sec i) 5 °C/sec [6]

Some studies in the literature [2,7,8] have proposed that there is a great negative effect of microstructural banding on the ductility and the impact energy of the steel. In addition to this, the fact that anisotropy of these properties is worsened as banding intensity increases has been revealed. On the other hand, it has been seen that microstructural banding does not affect the strength properties of the material. If the martensite bands exist in the microstructure, it negatively affects machinability and cold formability of the steel [4,5].

2.1. Mechanism of Microstructural Banding Formation

The origin of microstructural banding is the inter-dendritic segregation of the alloying elements during solidification. If it is assumed liquid steel in which manganese is only alloying element with carbon, Mn is depleted in the first solidified dendrites since it lowers the melting point of iron. Then, Mn is rejected by growing dendrites to inter-dendritic regions [2]. As the liquid steel solidifies from the surface to the center, rejection of Mn increasingly continues since the solubility of Mn is lower in solidified dendrites than inter-dendritic liquid region. The alloying elements having partition coefficient less than unity (e.g. Mn, Si, S and P) are very prone to be rejected from first formed δ -ferrite dendrites to the inter-dendritic regions during solidification of steel [9]. This can result in microstructural banding in hot rolled products.

Yetkin [10], in his study, has examined manganese segregation. As it can be seen in Figure 2.3, at 1529 °C, which is close to pouring temperature for steels, the solubility of manganese in delta ferrite is 10% in mass. The red line in the diagram indicates that mass percent of manganese (1.5%) in steel examined in his study. In the diagram, it is also seen that manganese solubility of the delta ferrite decreases to 0 at 1394 °C. During solidification of steel, manganese is rejected from solidified dendrites to inter-dendritic liquid regions. By this way, these regions become enriched by manganese elements at the end of the solidification.

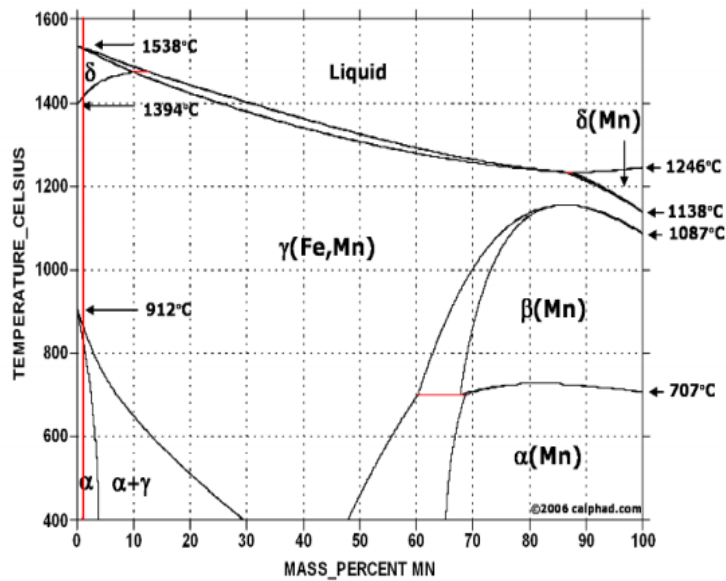


Figure 2-3. The Fe-Mn phase diagram [10]

Rejection of solutes from the solidified dendrites into the inter-dendritic liquid regions is called as micro segregation and it causes differences in chemical composition between dendrite arms. Micro segregation distances are typically on the order of 10 to 100 μm . So it can be removed by homogenizing heat treatment since diffusion distance is very small in this type of segregation. By the movement of micro segregated regions due to the motion of liquid and free crystals, they extend to macroscopic distances. By this way, macro segregation takes places on the order of 500 to 1000 μm [11].

After solidification, a concentration profile with positive and negative segregation regions is obtained. Before hot rolling, billets are heated to elevated temperatures (1250 $^{\circ}\text{C}$) and kept at this temperature for 2.5 hours in an annealing furnace. In this step, segregated regions can be partially homogenized, the extent of this homogenization will be detailed later. After annealing treatment, billets are hot rolled to final products having different sections and dimensions. Because of the plastic deformation during hot rolling, the concentration profile is altered. In this profile, positive and negative segregation regions are aligned parallel to each other and rolling

direction. At the end of the rolling process, the temperature of the material is about 900 °C. Through cooling of products on cooling bed, the phase transformation from austenite to room temperature phases occurs and different phases are formed in positive and negative segregation regions, which leads banded microstructure [2].

Nagode et al. [4] have investigated development of banded microstructure in 34CrNiMo6 steel by using SEM/EDS analysis and a computer programme, JMatPro 7.0. In Figure 2.4, microstructure of 34CrNiMo6 steel under light microscope and SEM can be seen.

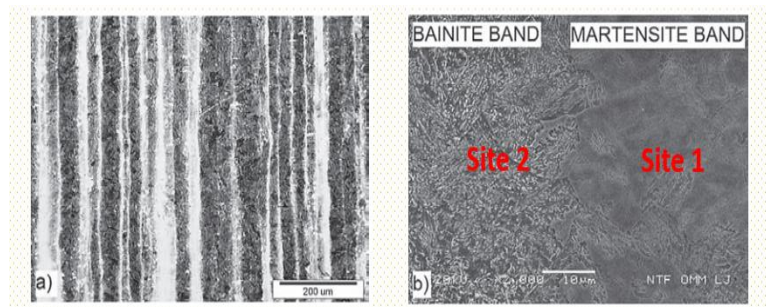


Figure 2-4. Banded microstructure in 34CrNiMo6 steel a) LM and b) SEM [4]

Results of EDS analysis show that site 1 is positive segregation region whereas site 2 is negative segregation region.

Table 2-1. Results of EDS analysis (wt%) of Site 1 and Site 2 [4]

Element	Si	Cr	Mn	Ni	Mo	Cu	Fe
Site 1	0.37	1.92	0.67	1.68	0.61	0.32	Balance
Site 2	0.21	1.08	0.42	1.34	0.18	0.27	Balance

By using JMatPro 7.0, CCT diagrams were calculated for site 1 and site 2. Figure 2.5 shows that under the same cooling conditions different phases can form since the CCT behaviors of two regions next to each other are different.

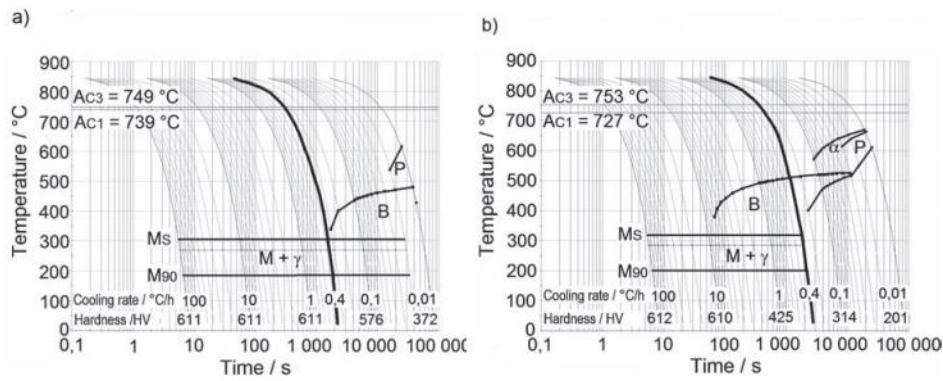


Figure 2-5. CCT diagrams of a) Site 1 and b) Site 2 [4]

2.2. Factors Affecting Formation of Microstructural Banding

There is a strong relationship between the morphology of the cast structure and segregation phenomena. As described in Figure 2.6, billets produced by continuous casting have distinctly three macrostructural zones: the chill zone, the columnar zone and the equiaxed zone [12].

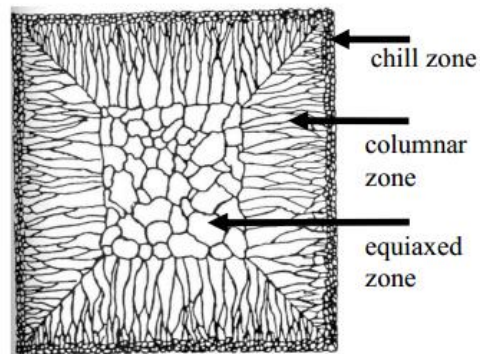


Figure 2-6. Sketch of continuous casting billet structure [13]

The formation of these zones is strictly dependent upon the cooling conditions of the casting. Chill zone consisting of equiaxed crystals and randomly oriented dendrites is formed near the billet surface as a result of rapid heat transfer occurring when the liquid steel is into contact with the mould wall. As the heat transfer rate is decreased,

the grains start to grow towards the center in parallel with heat flow. Such growth causes the formation of the columnar zone which is undesirable because of its anisotropic behaviors. On the other hand, the equiaxed zone which is observed at the center has isotropic behaviors since all crystals and dendrites in this region are oriented at random [12,13]. In other words, there is no specific growth direction in the equiaxed zone. By this means, rejected impure liquid by the solidifying dendrites is distributed more uniformly in the equiaxed zone, which reduces the segregation of alloying elements. Therefore, promotion of early columnar-to-equiaxed transition forming a wider equiaxed zone is very important to minimize segregation [14-16]. Choudhary et al. [14] have demonstrated that the center segregation index of carbon decreases as equiaxed zone ratio increases. Center carbon segregation index can be defined as the ratio of carbon content at the center of the semi-finished of continuous casting product which can be billet, bloom or slab to the carbon content of liquid steel in tundish before pouring.

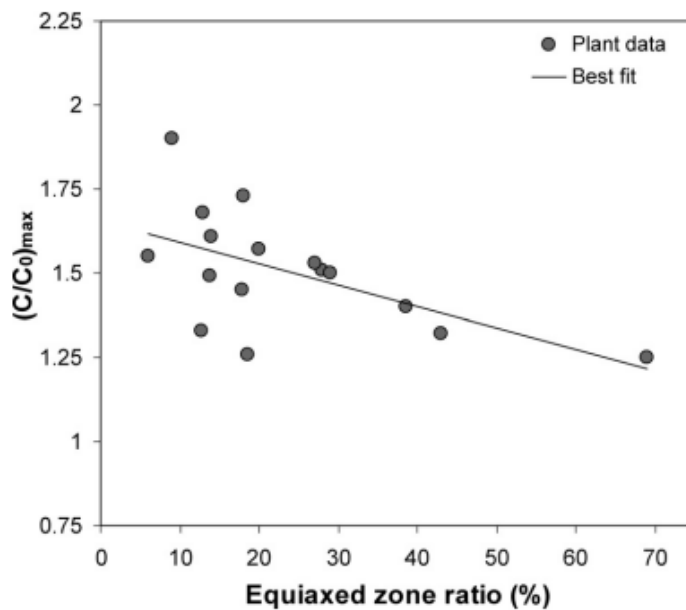


Figure 2-7. Variation of maximum degree of center carbon segregation index with equiaxed zone ratio [14]

In addition to the promotion of equiaxed grain ratio in the macrostructure of billets, reducing secondary dendrite arm spacing (SDAS) is considered to be one of the important parameters for removing segregation of alloying elements. Reducing SDAS decreases the diffusion distance for alloying elements and provides shorter homogenization time according to the below equation [17].

$$\text{Homogenization time} = c \frac{(\text{SDAS})^2}{D_s} \quad (1)$$

where D_s is the rate of diffusion of the solute, and c is a constant.

In order to decrease SDAS, the local cooling rate around dendrite tips should be accelerated. Local solidification time (LST) is the time duration for the removal of only heat of fusion at a particular location in the casting [18]. This has an important role in determining SDAS, however, it is hard to find out its exact value. Then, Gao et. al. [19] have used effective solidification time (EST) representing the time from the pouring temperature to the solidus temperature instead of LST. Their studies showed that EST and SDAS are directly proportional.

A study [20] has been carried out to explain the relationship between homogenization time and SDAS. Figure 2.8 shows that for the 90% reduction in degree of segregation which indicated with red line on the diagram, the homogenization times for nickel are 2280, 206, 2.06 and 0.23 hours for different dendrite arm spacings which are 1000, 300, 30 and 10 microns, respectively. Dendrite arm spacing is represented with “d” in the diagram.

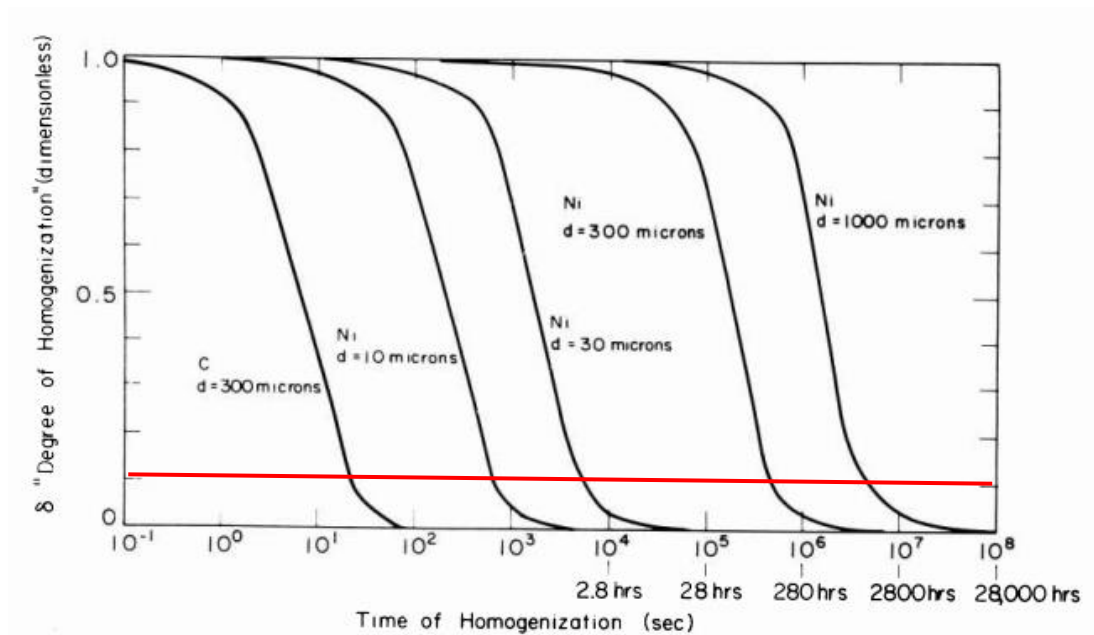


Figure 2-8. Degree of homogenization versus time at 1200 °C for nickel and carbon for different dendrite arm spacings [20]

To sum up, the enrichment of the inter-dendritic regions with alloying elements during solidification can be reduced by increasing ratio of the equiaxed zone and the homogenization of segregation can be improved by shortening SDAS. Thus, it becomes possible to minimize micro segregation induced microstructural banding. The production parameters affecting equiaxed grain ratio and SDAS are listed below.

- Micro alloying elements
- Continuous casting machine (CCM) parameters
 - Primary and secondary cooling intensity
 - Superheat
 - Strand velocity
 - Electro-magnetic stirring

Furthermore, hot rolling parameters which are listed below affect the development of banded microstructure. Unlike CCM parameters, hot rolling parameters cannot

remove the main reason for microstructural banding which is segregation of alloying elements.

- Annealing treatment before hot rolling
- Reduction ratio
- Cooling rate after hot rolling

2.2.1. Micro Alloying Elements

As the content of micro alloying elements such as Nb, Ti and V increases, liquid steel becomes more conductive thermally. The increase in thermal conductivity of liquid steel lowers the EST. In Figure 2.9, it is seen that as Nb mass fraction is increased from 100 ppm to 300 ppm, the EST decreases by approximately 61 seconds.

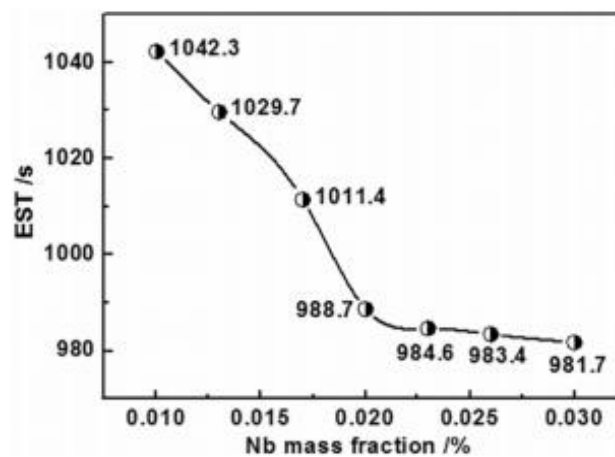


Figure 2-9. EST (sec) with different mass fractions of Nb (%) [19]

In line with this, the average SDAS also decreases from 116.2 μm to 82.1 μm if the amount of Nb added to the liquid steel is increased by 200 ppm.

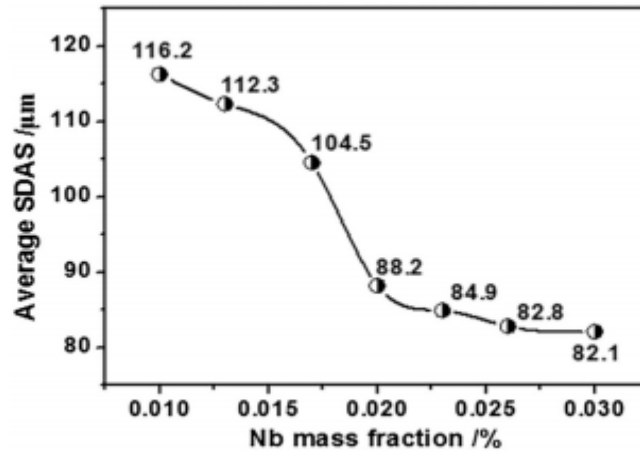


Figure 2-10. Average SDAS (μm) with different mass fractions of Nb (%) [19]

2.2.2. Continuous Casting Parameters

2.2.2.1. Primary and secondary cooling intensity

In the steel production with continuous casting, molten steel which is produced by melting of scraps in the electric arc furnace is transported to the ladle furnace. After secondary metallurgical operations such as alloying, adjusting of temperature and vacuum degassing, molten steel is tapped from the ladle into the mould through a tundish via a refractory shroud. There is a closed circuit cooling system around the mould to extract heat from liquid metal, which is primary cooling. When the molten metal is in contact with water-cooled mould, it starts to solidify and a thin solid shell at the interface between molten metal and mould wall forms. Heat conduction across this interface is the first stage of primary cooling. When the solid shell is thick enough to contract away from the mould wall, air gap at steel-mould interface forms and then air gap cooling starts. At this stage of primary cooling, heat transfer rate dramatically decreases [21,22].

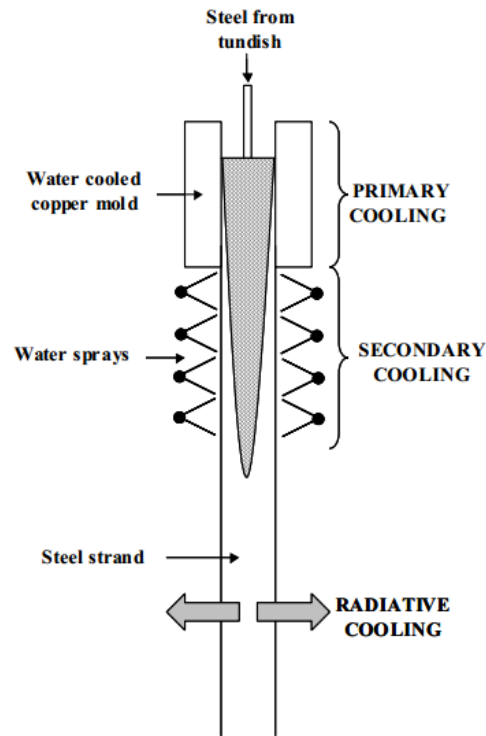


Figure 2-11. Schematic cooling process for continuous casting of steel [21]

Primary cooling is very important for both the macrostructure of billets and surface quality of the last products. If the heat transfer rate is too fast, the risk of crack formation on the billet surface increases, which naturally have a negative effect on the surface quality of the last products. On the other hand, if the heat transfer is not enough in the mould, solid shell thickness is insufficient to prevent bleeding which is flowing of molten metal out from the solid shell because of ferro-static pressure of liquid within the strand.

After the strand exits the mould, it passes through a spray chamber in which hot metal surface and cooling water are in direct contact. This is called secondary cooling. In this region, there are rolls which are needed to support the strand against bulging due to the ferro-static pressure. In addition to cooling due to spray water, another

mechanism operating in this region is roll contact cooling at the contact point of rolls and strand surface [21].

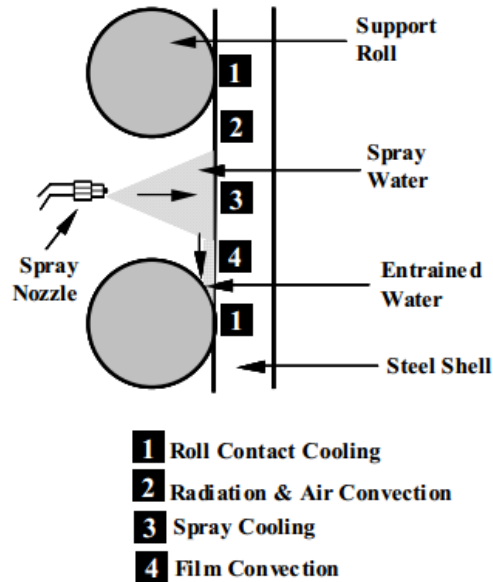


Figure 2-12. Different cooling mechanisms in the secondary cooling region [21]

In the literature, there are several studies which have reported that SDAS decreases with increase in secondary cooling rate. As the secondary cooling becomes more intense, the local cooling rate around dendrite tips also increases, which reduces SDAS, and thereby, homogenization time [20, 23]. Equation 2 [14] shows the relationship between the secondary cooling rate and SDAS.

$$SDAS = \alpha \varepsilon^{-n} \quad (2)$$

where α and n are constants and ε represents secondary cooling rate which is expressed in K / sec. Jacobi and Schwerdtfeger [24] have performed experiments to calculate these constants and they modified above equation as:

$$SDAS = 109.2 \varepsilon^{-0.44} \quad (3)$$

2.2.2.2. Strand Velocity

Strand velocity is one of the important CCM parameters affecting the segregation of alloying elements which is the main reason for microstructural banding. When the strand velocity is decreased, the cooling intensity increases since strand passes slower through the spray chamber on condition that the flow rate of cooling water is constant. Zeng et al. [25] have found that the grain compactness in equiaxed grain zone increases because more intense cooling promotes breaking dendrite tips and create nucleating sites for new grain formation. In addition to this, they have reported that SDAS is reduced from 190 microns to 140 microns when strand velocity is decreased 1.35 m/min to 1.25 m/min. Consequently, center carbon segregation remarkably removed with decreasing strand velocity as shown in Figure 2.13.

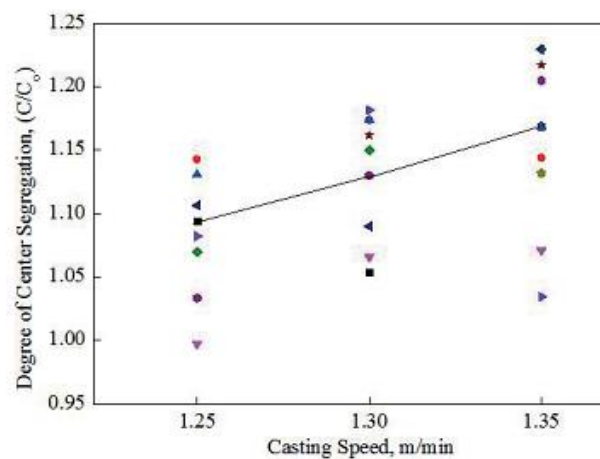


Figure 2-13. The effect of casting speed (strand velocity) on the degree of center segregation for carbon [25]

It should be also noted that strand velocity affects the efficiency of electro-magnetic stirring, which will be mentioned later.

2.2.2.3. Casting Superheat

Casting superheat is defined as the amount of difference between tundish temperature and liquidus temperature of the steel. There is a proportionality between casting

superheat and EST which is an important factor for SDAS, as previously mentioned. Figure 2.14 shows how SDAS changes with increasing superheat. If the superheat value exceeds 35 °C, a sharp increase in average SDAS is seen.

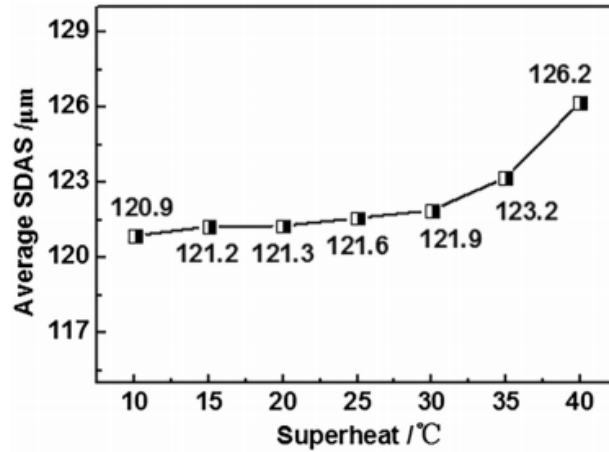


Figure 2-14. SDAS (μm) with different superheat [19]

In addition to this, it has been shown that in several researches as the casting superheat is reduced, the ratio of equiaxed grain zone and homogeneity of steel increases. As a result of these, central segregation of alloying elements is reduced which is the best way for minimizing of microstructural banding [14,26,27].

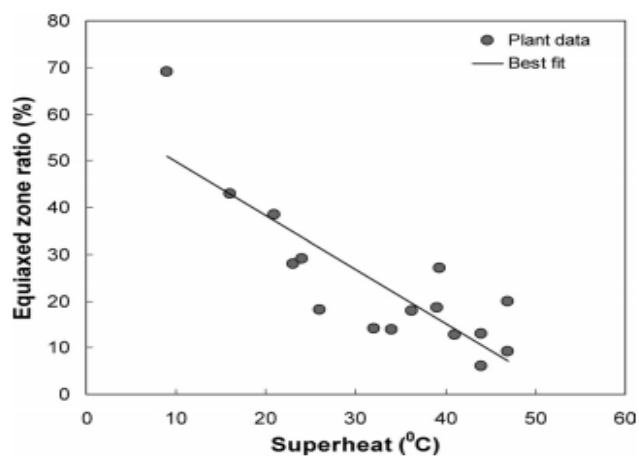


Figure 2-15. Variation of equiaxed zone ratio with the casting superheat [14]

2.2.2.4. Electro-Magnetic Stirring

Electro-magnetic stirring (EMS) is another method to solve the segregation problem in continuous casting of steel. EMS can be defined as stirring the liquid steel by electro-magnetic forces which are created by electromagnetic stirrers at different positions of CCM.

As it is seen in Figure 2.16, there are different zones in a dendrite according to its mechanical properties. The dendrite tip is surrounded by alloying enriched molten steel and this region is called zero strength zone. Between the dendrite tip and the main body of the dendrite which is called zero ductility zone, there is liquid impenetrable zone which can resist ferro-static pressure of liquid steel. By applying EMS, dendrite tips are broken from zero strength zone to liquid impenetrable zone. By broken dendrite arms, it is possible to promote wider equiaxed zone and to provide more uniform distribution of alloying elements [10,28,29].

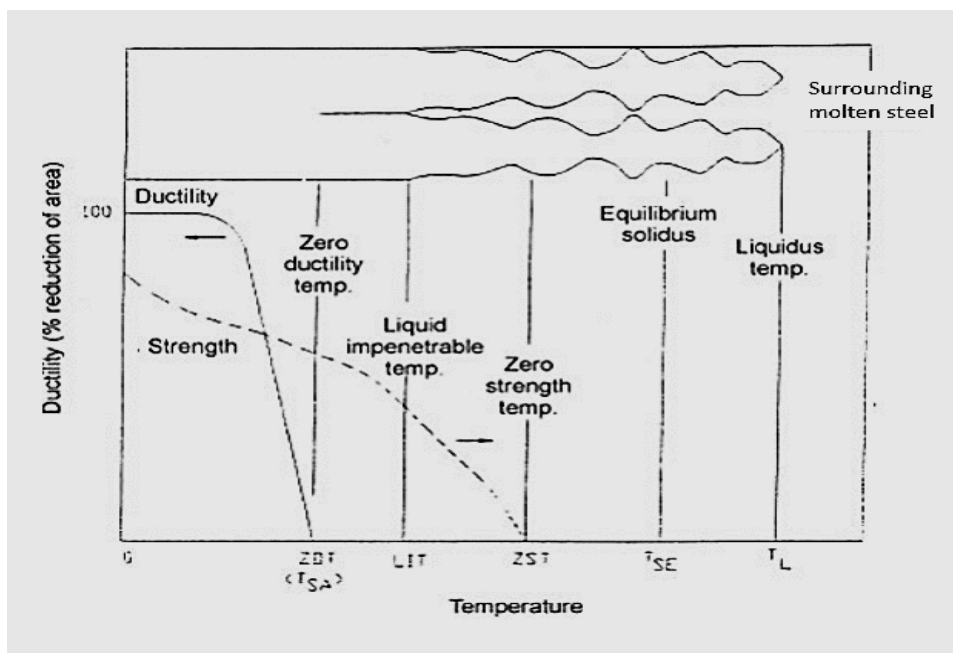


Figure 2-16. Mechanical properties of dendrites in mushy zone [28]

There are two common types of EMS which are Mould-EMS (M-EMS) and Final-EMS (F-EMS) as shown in Figure 2.17.

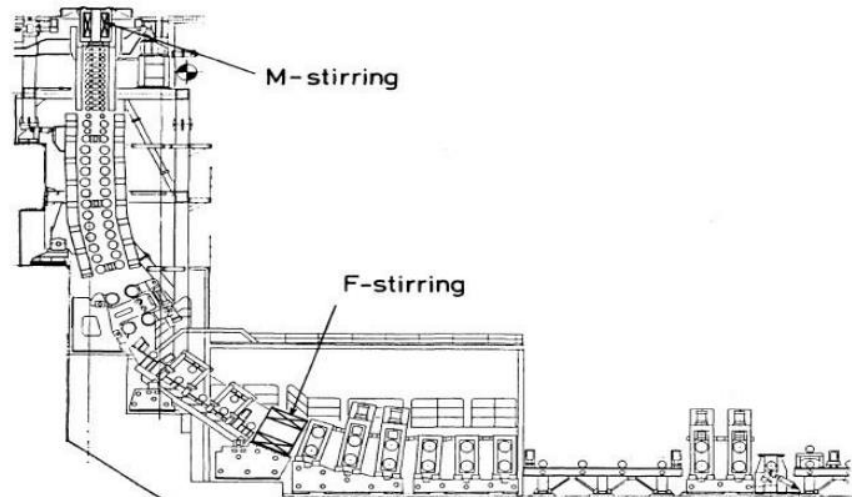


Figure 2-17. Position of M-EMS and F-EMS on a CCM [30]

M-EMS is located at the bottom part of the mould at the position where 85-90% of strand interior is liquid. In addition to increase in the ratio of the equiaxed zone by breaking dendrite tips, M-EMS also provides shell homogenization and reduces subcutaneous inclusions and pinholes. When the intensity of M-EMS is too high, however, some casting defects such as white band and mould powder entrapment can be seen. The second electro-magnetic stirrer, F-EMS, is located at the final solidification zone where the mushy interior of strand has a liquid fraction of 30-40% and it is very effective in reducing central segregation by refining equiaxed grains and breaking columnar bridges in the mushy zone [31,32].

White band is a negative segregation region in which content of alloying elements is low and its formation is inevitable for both M-EMS and F-EMS. Although white band formation mechanism cannot be exactly explained, there are several studies to determine which mechanism leads to its formation. For example, “solute washing” mechanism proposes that the turbulence induced by EMS sweeps out enriched inter-

dendritic liquid from leading edge of solidifying strand. Additionally, one of the alternative explanations states that the formation of white band is a result of changes in growth rate at the start and end of the EMS [33,34]. Figure 2.18 shows the difference between carbon distributions in billets produced with and without EMS. It is seen that width of the white band can be 7-8 mm. Macro etching of billet surfaces with hydrochloric acid makes it visible with naked eye. Width of white band, its location and severity of negative segregation in this region depend on intensity of EMS as well as strand velocity and secondary cooling intensity.

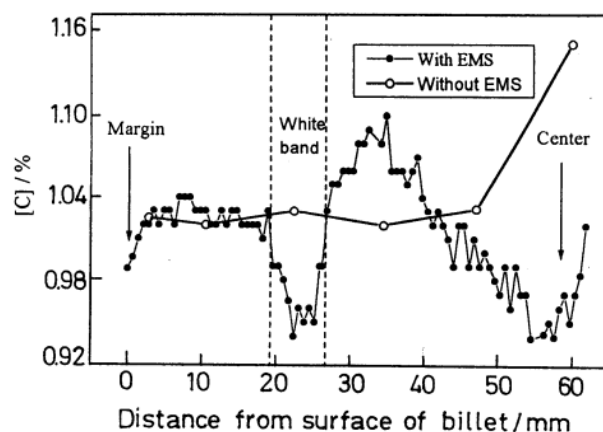


Figure 2-18. Carbon distribution in 120x120 mm billets with and without EMS [34]

Determination of suitable stirring velocity of F-EMS is very important for reducing central segregation with an acceptable white band. The stirring velocity of the molten metal, U (cm/sec), is given by below equation [35].

$$U = K \times B \times \sqrt{f} \times R^n \times \sqrt{\sigma/\rho} \times \mu^{-0.44} \quad (4)$$

where K is constant depending on rotary type, B is the magnetic flux density (Gauss), f is the frequency (Hz), R is the radius of molten metal pool stirred, σ is the electric conductivity (Ω/cm), ρ is the density of molten metal (g/cm^3) and μ is the viscosity of

molten metal (c.p.). Equation 4 indicates that if the current intensity and frequency of F-EMS is increased, more effective stirring can be obtained.

In addition to current intensity and frequency, the efficiency of EMS in the final zone also depends on the secondary cooling intensity and strand velocity. This is because these parameters affect metallurgical length which can be defined as the distance from the meniscus level to the point at which the strand becomes completely solid [36]. F-EMS should be located before the metallurgical length ends otherwise its metallurgical effect decreases.

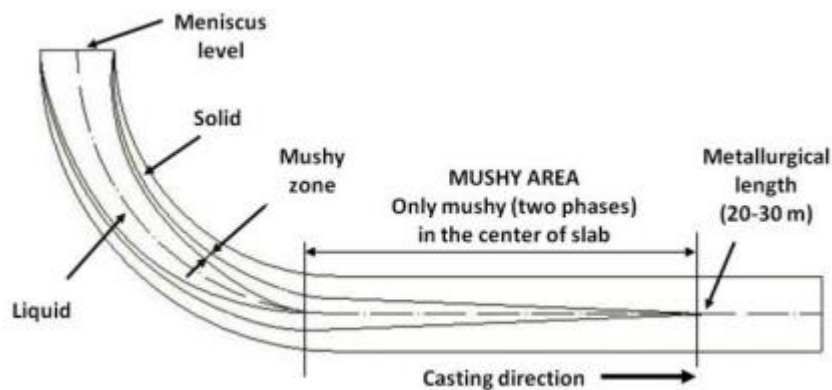


Figure 2-19. Sketch of inner structure of continuously casted billet [37]

Excessive secondary cooling intensity shortens the metallurgical length and causes that the mushy interior of the strand has a high fraction of solid. In such a case, F-EMS cannot function properly because it cannot create liquid turbulence. On the contrary, when the secondary cooling is not enough, the liquid fraction in the strand can be high. The stirring efficiency of F-EMS decreases in this situation. To overcome this problem, it is very important to adjust the solid-liquid ratio of the strand correctly at the F-EMS position [26,38]. Strand velocity can have both positive and negative effects on F-EMS efficiency. When the strand velocity is high, stirring becomes more effective because of the turbulence [10]. However, high casting rate also causes that the strand passes through F-EMS region more rapidly, so the stirring time decreases.

As a consequence, the optimization of secondary cooling intensity and strand velocity is necessary to maximize the efficiency of electromagnetic stirring which has a significant effect on segregation of alloying elements.

2.2.3. Hot Rolling Parameters

Billets which are produced at CCM as semi-finished products are annealed at about 1250 °C for 2.5 hours before hot rolling, which is typical industrial annealing heat treatment. Even after this annealing treatment, it is seen that the distribution of alloying elements cannot be homogenized. Longer annealing treatments are needed for removing segregation of alloying elements completely. For complete homogenization of segregated regions and complete disappearing of microstructural banding, an annealing treatment at 1225 °C for 8 hours has been reported by Beguinot [39] in his study because substitutional alloying elements (Mn, Cr, etc.) have low diffusivity. Furthermore, in the same study, it has been found that micro segregation rates of the same element in the similar areas of the billet and hot rolled plate are very close after an annealing treatment at 1300 °C for 4 hours, which proves that the effect of typical annealing treatment before hot rolling on inter-dendritic segregation is very low because of longer diffusion distances. In a similar study, Jatczak et al. [40] have focused on pearlite-martensite banding in 4340 steel. They have still observed microstructural banding even after annealing treatments at 1200 °C for 200 hours. This type of long annealing treatments are not economically (energy, production rate) and metallurgically (decarburization, scale formation) feasible.

Although the diffusion coefficient of carbon is much higher than that of substitutional alloying elements, manganese and chromium prevent homogenization of carbon by heat treatment because they lower the activity of carbon [4,41]. Bode et al. [38] have demonstrated a relationship between center segregation indexes of carbon and that of manganese and chromium as in Figure 2.20.

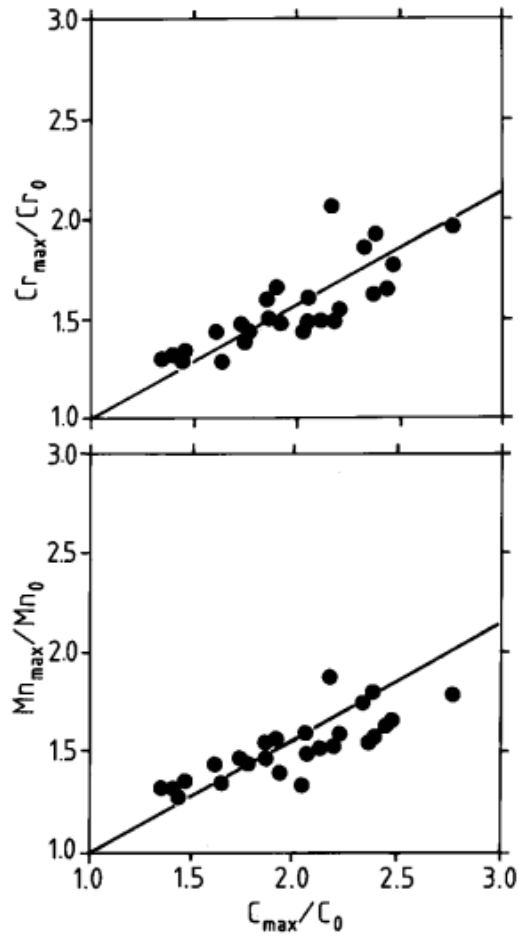


Figure 2-20. The relationship between center segregation indexes of carbon, chromium and manganese [38]

The second important hot rolling parameter is the cooling rate applied to the products after rolling which is very important for the development of microstructural banding. Studies show that increasing the cooling rate after hot rolling reduces the microstructural banding intensity in the products. However, although microstructural banding can be suppressed by this way, segregation of alloying elements which is the main reason of the banding cannot be removed by fast cooling. In other words, bands can reappear if the product is reheated and cooled for subsequent operations of the manufacturing process [2,4,8].

Additionally, the ratio between cross-section areas of the billet and product is also one of the important hot rolling parameters affecting microstructural banding. This ratio is called as reduction ratio. Simply, as the reduction ratio increases, the thickness of microstructural bands decreases as in other discontinuities such as voids and inclusions.

CHAPTER 3

EXPERIMENTAL PROCEDURE

3.1. Production of the Experimental Castings

The 52CrMoV4 steel grade was used in this study. The nominal composition of this steel grade according to DIN EN 10089 and target analysis of experimental castings are given in Table 3.1. Experimental castings were produced by this target analysis with the admissible deviations.

Table 3-1. Nominal composition of 52CrMoV4 steel and target analysis of experimental castings

Element	C	Si	Mn	Cr	Mo	V	P	S
52CrMoV4	Wt. %							
Nominal	0.48- 0.56	Max. 0.40	0.70- 1.10	0.90- 1.20	0,15- 0,30	0,10- 0,20	Max. 0,025	Max. 0,025
Target Analysis	0,55	0,28	0,84	1,10	0,18	0,12	0,005	0,005

The experimental billets were produced by the continuous casting process at ÇEMTAŞ Steel Plant. Continuous casting machine (SMS CONCAST) has 2 strands in ÇEMTAŞ. To eliminate the effect of strand variability, all experimental castings were produced in one particular strand. In Table 3.2, 18 different experimental castings produced with different parameters are listed. In the first 6 experiments, the flow rate of secondary cooling water is 34 L/min. called as mild cooling. The experiments from 7 to 12 are in group of medium cooling in which the flow rate of secondary cooling water is 40 L/min. The last six experiments have the highest flow rate, 51 L/min, which was called as intense cooling. Additionally, each of these 3 main groups has the combinations of 2 F-EMS frequencies (7 Hz and 10 Hz) and 3 F-EMS currents (350 A, 400 A, 450 A).

Table 3-2. Experimental matrix

Experiment No.	F-EMS Frequency (Hz)	F-EMS Current (A)	Flow rate of secondary cooling water (L/min)		Carbon amount in tundish (wt%)
1	10	350	34	Mild Cooling	0.55
2	10	400	34		0.55
3	10	450	34		0.54
4	7	350	34		0.54
5	7	400	34		0.54
6	7	450	34		0.54
7	10	350	40	Medium Cooling	0.54
8	10	400	40		0.54
9	10	450	40		0.55
10	7	350	40		0.54
11	7	400	40		0.54
12	7	450	40		0.54
13	10	350	51	Intense Cooling	0.55
14	10	400	51		0.55
15	10	450	51		0.55
16	7	350	51		0.54
17	7	400	51		0.55
18	7	450	51		0.55

Although the F-EMS and flow rate of secondary cooling water are variables of this thesis study, other CCM parameters such as primary cooling intensity, strand velocity, and M-EMS also affect inter-dendritic segregation of alloying elements during continuous casting of steels. The liquidus temperature of 52CrMoV4 steel is 1474 °C. The superheat was kept about 50 °C, meaning that the temperature of the liquid steel in tundish was around 1524 °C. The same flow rate for primary cooling water was set to the experimental castings. In addition to these, the strand velocity and M-EMS parameters were also exact same with the normal production practice.

200x200 mm square sectioned billets were hot rolled to the plate products with dimensions of 90x45 mm. The reduction ratio for them is 9.9 which is constant because all experimental billets and plate products were also in the same size. Annealing temperature and time were kept almost constant for all experimental

castings. The cooling rate after hot rolling affects directly the amount and type of banded phases in the final microstructure although it cannot remove micro segregation of alloying elements. To eliminate the effect of cooling rate on results, specimens prepared for micro examinations were austenitized at 850 °C for 10 minutes and then they were cooled by air cooling as similar to the method defined in SEP 1520 standard.

3.2. Sampling and Investigations

To investigate the effects of CCM parameters on the segregation pattern of billets, the chemical composition analyses were conducted by Test Master Pro mobile spectrometer. For this purpose, about 15 mm thick transverse slice was cut from the billets with a cross-section area of 20x20 cm and divided 169 regions as shown in Figure 3.1.

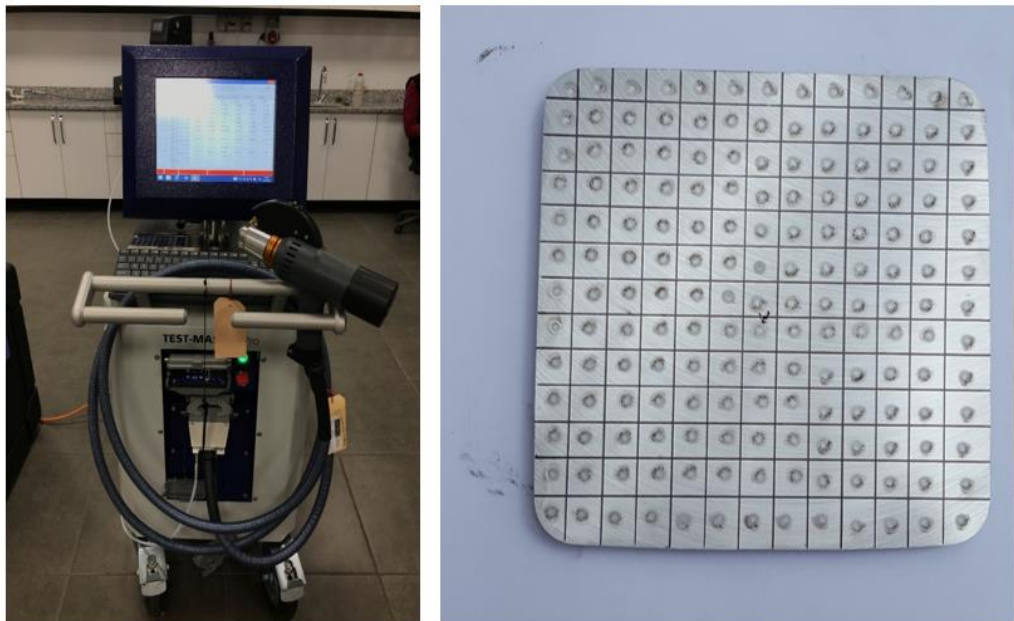


Figure 3-1. Test Master Pro mobile spectrometer and chemical composition measurements on transverse billet slice

For micro examinations, samples with the dimensions of 15x10x25 mm were taken from the middle of the 90x45 mm plate products. From each experiment, 4 samples

were examined with a digital microscope which is Keyence VHX-5000. As defined above, samples were heat treated before they were grinded and polished. Then, the samples were etched by using 4% Picral solution containing 4% picric acid in ethanol for 60 seconds. 200X microstructure figures were taken to examine the structure of martensite bands at the center of the samples. In addition to this, the area ratios of the banded phases were calculated by using image analysis software of the digital microscope. After 4 samples from all experiments were examined, only the region with highest microstructural banding intensity was reported.

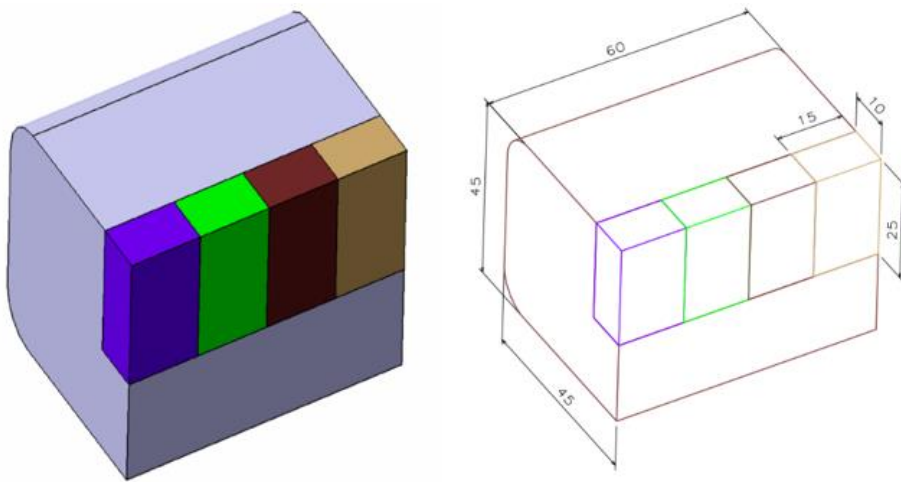


Figure 3-2. Sampling for micro examinations

After micro examinations, micro and macro hardness measurements were carried out. Micro hardness measurements were done on each phase existing in the microstructures of the samples by using Emco Test Durascan 20.

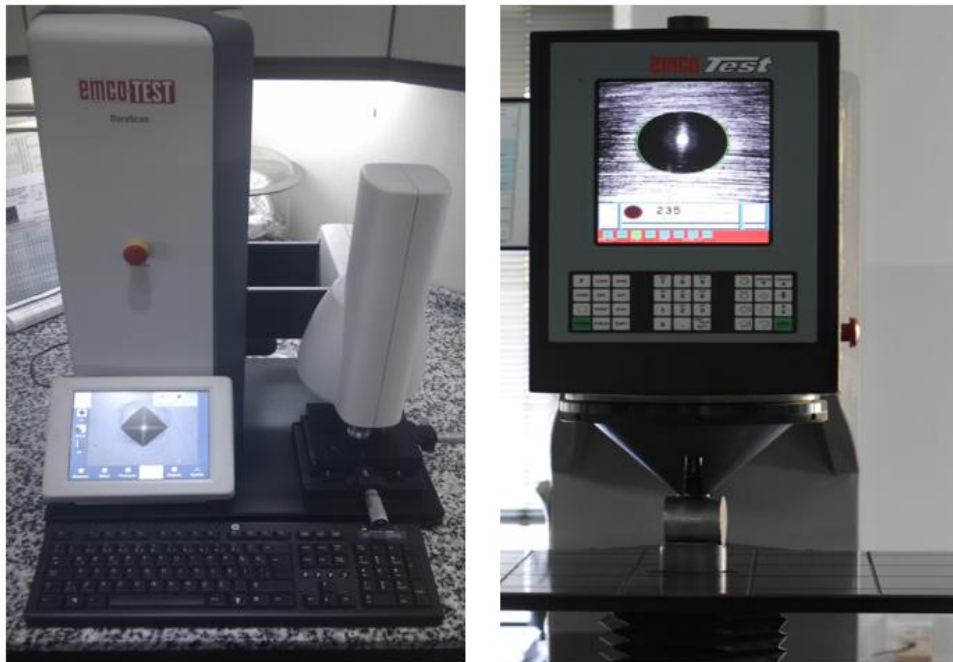


Figure 3-3. Emco Test Durascan 20 micro hardness test device and Emco Test M5C hardness test device

Hardness measurements in the Rockwell scale were also conducted at the middle of the 90x45 mm plate products. Hardness measurement points are shown in Figure 3.4. The hardness test device is Emco Test M5C.

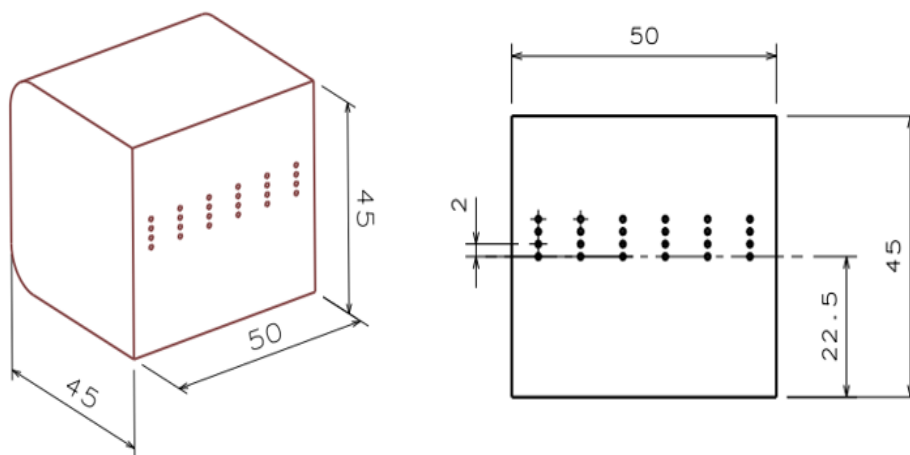


Figure 3-4. Hardness measurement points

Lastly, to evaluate the effect of microstructural banding on cutting and drilling performance of the materials, 25 tons of cast were produced with the parameters used in the experiment which have best results in terms of banding intensity and center hardness. Hot rolled products from this cast were cut by band saws which are EBERLE – M51 and center holes were drilled by TiN coated drilling heads as in normal production route. Then, usage capacities of these tools in this cast were compared with that in products produced with the parameters used in normal production practice.

CHAPTER 4

RESULTS AND DISCUSSION

The main objective of this thesis is to minimize the fraction of micro segregation induced banded martensite phase in 52CrMoV4 steel grade by optimizing F-EMS frequency, F-EMS current, and secondary cooling intensity. Initially, chemical composition measurements were conducted to clarify the effect of changing these parameters on the distribution of alloying elements in experimental billets. Then, the banding intensities at the center of the products hot rolled from these billets were measured. Furthermore, how the center hardness of the material is affected by banding intensity were investigated. Finally, the capability of cold sawing and center hole making of the products were compared by considering equipment life used for these operations to see the effect of banding intensity.

4.1. Characterization of the Microstructural Banding in 52CrMoV4 Steel

Firstly, LePera solution was used as etchant to characterize phases existing in 52CrMoV4 steel. It was prepared by mixing an equal amount of 1% $\text{Na}_2\text{S}_2\text{O}_5$ in aqueous dilution and 4% picric acid in ethanol. It is known that 4-minute etching by LePera forms on martensite a white, on pearlite a light brown and on bainite a dark structured surface layer [42,43]. In the light of this information, banded phases in hot rolled 52CrMoV4 steel were identified as in Figure 4.1.

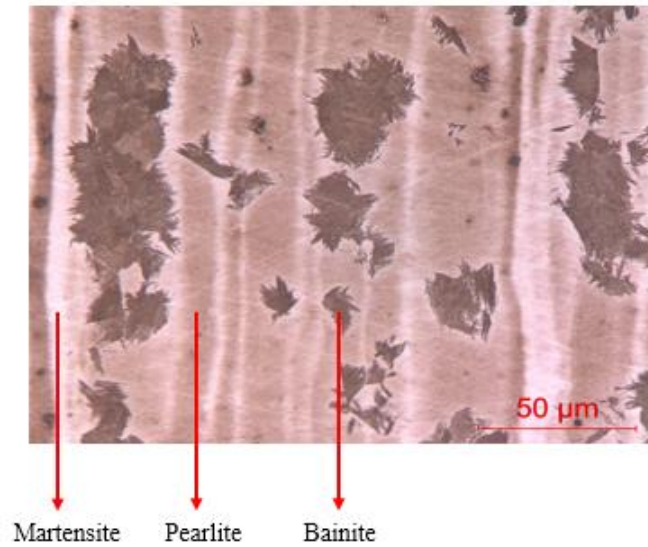


Figure 4-1. Microstructure of the sample taken from center of the plate product, 52CrMoV4, 90x45 mm (LM, LePera, 4 minutes, 100X)

In addition, EDS analysis was also performed to support this finding. As shown in Figure 4.2, the first spectrum was measured on martensite band (site 1), the second spectrum was measured on bainite (site 2), and the third spectrum was measured on pearlite (site 3).

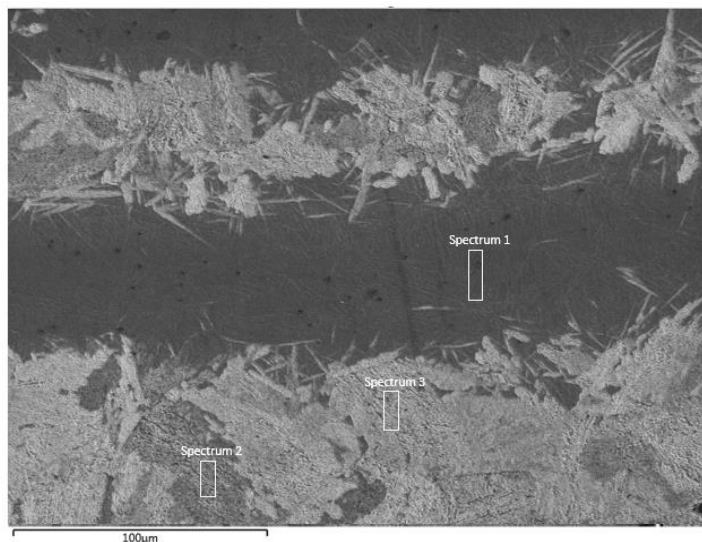


Figure 4-2. SEM micrograph of banded microstructure of 52CrMoV4 steel

EDS analysis showed that the contents of alloying elements in Site 1 and Site 2 were higher than target analysis given in Table 3.1. On the contrary, the content of alloying elements in Site 3 was lower than the target analysis.

Table 4-1. Results of EDS analysis (wt%) of different phases in 52CrMoV4 steel

Element	Si	Mn	Cr	Mo	V	Fe
Site 1	0.38	1.65	1.87	0.49	0.33	Balance
Site 2	0.30	1.10	1.29	0.25	0.17	Balance
Site 3	0.21	0.67	0.94	0.13	0.10	Balance

To see the effect of the change in the content of the alloying elements, the continuous cooling transformation (CCT) diagrams of each site were calculated by using JMatPro software. It should be noted that the content of light elements like carbon cannot be measured properly by the EDS method [4]. For this reason, the change in carbon content was ignored for these calculations.

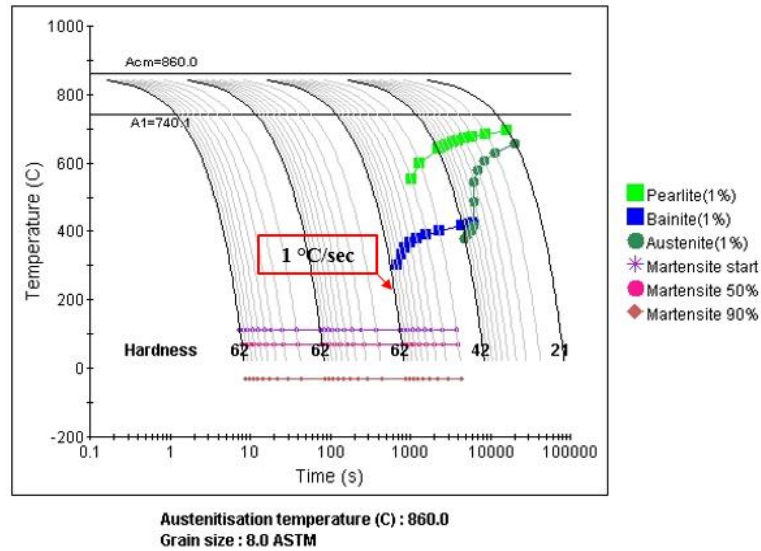


Figure 4-3. CCT of Site 1 calculated by JMatPro software

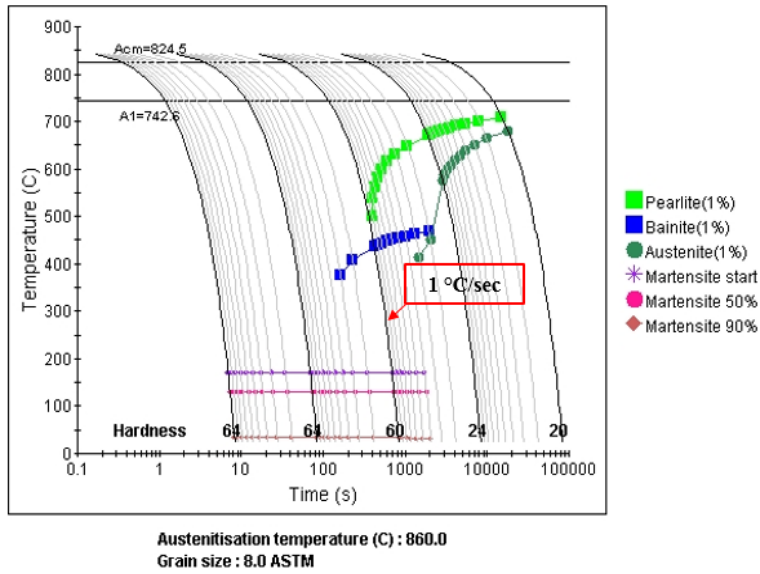


Figure 4-4. CCT of Site 2 calculated by JMatPro software

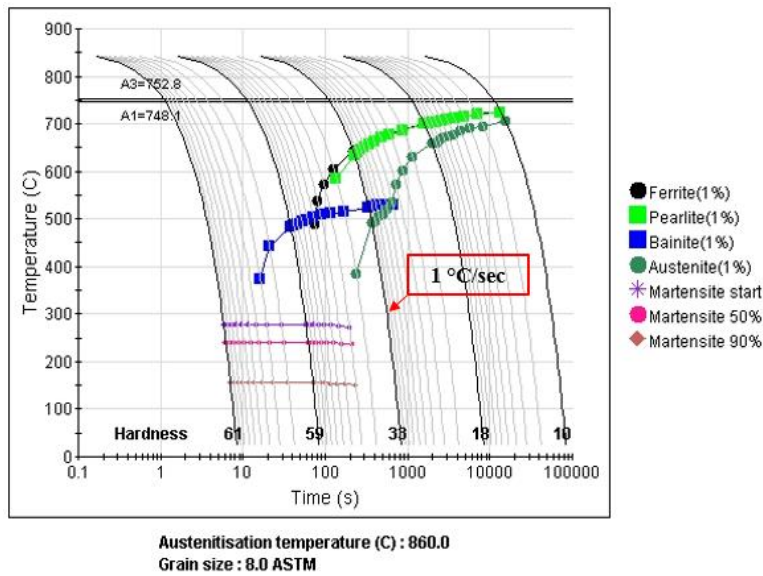


Figure 4-5. CCT of Site 3 calculated by JMatPro software

Calculated CCT diagrams showed that martensite formation becomes favorable in Site 1 even in industrial cooling rate which is about 1 °C/sec. Due to decrease in the content of alloying elements in other sites, the noses of bainite and pearlite curves shift to left. Therefore, different phases can form in alternate regions at the same cooling rate.

4.2. The Amount of Heat Extracted by Primary Cooling in Mould

As referred in the literature review, heat transfer at the mold/metal interface affects directly the quality of both semi-finished and last products. The flow rate of the water circulating around the mould is main responsible for heat transfer at liquid metal – mould interface. To calculate the flow rate of primary cooling water, the following calculation should be done carefully by considering heat conduction in the mould [10,21,44].

First of all, a ThermoCalc analysis was carried out to find thermal properties of 52CrMoV4 steel according to target analysis in Table 3.2.

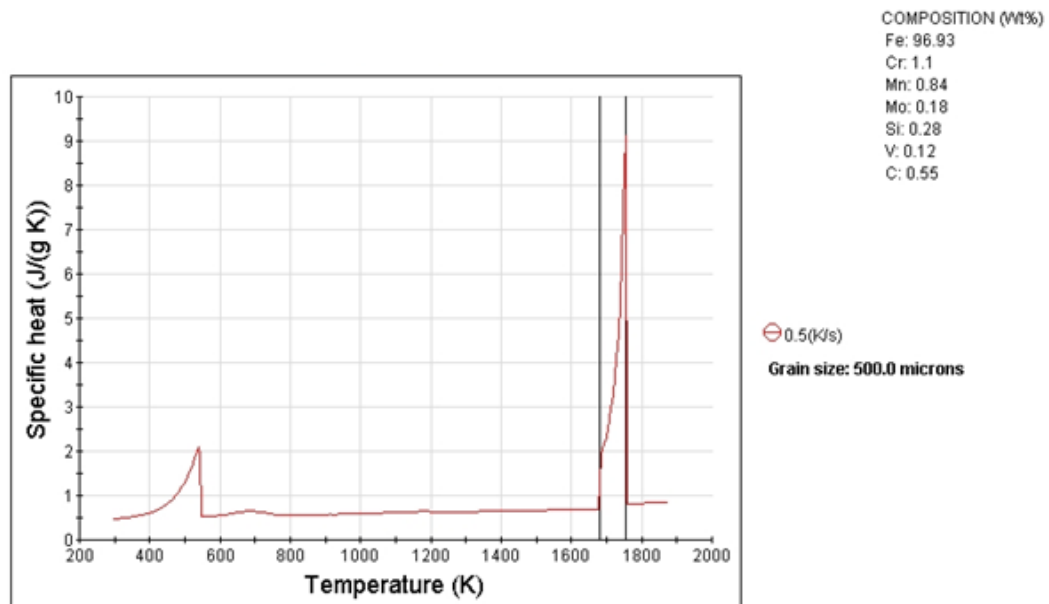


Figure 4-6. Specific heat of 52CrMoV4 steel at various temperatures

According to this analysis;

- Heat capacity of 52CrMoV4 steel at 298 K is 0.47 J/g K,
- Heat capacity of 52CrMoV4 steel at 1797 K is 0.82 J/g K,
- Latent heat of fusion for this steel grade is 250 J/g.

By using these values, the effective latent heat of fusion can be calculated as below.

$$H'_f = H_f + C_p(T_p - T_m) \quad (5)$$

where C_p is the liquid heat capacity of 52CrMoV4 steel,

T_p is the tundish temperature (1797 K if it is assumed that super heat is 50 K),

T_m is the liquidus temperature (1747 K for 52CrMoV4).

Then,

$$H'_f = 2.5 \times 10^5 \frac{J}{kg} + 820 \frac{J}{kg K} \times (1797 K - 1747 K) = 291000 \frac{J}{kg} \quad (6)$$

Figure 4.7 was used to calculate the heat removal rate at the various positions of the mould when the mould temperature is maintained at T_o . Lines in the diagram represent dimensionless variable:

$$\frac{H_f}{C_p(T_m - T_o)} = \frac{291000}{470 \times (1747 - 303)} = 0.43 \quad (7)$$

where T_o is the mould inlet temperature of the cooling water (303 K) which was taken from SMS concast programme and C_p in this equation is the solid heat capacity of 52CrMoV4 steel. X-axis of this diagram represents another dimensionless parameter.

$$\frac{h^2 y}{u k \rho C_p} = \frac{1700^2 \times 0.64}{0.013 \times 44 \times 7800 \times 470} = 0.78 \quad (8)$$

where h is the heat transfer coefficient and it is assumed that h is 1700 W/m² K,

y is the mould length which is 0.64 m,

u is the casting speed which is 0.8 m/min. (0.013 m/sec),

k is the solid thermal conductivity of 52CrMoV4 steel which is 44 W/m K

ρ is the density of 52CrMoV4 steel which is 7800 kg/m³

C_p is the solid steel heat capacity which is 470 J/kg K.

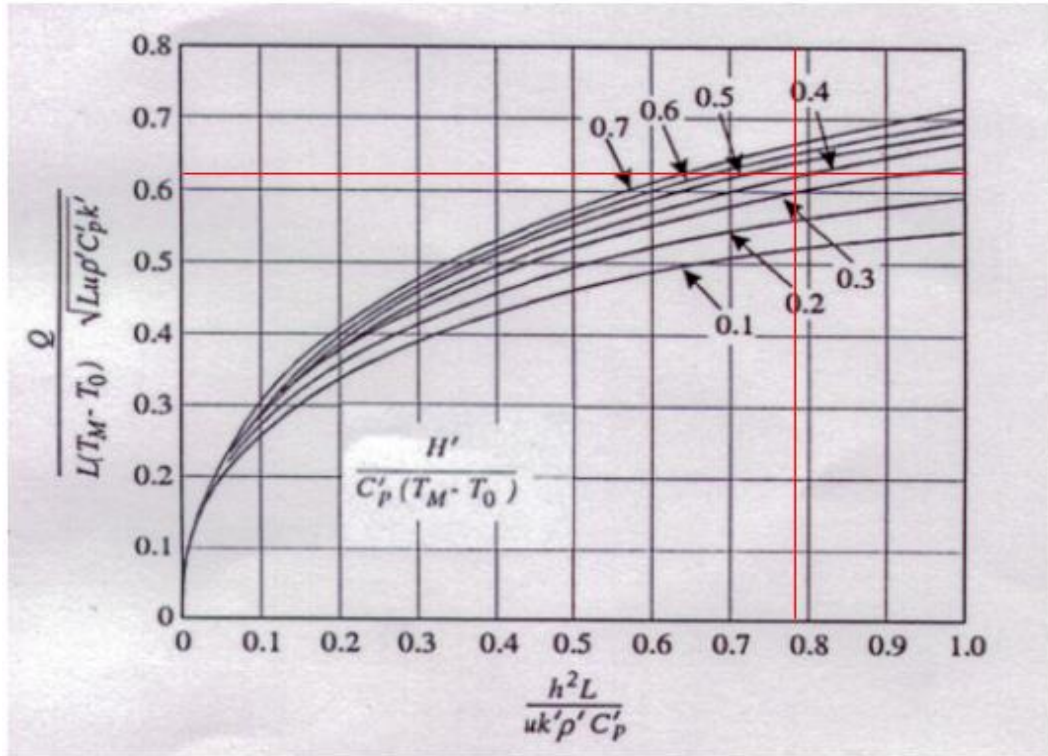


Figure 4-7. Rate of heat removal by mould cooling water versus mould length [44]

According to Figure 4.7,

$$\frac{Q}{L(T_m - T_o)\sqrt{Lu\rho C_p k}} \cong 0.62 \quad (9)$$

$$Q = (0.62)(0.64)(1747-303)\sqrt{(0.64)(0.013)(7800)(470)(44)} \quad (10)$$

$$Q = 663778.4 \text{ W} \quad (11)$$

According to SMS Concast programme, the temperature difference between inlet and outlet cooling water is 4.6 K. So,

$$\text{Flow rate} = 663778.4 \times \frac{J}{\text{sec}} \times \frac{\text{kg K}}{4184 \text{ J } 4.6 \text{ K}} = 33.5 \text{ kg/sec} \quad (12)$$

where 4184 J/kg K is the specific heat of water.

$$\text{Flow rate} = 2069 \text{ kg/min} \cong 2069 \text{ L/min} \quad (13)$$

The minimum and maximum flow rates are 2066 L/min and 2080 L/min for this heat conduction according to SMS Concast software program. It is seen that the calculated flow rate is consistent with actual value so the assumption of the heat transfer coefficient is reasonable regarding these values.

It is also possible to calculate the shell thickness associated with the primary cooling by this approach. Figure 4.8 shows how the solidified thickness of the strand is changed within the mould.

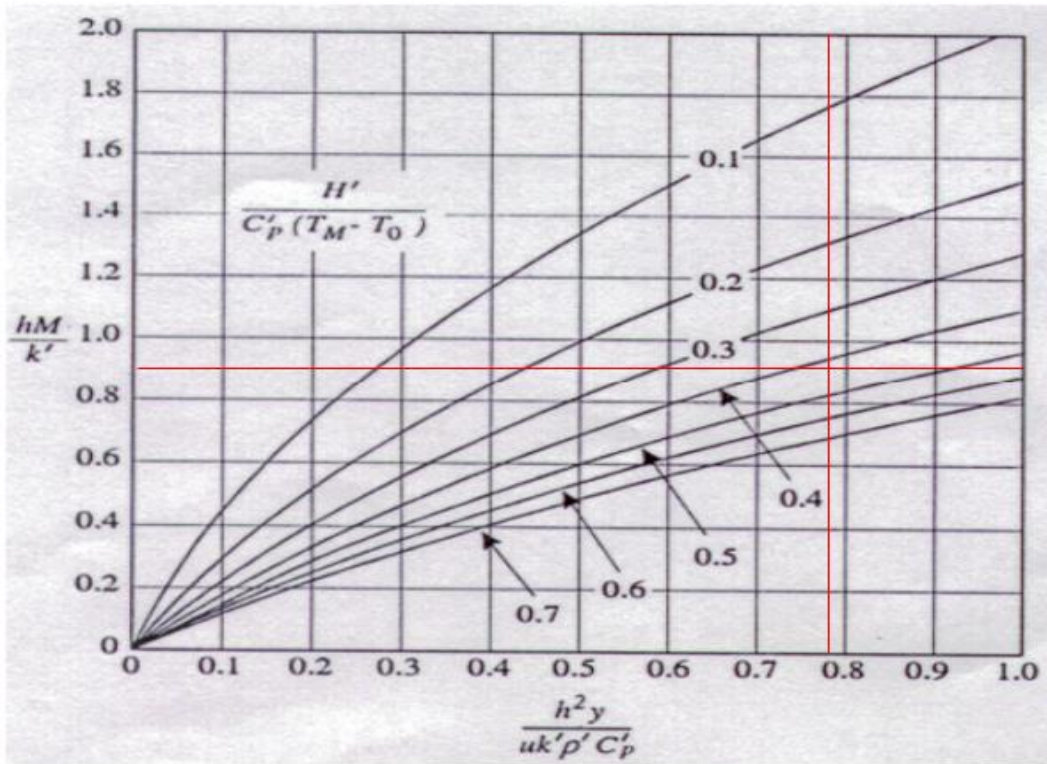


Figure 4-8. Thickness solidified, M , versus distance down the mould [44]

According to this figure,

$$\frac{hM}{k'} \cong 0.895 \quad (14)$$

$$\frac{1700M}{44} \cong 0.895 \quad (15)$$

Thickness of solid shell when the strand exits from mould,

$$M = 0.023 \text{ m} = 23 \text{ mm} \quad (16)$$

When the carbon distribution in the billet slices which will be detailed in the next part is considered, it is seen that the value of solidified thickness is coherent with the M-EMS region. In addition to this, thickness of 23 mm which is about 10% of billet's full thickness is enough to resist hydrostatic pressure of liquid metal in the strand against bleeding.

4.3. Carbon Segregation Pattern in Transverse Billet Slices

As the first step of evaluating the project's results, distribution of carbon which is the main alloying element in steel was investigated. Then, carbon segregation indexes at the center of the experimental billets were calculated. By this way, the effects of F-EMS frequency, F-EMS current and secondary cooling intensity on the distribution of alloying elements in semi-products, in this case these are billets, were revealed. As previously mentioned, transverse billet slices with 20x20 cm cross-section area taken from all 18 experimental castings were divided 169 regions and chemical analyses were performed in each region. Figure 4.9 shows the carbon distribution of Experiment 8 produced by using the normal production parameters of 52CrMoV4 steel at ÇEMTAŞ steel plant.

Carbon amount of Experiment 8 in tundish is 0,54%. Measurements show that average carbon amount in billet is 0,55% although carbon content varies from region to region. As previously defined in literature review, there exists a concentration profile consisting of both positive and negative segregation region in billets. However, the ratio between them can be different in each region. Since segregation of alloying

elements becomes more severe towards the center of the billet resulting in more positive segregated regions, the carbon content increases at center region. On the other hand, carbon content decreases at white band regions which are caused by M-EMS and F-EMS. White band caused by M-EMS is seen 1.5 - 3 cm below the surface. This also proves that shell thickness calculation regarding the conduction method which was 2.3 cm. Decreasing of carbon content due to F-EMS is about 6 - 7.5 cm below the surface in the Experiment 8. It is noted that chemical composition analysis of billets showed that the other alloying elements such as chromium and manganese have similar distribution with carbon as stated in literature review part. This distribution pattern is almost same for other experimental castings. However, the severities of change in the amount of alloying elements differ greatly depending on parameters used in experiments.

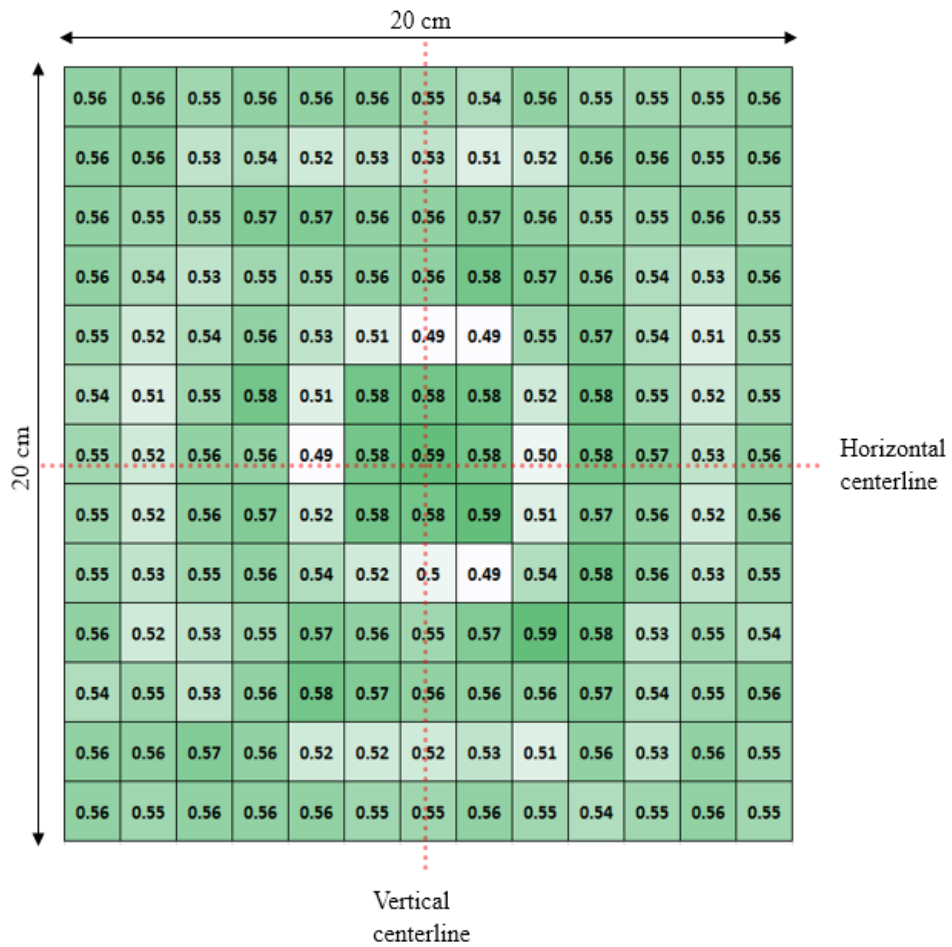


Figure 4-9. Carbon distribution of Experiment 8

Especially, the increase in the amount of alloying elements at the center of the billets causes the banded martensitic structure to become more intense in this region. To estimate the effects of parameters used in experimental castings on the severity of segregation, the center carbon segregation indexes were calculated by using center carbon distribution. It was generated by averaging carbon content at equivalent regions of billet throughout vertical and horizontal centerlines shown in Figure 4.9. Then, the center carbon segregation index was calculated by dividing the average carbon amount at the center region to tundish carbon amount of casting. The example

calculation for Experiment 8 is shown below. Calculations of center carbon segregation indexes for other experiments can be seen in Appendix B.

Table 4-2. Carbon distribution through vertical and horizontal centerline for Experiment 8

Position	0.5-1.5 cm	1.5-3 cm	3-4.5 cm	4.5-6 cm	6-7.5 cm	7.5-9 cm	9-10.5 cm	10.5-12 cm	12-13.5 cm	13.5-15 cm	15-16.5 cm	16.5-18 cm	18-19.5 cm
Vertical centerline	0.55	0.52	0.56	0.56	0.49	0.58	0.59	0.58	0.50	0.58	0.57	0.53	0.56
Horizontal centerline	0.55	0.53	0.56	0.56	0.49	0.58	0.59	0.58	0.50	0.55	0.56	0.52	0.55
Average	0.55	0.53	0.56	0.56	0.49	0.58	0.59	0.58	0.50	0.57	0.57	0.53	0.55
	Sub-surface	M-EMS Region	Unstirred Region		F-EMS Region	Center Region			F-EMS Region	Unstirred Region		M-EMS Region	Sub-surface

$$\text{Center carbon segregation index} = \frac{\text{Average carbon content at center}}{\text{Carbon content in tundish}} \quad (17)$$

Then, for experiment 8:

$$\text{Center carbon segregation index} = \frac{\frac{0.58 + 0.59 + 0.58}{3}}{0.54} \quad (18)$$

$$\text{Center carbon segregation index} = 1.08 \quad (19)$$

In Table 4.3, average carbon distributions through centerline and center carbon segregation indexes for all 18 experimental castings are seen.

Table 4-3. Center carbon distributions of experimental billets and center carbon segregation indexes

Experiment No	Sub-surface	M-EMS Region	Unstirred Region		F-EMS Region	Center Region			F-EMS Region	Unstirred Region		M-EMS Region	Sub-surface	Segregation Index
1	0.56	0.54	0.58	0.58	0.47	0.61	0.65	0.61	0.47	0.58	0.58	0.54	0.56	1.13
2	0.56	0.53	0.56	0.56	0.48	0.61	0.62	0.60	0.47	0.57	0.56	0.53	0.55	1.11
3	0.55	0.53	0.58	0.55	0.50	0.59	0.60	0.58	0.47	0.55	0.57	0.54	0.55	1.09
4	0.54	0.51	0.55	0.55	0.50	0.60	0.64	0.60	0.49	0.53	0.55	0.51	0.54	1.14
5	0.56	0.54	0.57	0.57	0.47	0.59	0.63	0.61	0.48	0.57	0.56	0.54	0.56	1.13
6	0.55	0.52	0.56	0.56	0.48	0.60	0.61	0.58	0.48	0.56	0.56	0.53	0.56	1.10
7	0.55	0.52	0.56	0.56	0.49	0.59	0.60	0.59	0.49	0.57	0.56	0.53	0.56	1.10
8	0.55	0.53	0.56	0.56	0.49	0.58	0.59	0.58	0.50	0.57	0.57	0.53	0.56	1.08
9	0.55	0.52	0.57	0.57	0.47	0.58	0.59	0.59	0.47	0.57	0.56	0.52	0.56	1.07
10	0.55	0.52	0.56	0.56	0.48	0.60	0.61	0.59	0.48	0.56	0.56	0.52	0.55	1.11
11	0.55	0.53	0.57	0.58	0.47	0.60	0.60	0.59	0.48	0.57	0.57	0.53	0.56	1.10
12	0.55	0.51	0.55	0.56	0.47	0.59	0.60	0.58	0.47	0.56	0.57	0.52	0.55	1.09
13	0.55	0.52	0.56	0.56	0.55	0.56	0.57	0.56	0.55	0.55	0.55	0.52	0.55	1.02
14	0.56	0.52	0.55	0.57	0.54	0.56	0.56	0.55	0.53	0.57	0.57	0.52	0.55	1.01
15	0.56	0.53	0.57	0.56	0.55	0.56	0.57	0.56	0.53	0.57	0.57	0.53	0.56	1.02
16	0.54	0.51	0.54	0.55	0.52	0.55	0.56	0.55	0.52	0.56	0.55	0.51	0.54	1.02
17	0.55	0.53	0.57	0.57	0.54	0.56	0.56	0.55	0.53	0.57	0.57	0.52	0.56	1.01
18	0.54	0.52	0.55	0.57	0.55	0.55	0.56	0.56	0.53	0.55	0.55	0.52	0.54	1.01

When the experimental castings produced by medium cooling are examined, it is seen that center carbon segregation indexes decrease as the F-EMS current is increased. In addition to this, when 7 Hz F-EMS frequency is used instead of 10 Hz center carbon segregation in billets become worse as shown in Figure 4.10. In the experiments produced with mild cooling, this tendency is almost the same. These results are expected because as the intensity of electro-magnetic stirring increases, the ratio of equiaxed zone increases and also secondary dendrites are broken resulting in smaller SDAS. These provide a more uniform distribution of alloying elements. Therefore, billets become more homogenous as F-EMS frequency and current increase.

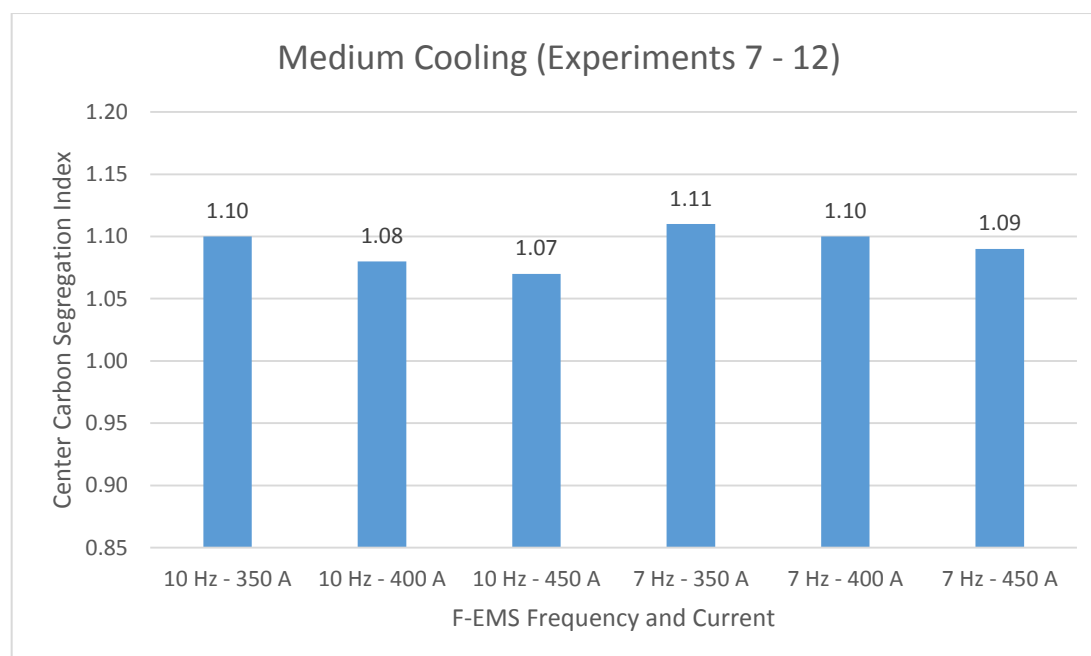


Figure 4-10. Center carbon segregation indexes for experiments with medium secondary cooling

On the other hand, when the flow rate of secondary cooling water is increased to 51 L/min, the effect of F-EMS disappears as shown in Figure 4.11. It is seen that increasing of F-EMS current and frequency has no remarkable effect on center carbon segregation indexes for experimental castings in which intense cooling regime was used. As stated in the literature review part, the efficiency of electromagnetic stirring

depends on the liquid-solid ratio in the mushy interior of the billet when it passes through F-EMS. Intense cooling naturally causes that billets are cooled more rapidly. Therefore, metallurgical length becomes smaller for these experiments, which lowers the efficiency of electro-magnetic stirring. Carbon distributions in Table 4.3 also showed that there is no distinct decreasing of carbon content in billets produced with intense cooling due to F-EMS although the white band formation is signally seen in experiments in which mild and medium cooling are used. This can be also evidence of the above phenomena.

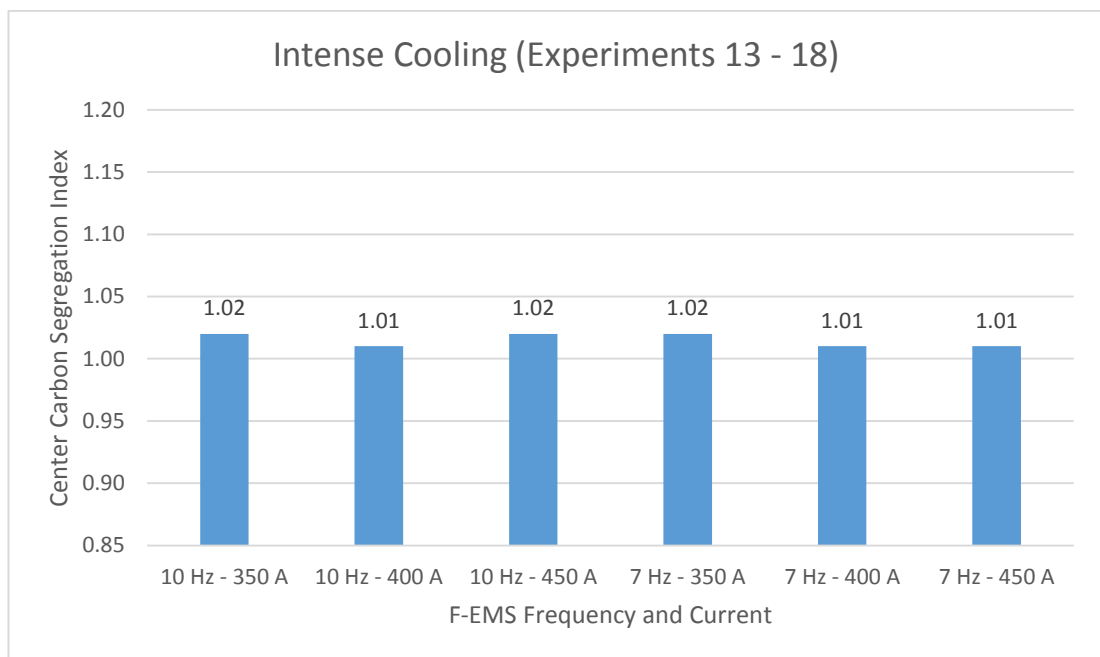


Figure 4-11. Center carbon segregation indexes for experiments with intense secondary cooling

After the secondary cooling region at the exit of the CCM, surface temperatures of the billets were measured by pyrometer device. These measurements show that when the medium cooling regime is used, the average temperature of the billets is 1075 °C. In the experiments having mild cooling regime, the flow rate of secondary cooling water decreases from 40 L/min to 34 L/min, and it is seen that the average surface temperature of billets slightly increases to 1090 °C. When intense cooling is used

instead of medium cooling, the flow rate of secondary cooling water increases by 11 L/min, and in this case, the average surface temperature of billets significantly decreases to 1010 °C.

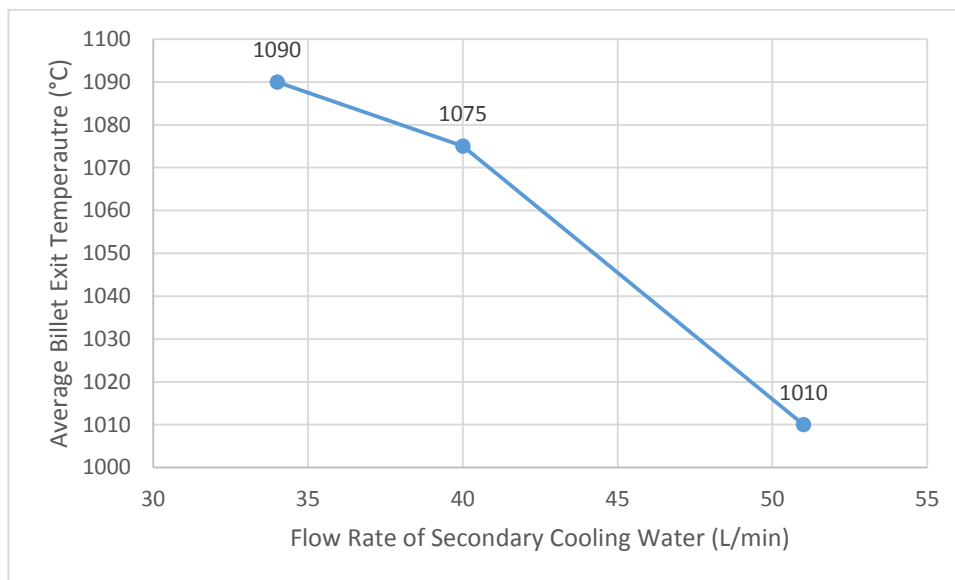


Figure 4-12. Average billet exit temperatures for different flow rates of secondary cooling water

Figure 4.13 shows the effect of the flow rate of secondary cooling water on center carbon segregation index for experiments in which 350 – 400 – 450 A with 10 Hz are used as F-EMS parameters. It should be also noted that results are similar for the experiments produced with 7 Hz of F-EMS frequency.

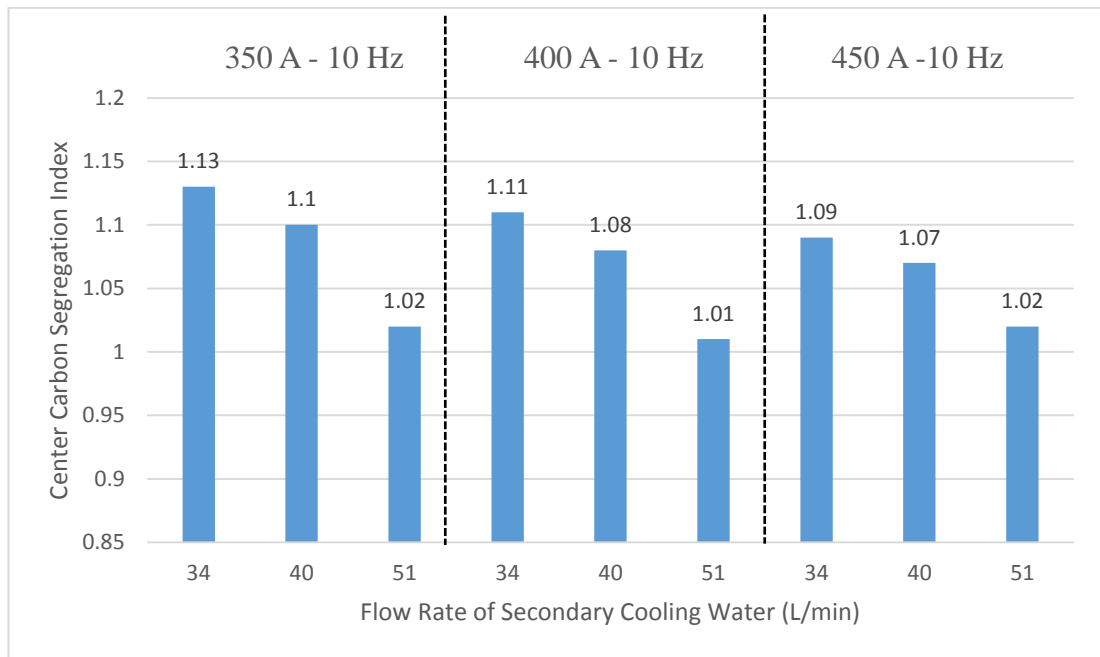


Figure 4-13. The effect of cooling intensity on center carbon segregation index

It is seen that when the flow rate of secondary cooling water is 34 L/min, center carbon segregation indexes have the highest values. If the flow rate is increased from 34 L/min to 40 L/min, center carbon segregation indexes slightly decrease. There exists a 15 °C difference between the average billet exit temperatures of the billets which were produced with mild cooling regime and medium cooling regime since flow rates of these regimes are close each other. Therefore, there is very small difference between their homogeneity according to center carbon segregation indexes. However, there is a sharp decrease in center carbon segregation indexes for experimental castings in which flow rate of secondary cooling water is 51 L/min. Temperature difference between medium cooling and intense cooling is 65 °C. As a result of this, the experiments produced with intense cooling regime have the most homogeneous carbon distribution and the smallest carbon segregation indexes.

The importance of secondary cooling rate due to its effect on SDAS, thereby on homogenization time, was emphasized in the literature review. According to SMS

Concast software program, the surface temperature of the billets at the exit of the mould is approximately 1300 °C. The distance between the mould exit and measurement point is 10 meters. Since the strand velocity is 0.8 m/min, the time period between them is 12.5 min. According to the pyrometer measurements after secondary cooling zone, cooling rates are 0.28 °C/sec, 0.30 °C/sec and 0.39 °C/sec for mild, medium and intense cooling regimes, respectively.

Table 4-4. Secondary cooling rate and theoretical SDAS values for mild, medium and intense secondary cooling regimes

Secondary Cooling Regime	Secondary Cooling Rate	Theoretical SDAS
Mild	0.28 °C / sec	191.2 µm
Medium	0.30 °C / sec	185.5 µm
Intense	0.39 °C / sec	165.2 µm

Theoretical SDAS values calculated by equation 3 show that SDAS value reduces by 26 microns when the intense cooling regime is used. As a result of this, it is seen that center carbon segregation indexes significantly decrease since an increase in the flow rate of secondary cooling water decreases SDAS.

Figure 4.14 summarizes the effect of CCM parameters on center carbon segregation indexes for all experiments.

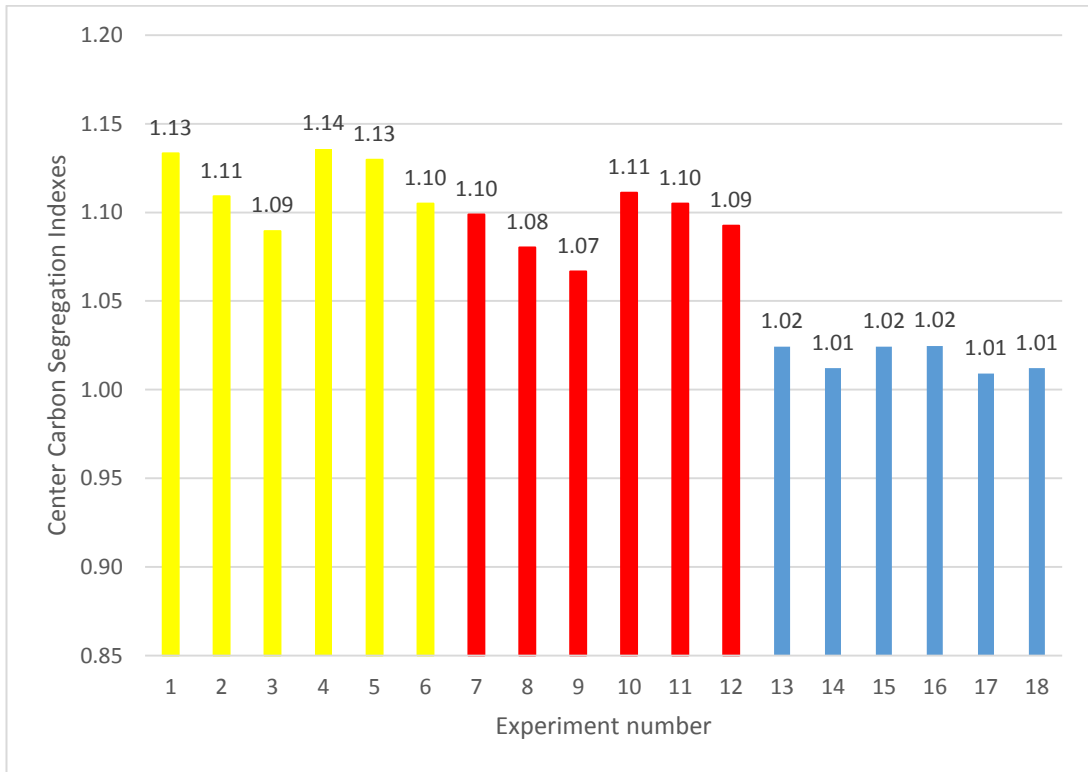


Figure 4-14. Center carbon segregation indexes for all experiments

4.4. Microstructure Examination Results

All experimental billets were hot rolled to 90x45 mm plate products. After the hot rolling process, the samples were taken from the center of these products and area ratio of martensite and bainite bands were measured to see the effect of homogeneity of billets on banding intensity in last products. In the following figures, there are microstructures of experiments having best and worst results in terms of microstructural banding for three main experiment groups; mild, medium and intense cooling experiments. Rest of the microstructures and image analysis for measuring area ratios of the banded phases can be found in Appendix C.

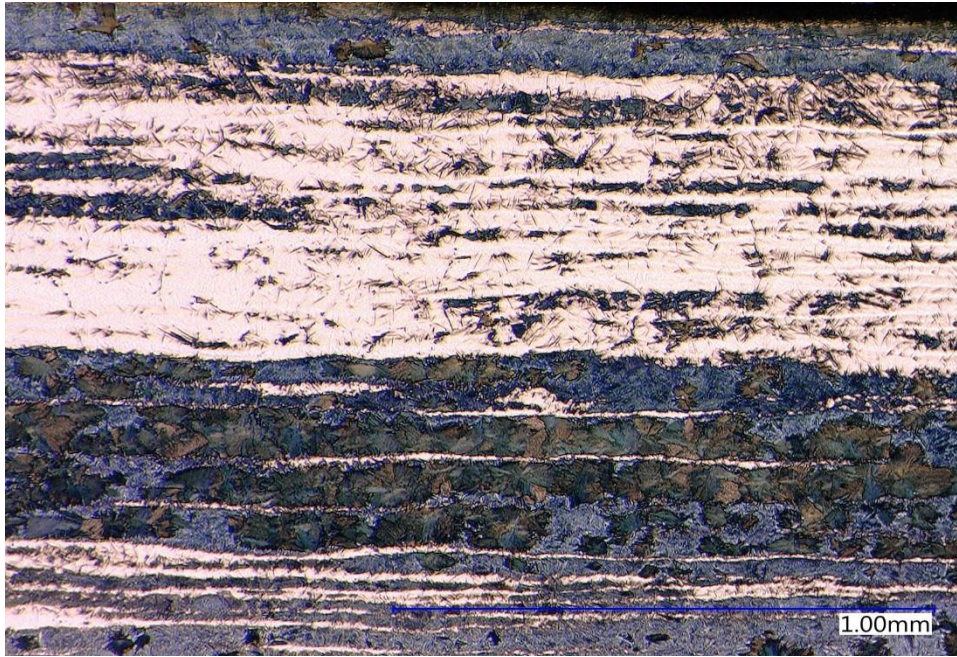


Figure 4-15. Microstructure of Experiment 1 having the highest banding intensity among the mild cooling experiments (200X, 4% Picral, 60 sec.)

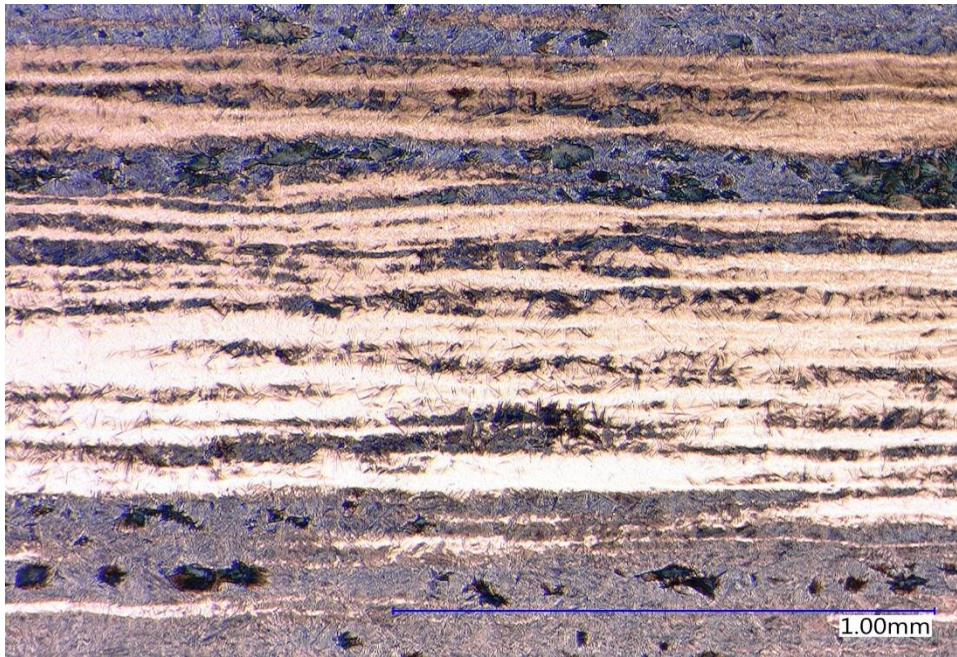


Figure 4-16. Microstructure of Experiment 2 having the lowest banding intensity among the mild cooling experiments (200X, 4% Picral, 60 sec.)



Figure 4-17. Microstructure of Experiment 10 having the highest banding intensity among the medium cooling experiments (200X, 4% Picral, 60 sec.)

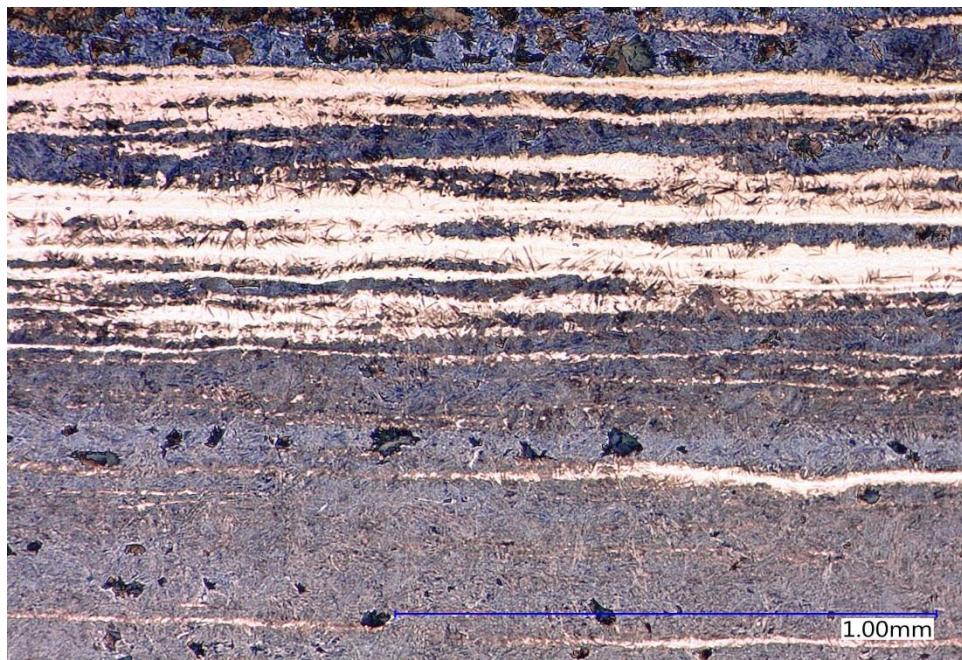


Figure 4-18. Microstructure of Experiment 8 having the lowest banding intensity among the medium cooling experiments (200X, 4% Picral, 60 sec.)

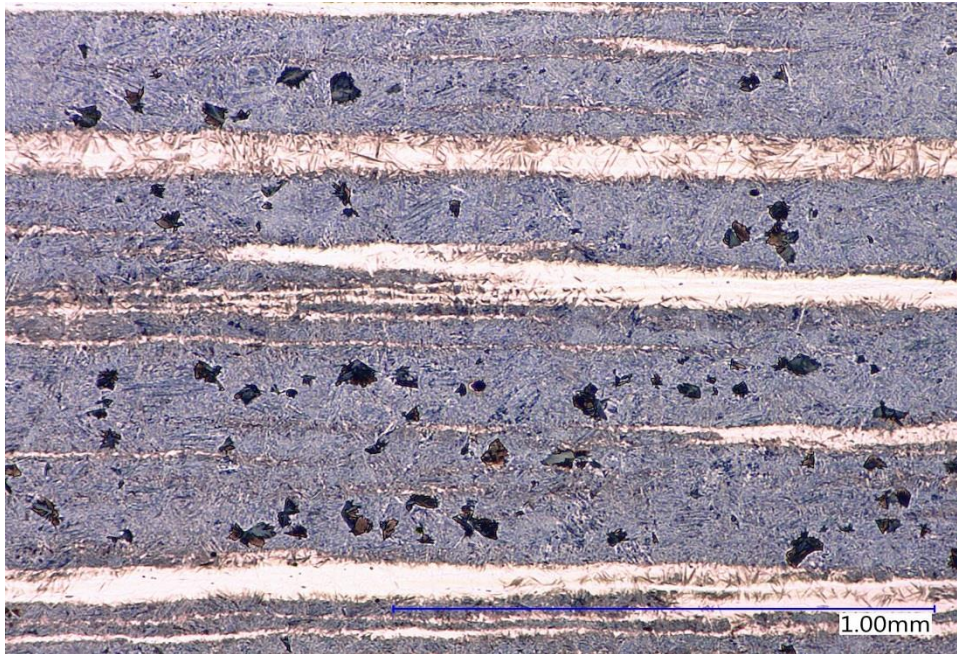


Figure 4-19. Microstructure of Experiment 13 having the highest banding intensity among the intense cooling experiments (200X, 4% Picral, 60 sec.)

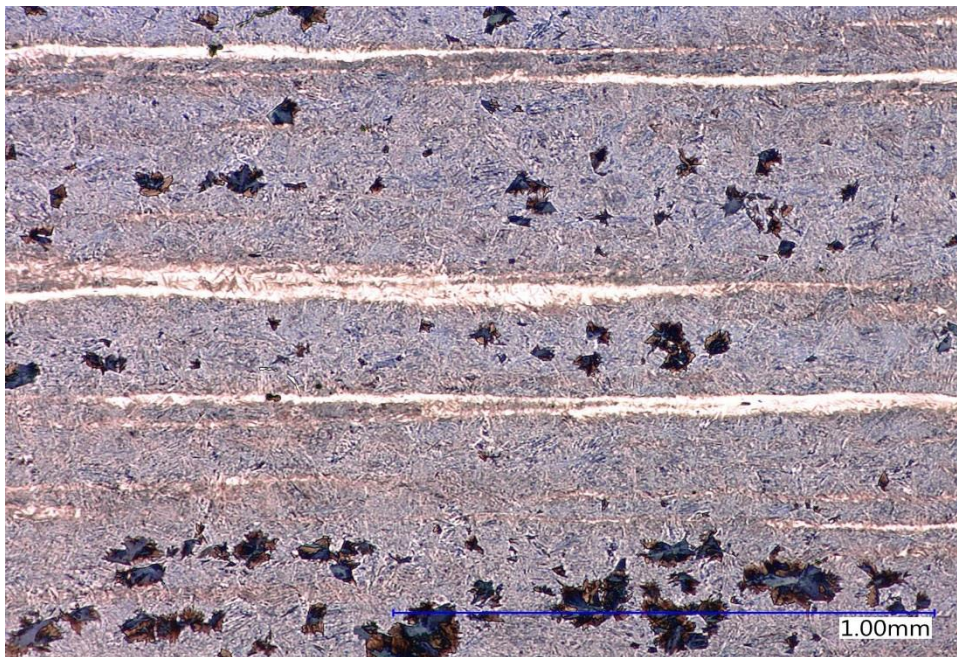


Figure 4-20. Microstructure of Experiment 14 having the lowest banding intensity among the intense cooling experiments (200X, 4% Picral, 60 sec.)

Figure 4.21 shows the area ratios of martensite bands are close to each other in the experiments produced with mild cooling and it is about 40%. However, the amounts of bainite bands are higher in Experiment 1 and Experiment 4 than other experiments. In terms of center carbon segregation indexes, the worst results also were belong to Experiment 1 and Experiment 4 in which F-EMS current is 350 A. Calculated center carbon segregation indexes also have shown that billets become more homogeneous as F-EMS current is increased from 350 A to 450 A. Therefore, it is expected that the products rolled from billets of experiments in which F-EMS current is 450 A have lower banding intensities. Nevertheless, the total banding intensities are minimum for Experiment 2 and Experiment 5 in which 400 A is used as F-EMS current. Although the area ratios of martensite bands of these experiments are not different from other experiments, the amount of banded bainite is very small in these two experiments.

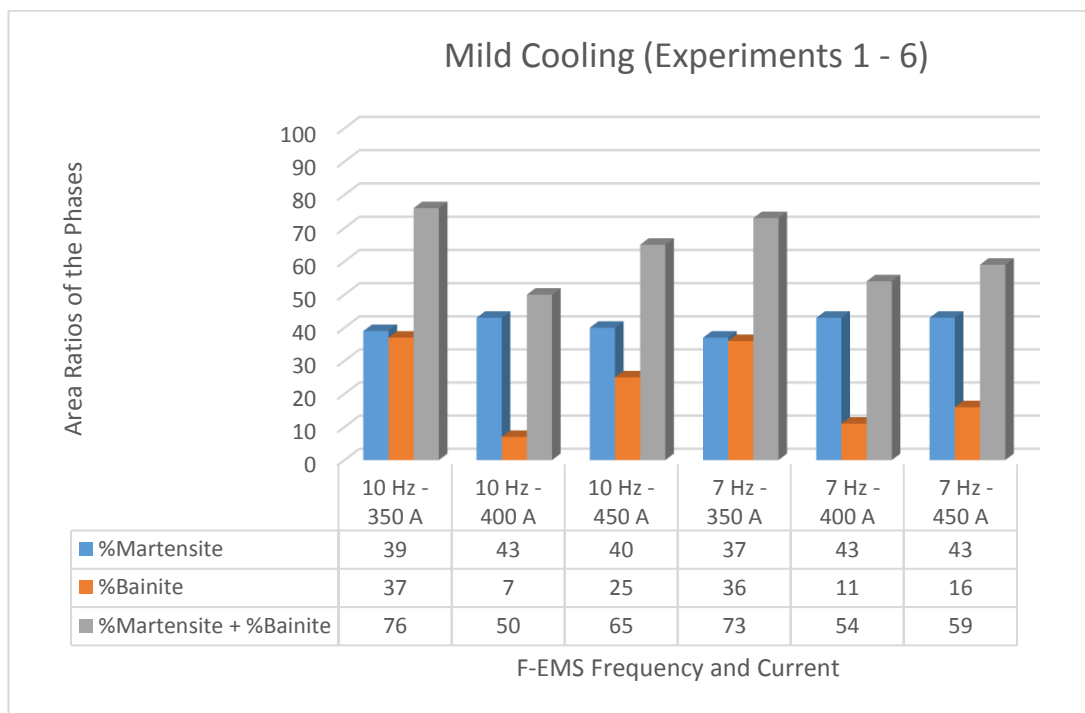


Figure 4-21. The area ratio of the phases for mild cooling experiments

In terms of the area ratio of the banded martensite phase, it is seen that the best results for medium cooling experiments belong to Experiment 9 and Experiment 12 in which F-EMS current is 450 A in Figure 4.22. However, if the bainite is also considered, it is seen that Experiment 8 and Experiment 11 have the lowest banding intensity since the banded bainite amounts are low in these experiments. Nevertheless, micro examinations show that martensite bands are the loosest in the microstructure of the sample taken from Experiment 9 among the experiments produced with the medium cooling regime. It should be noted that Experiment 9 has also the lowest center carbon segregation index in this group of experiments.

In addition to these, the effect of F-EMS frequency on the microstructural banding intensity is very little for both mild and medium cooling experiments.

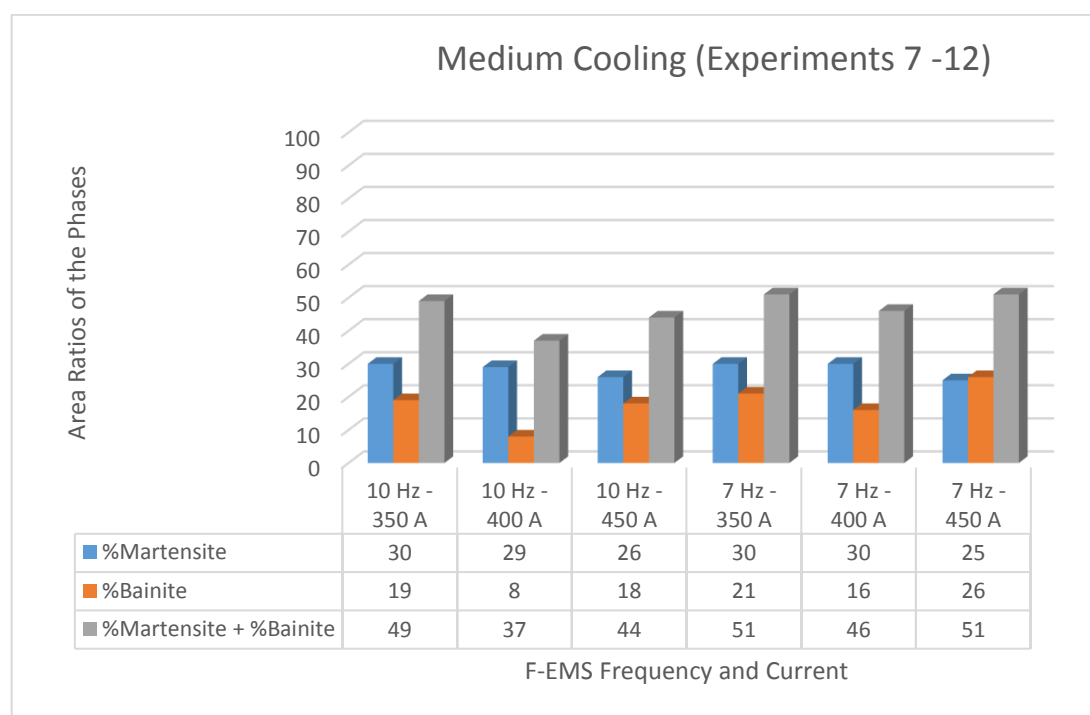


Figure 4-22. The area ratio of the phases for medium cooling experiments

In the previous part, carbon distributions showed that the efficiency of the F-EMS decreases when the intense cooling regime is used due to a high solid fraction in the strand. This finding was also supported by the amounts of banded phases in the samples taken from experiments produced with the intense cooling regime. As it can be seen in Figure 4.23, the amounts of banded phases are almost the same for all experiments in which intense cooling regime is used.

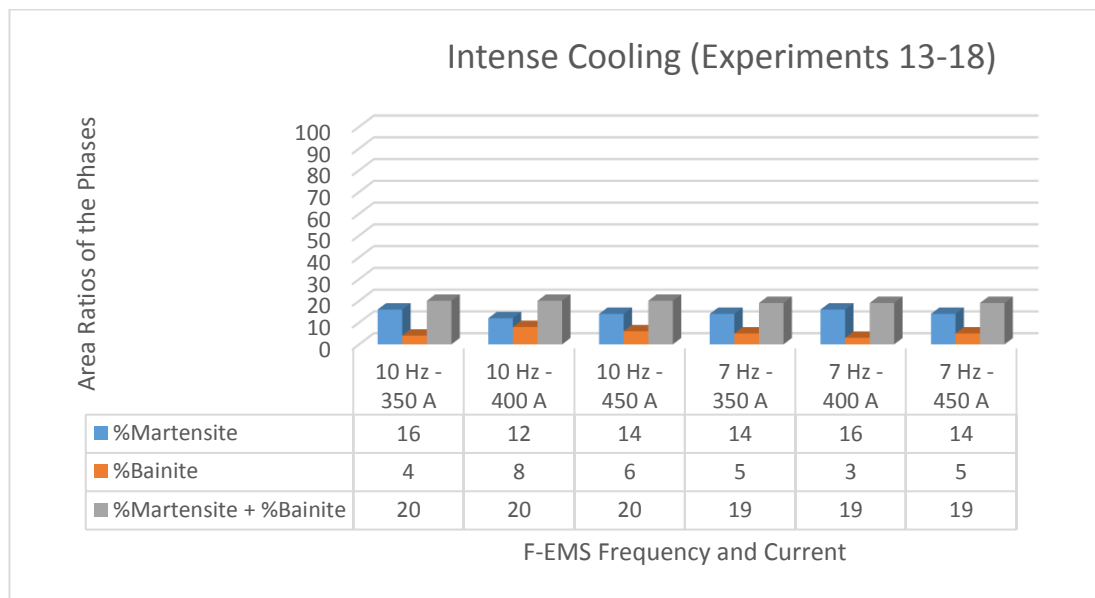


Figure 4-23. The area ratio of the phases for intense cooling experiments

Figure 4.24 shows the effect of rolling more homogeneous billets on the area ratio of the banded phases in the last products for experiments in which 350 – 400 – 450 A with 10 Hz are used as F-EMS parameters. It is seen that area ratios of both martensite and bainite bands decrease considerably for the experiments produced with the intense cooling regime. On the other hand, the experiments with the mild cooling regime have the highest amount of banded structure in parallel with the homogeneity of the billets. In addition to this, micro examinations also show that martensite and bainite bands are more compact in the experiments with the mild cooling. Although the samples of experiments with the medium cooling consist of a remarkable amount of banded

phases, band structures are more scattered for these comparing the samples of experiments with the mild cooling regime. According to the literature, the products which are hot rolled from more homogeneous billets have less banding intensity. Figure 4.24 also shows that the amounts of banded phases decrease as the center carbon segregation indexes decrease.

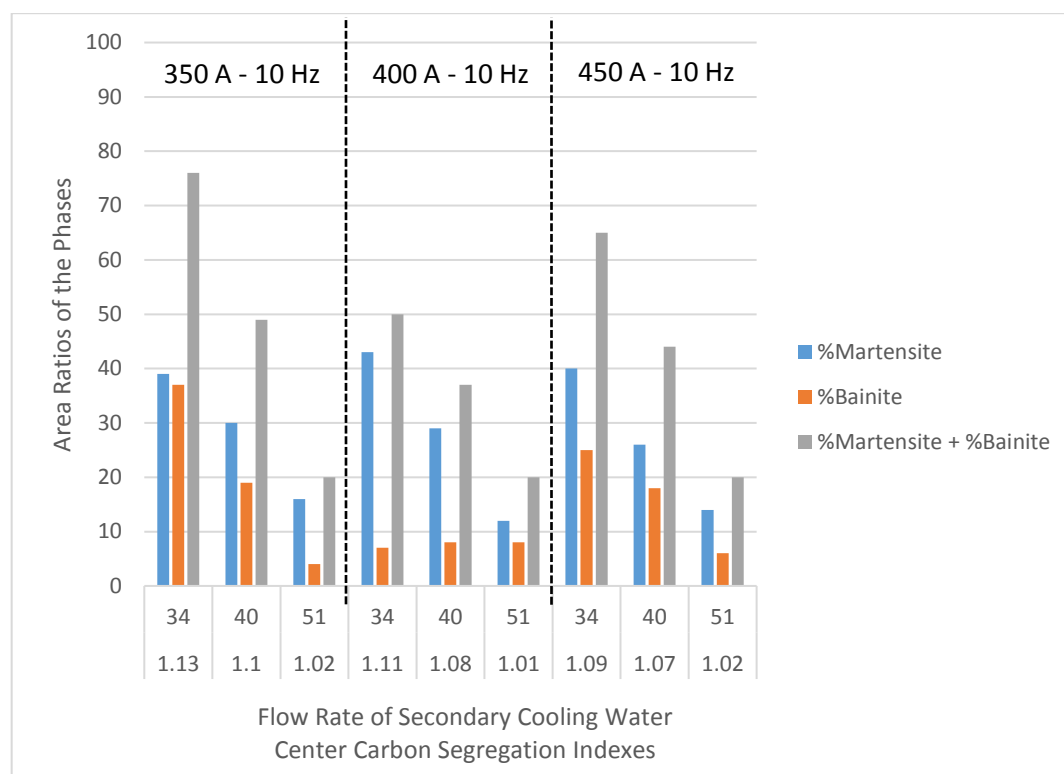


Figure 4-24. The effect of flow rate of secondary cooling water on microstructural banding intensity

4.5. Micro and Macro Hardness Measurements

Firstly, micro hardness measurements were done on the phases existing at the center of the samples taken from all experiments. These measurements showed that micro hardness values of the phases were similar for all different experiments although their amount varies. The micro hardness value of the martensite phase was between 750 HV (~62.1 HRC) and 850 HV (~65.6 HRC). In leaf spring manufacturing, bi-metal band saws and TiN coated drilling heads are used for cutting and hole-making

operations. These tools are suitable for use in materials having hardness up to 50 HRC according to product's catalogs. The micro hardness value of the banded martensite phase is higher than this value. Therefore, it can be said that banded martensite phase is detrimental for machinability of the leaf springs.

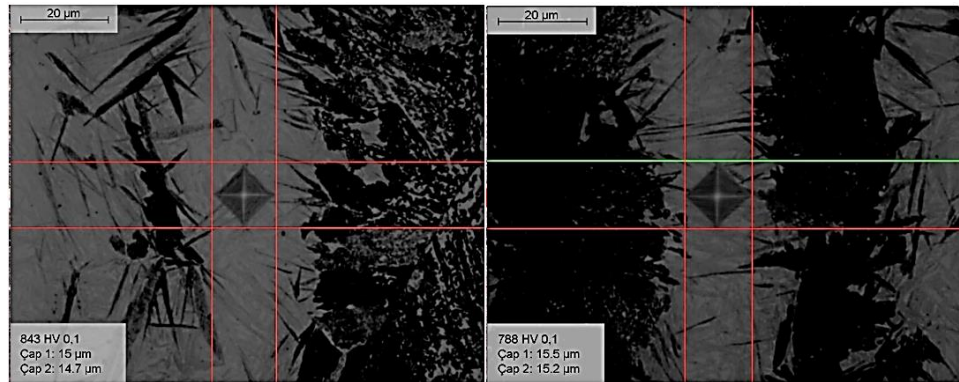


Figure 4-25. Micro hardness measurements on martensite bands (843 HV 0.1 and 788 HV 0.1)

In addition to this, micro hardness measurements carried out on the bainite and pearlite. According to these, the micro hardness of the bainite was between 450 HV (~43.3 HRC) and 500 HV (~49.1 HRC), which is also high for machining tools. However, on the pearlite micro hardness was measured between 350 HV (~35.5 HRC) and 400 HV (~40.8 HRC).

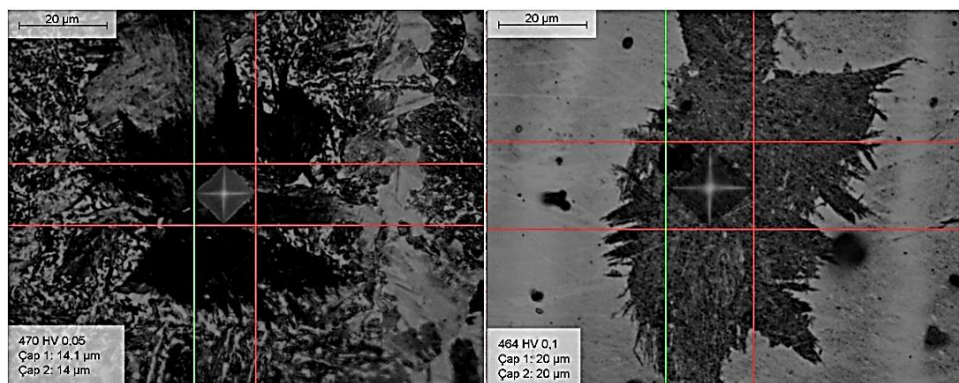


Figure 4-26. Micro hardness measurements on bainite (470 HV 0.05 and 464 HV 0.1)

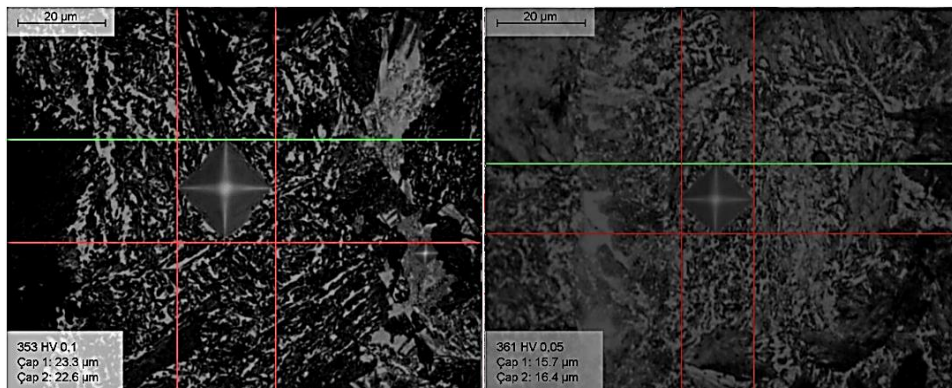


Figure 4-27. Micro hardness measurements on pearlite (353 HV 0.1 and 361 HV 0.05)

After micro hardness measurements, macro hardness measurements were carried out to clarify the effect of banding intensity on hardness distribution in the last products. The hardness values at the center of the samples were almost completely in parallel with the area ratio of the martensite phase. The average center hardness was 55.9 HRC in Experiment 6 which have the highest area ratio of the banded martensite phase. In Experiment 14 in which the area ratio of the banded martensite phase is only 12%, it was seen that the center hardness decreases to 39.8 HRC. Hardness measurements also showed that hardness values at 2 mm below the center are still proportional to the area ratio of the martensite phase. However, hardness values became stable in the range of 32 – 34 HRC beyond this point.

Table 4-5. Hardness values (in HRC) at the center, 2 mm, 4 mm, 6 mm below the center

Experiment No.	%Martensite	Hardness Values (Average of 6 Measurements)			
		Center	2 mm below the center	4 mm below the center	6 mm below the center
1	39	55.6 ± 3.1	39.5 ± 3.5	32.8 ± 1.9	34.1 ± 1.8
2	43	55.2 ± 3.3	39.1 ± 3.4	34.2 ± 2.0	33.1 ± 2.3
3	40	54.5 ± 3.2	38.2 ± 3.7	32.8 ± 1.6	32.4 ± 1.9
4	37	55.2 ± 2.9	39.4 ± 3.7	33.7 ± 2.2	31.9 ± 1.6
5	40	55.1 ± 3.2	39.5 ± 3.4	32.5 ± 2.1	33.8 ± 1.7
6	43	55.9 ± 3.0	38.9 ± 3.5	33.2 ± 1.8	34.1 ± 1.8
7	30	48.1 ± 3.1	36.2 ± 3.3	34.1 ± 1.5	34.3 ± 2.2
8	29	46.9 ± 2.8	36.5 ± 3.2	33.9 ± 2.3	33.6 ± 1.9
9	26	46.4 ± 3.2	37.5 ± 3.4	33.5 ± 1.6	33.8 ± 1.6
10	30	48.5 ± 2.7	36.8 ± 3.7	32.9 ± 1.9	32.7 ± 1.7
11	30	47.7 ± 2.8	37.9 ± 3.9	33.4 ± 2.3	32.8 ± 1.8
12	25	47.1 ± 3.2	36.2 ± 3.8	33.7 ± 2.4	32.1 ± 2.0
13	16	40.5 ± 3.1	34.5 ± 3.3	34.1 ± 1.8	33.6 ± 2.0
14	12	39.8 ± 3.3	33.7 ± 3.5	33.7 ± 2.0	32.9 ± 1.8
15	14	41.2 ± 3.1	34.8 ± 3.8	32.8 ± 1.7	34.4 ± 1.6
16	14	41.4 ± 3.2	33.6 ± 3.2	33.9 ± 2.0	32.5 ± 1.8
17	16	40.8 ± 3.0	33.2 ± 3.6	33.6 ± 1.9	33.9 ± 2.1
18	14	40.9 ± 3.3	34.5 ± 3.3	32.5 ± 1.7	34.1 ± 1.9

4.6. The Effect of Banding Intensity on the Cutting and Drilling Operations

As a result of the microstructure examinations and hardness measurements, it was seen that best results belong to Experiment 14 in terms of microstructural banding. In order to reveal the effect of banding intensity on the capability of cold sawing and center hole-making of the products, 25 tons of plate products were produced with the same parameters used in Experiment 14 and with the parameters used in Experiment 8 which are used in normal production practice. Firstly, cutting surfaces of these materials after cold sawing were compared. In Figure 4.28, it is seen that the cutting surface of Experiment 14 is much smoother than that of Experiment 8.

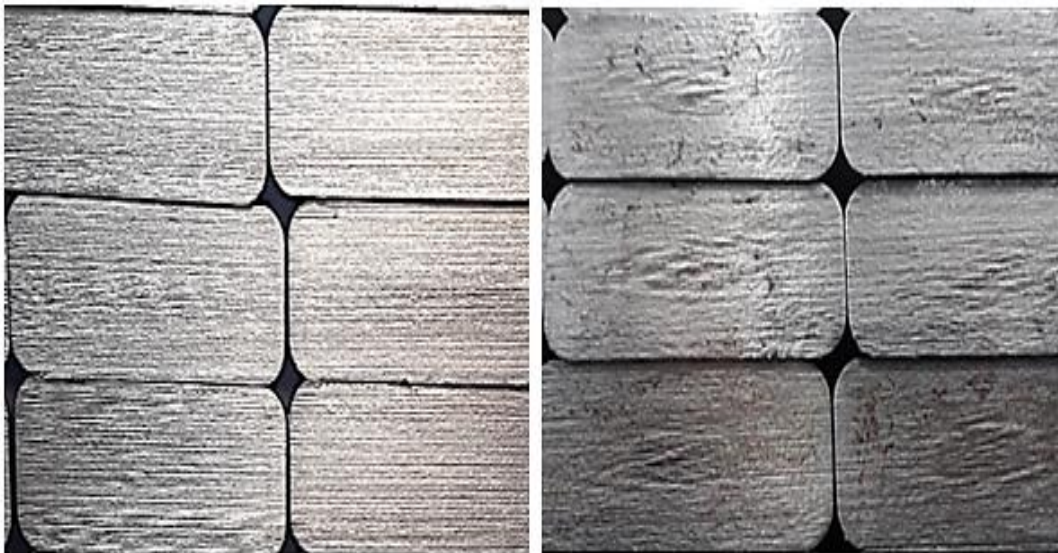


Figure 4-28. Comparison of cutting surfaces of the Experiment 14 (smooth) and Experiment 8 (uneven)

In addition, the consumption amounts of band saws and drilling heads during cutting and hole-making operations were recorded.

Table 4-6. Tool life in cutting and hole-making operations of Experiment 14 and Experiment 8

Experiment No.	Tool life	
	Band Saw (m ²)	Drilling Head (number of drillings)
14	0.90-1.20	55-65
8	0.21-0.35	30-40

Results showed that in cutting operation of plate products from Experiment 8, one band saw is capable of cutting 0.21-0.35 m² area. On the other hand, this value was increased by about 2.5 times for Experiment 14. In other words, one firsthand band saw could complete cutting operation of about 75 plate products from Experiment 8 whereas it could complete cutting operation of about 260 plate products from Experiment 14. It is also seen that the usage capacity of drilling heads used in center hole-making was doubled in Experiment 14.

CHAPTER 5

CONCLUSION

The main purpose of this thesis study is reducing of martensite band intensity in plate products of 52CrMoV4 steel which is produced as the raw material of leaf springs to increase the cutting and drilling performance of these products. Without any additional operation and cost, the main reason for microstructural banding, segregation of alloying elements during solidification, was tried to be removed by the optimization of some important CCM parameters. Consequently, the following major conclusions have been drawn;

- The characterization studies with etching by LePera solution showed that martensite-pearlite banding exists in 52CrMoV4 steel. There is also dispersed bainite in pearlite. These results also supported by JMatPro calculations by using chemical compositions of the different phases obtained by EDS analysis.
- The flow rate of the primary cooling water regarding conduction method is 2069 L/min by assuming that the heat transfer coefficient in the mould is 1700 W/m²K. According to SMS Concast program, the actual flow rate is between 2066 L/min and 2080 L/min. So, it was seen that the assumption of the heat transfer coefficient is correct. By this way, the thickness of solidified shell at the exit of the mould was also calculated as 23 mm. This was confirmed with considering position of the white band region due to M-EMS.
- Electro-magnetic stirring with higher currents and frequencies in the final region is an effective way to decrease segregation of alloying elements when mild and medium cooling is used as secondary cooling regime. However, the

efficiency of F-EMS is considerably decreased when secondary cooling intensity increased because of the liquid-solid ratio of the strand.

- Increase in the flow rate of secondary cooling water is much more effective than electro-magnetic stirring in reducing segregation of alloying elements. Although F-EMS efficiency is decreased in the intense cooling experiments, the center carbon segregation indexes are sharply decreased when the secondary cooling intensity is increased.
- Rolling more homogeneous billets is very beneficial to produce last products with less microstructural banding.
- In the products which were hot rolled from experimental castings produced with intense cooling, the area ratio of the banded phases is very low. On the other hand, the experiments with the mild cooling regime have the highest amount of banded phases. Although there is a remarkable amount of banded phases in samples taken from medium cooling experiments, martensite bands are more scattered in these experiments.
- Center hardness values are almost parallel with the area ratio of the banded martensite phase.
- In terms of microstructural banding intensity and center hardness, best results were obtained when the flow rate of secondary cooling water is 51 L/min, F-EMS current is 400 A and F-EMS frequency is 10 Hz. It was seen that the area ratio of the martensite phase is decreased to only 12% by using these CCM parameters. In parallel with this, center hardness is also decreased to 39.8 HRC.
- Comparing the products produced with parameters used in normal production practice, the tool life of band saw used in cutting operations was increased by about 2.5 times and tool life of drilling head used in hole-making operations was doubled when the area ratio of the martensite phase was minimized. By this way, it was provided that raw products of the leaf springs can be sawed

and drilled easier, which increases total production efficiency by reducing significantly production time and consumption of cutting and drilling tools.

CHAPTER 6

SUGGESTIONS FOR FUTURE WORK

- 1) The location of the F-EMS can be changed to increase the stirring efficiency. In addition, the clockwise – counterclockwise rotating mode of F-EMS can be tried instead of rotating in the same direction.
- 2) Other CCM parameters affecting segregation of alloying elements such as strand velocity, M-EMS and superheat can be changed to see their effects on microstructural banding.
- 3) The effect of microstructural banding intensity on the fatigue life of the leaf springs can be investigated because fatigue life is an important property for them.
- 4) The SDAS and equiaxed grain ratio in the billets can be measured.

REFERENCES

- [1] Verhoeven, J. 2000. A Review of Microsegregation Induced Banding Phenomena in Steels, Encyclopedia of Iron, Steel, and Their Alloys. Taylor and Francis: New York, 320-330, doi:10.1081/E-EISA-120052346.
- [2] Jäggle, E.A. 2007. Modelling of Microstructural Banding during Transformation in Steel (Master's Thesis), University of Cambridge.
- [3] Karagöz, Ş., Ünal, İ., Kahrıman, F., Demircan, F. G. 2009. Çeliklerde Segregasyon ve Etkileri, 5. Uluslararası İleri Teknolojiler Sempozyumu (IATS'09), Karabük, Türkiye.
- [4] Nagode, A., Resnik, A., Bizjak, M., Kosec, G., Karpe, B., Budak. I., Kosec, B., Zorc, B. 2016. Development of Banded Microstructure in 34CrNiMo6 Steel, Metallurgija, 55(3), 329-332.
- [5] Nagode, A., Resnik, A., Vertnik, R., Bizjak, M., Kosec, B., Gojic, M., Kosec, G., Sarler, B., Zorc, B. 2017. The development of a banded microstructure in S355J2 steel bar, Kovove Mater., 55, 51-56.
- [6] Hou, H., Huang, Y., Tian, Z., Chen, H., Liu, Y., An, Z. 2016. Microstructure evolution of spring steel 52CrMoV4 during continuous cooling transformation
- [7] Bor, A. Ş. 1991. Effect of Pearlite Banding on Mechanical Properties of Hot-rolled Steel Plates, ISIJ International, 31(12), 1445-1446.
- [8] Caballero, F. G., Garcia-Junceda, A., Capdevila, C., Garci de Andres, C. 2006. Evolution of Microstructural Banding during the Manufacturing Process of Dual Phase Steels, Materials Transactions, 47(9), 2269-2276.

- [9] Offerman, S. E., van Dijk, N. H., Rekveldt, M. Th., Sietsma, J., van der Zwaag, S. 2002. Ferrite/pearlite band formation in hot rolled medium carbon steel, *Materials Science and Technology*, 18, 297-303.
- [10] Yetkin, S. 2014. Elimination of Pearlite-Ferrite Band Using Soft Reduction during Continuous Casting of HSLA Steel (Master's Thesis), Middle East Technical University.
- [11] Garcia Nieto, P. J., Gonzalez Suarez, V. M., Alvarez Anton, J. C., Bayon, R. M., Sirgo Blanco, J. A., Diaz Fernandez, J. C. 2015. A New Predictive Model of Centerline Segregation in Continuous Steel Slabs by Using Multivariate Adaptive Regression Splines Approach, *Materials*, 8, 3562-3583, doi:10.3390/ma8063562.
- [12] Balas, M. M., 2010, Internal Model Expert control for slow cooling rate bronze casting, ResearchGate, doi:10.1109/SOFA.2010.5565590.
- [13] Raj, M. And Pandey, J. C. 2006. Evaluation of the Effect of Electro-Magnetic Stirring on Soundness of Continuously Cast Billets Using Ultrasonic Technique, Proc. National Seminar on Non-Destructive Evaluation.
- [14] Choudhary, S. K. And Ganguly, S. 2007. Morphology and Segregation in Continuously Cast High Carbon Steel Billets, *ISIJ International*, 47(12), 1759-1766.
- [15] Ghosh, A. 2001. Segregation in cast products, *Sādhanā*, 26(1), 5-24.
- [16] Zeng, J. And Chen, W. 2015. 'Effect of Secondary Cooling Conditions on Solidification Structure and Central Macrosegregation in Continuously Cast High-Carbon Rectangular Billet, *High Temp. Mater. Proc.*, 34, 577-583.
- [17] Askeland, D. R., Fulay, P. P., Wright, W. J. 2012. *The Science and Engineering of Materials*, Sixth Edition, CL Engineering, 401 p.

- [18] Askeland, D. R. And Wright, W. J. 2014. Essentials of Materials of Science and Engineering, Third Edition, Global Engineering, 294 p.
- [19] Gao, X., Yang, S., Li, J. 2016. Effects of micro-alloying elements and continuous casting parameters on reducing segregation in continuously cast slab, *Materials and Design*, 110, 284-295, doi:10.1016/j.matdes.2016.08.005
- [20] Foundry Section Metals Processing Division. 1961. Investigation of Solidification of High Strength Steel Casting, Technical Report WAL TR 311(49), Massachusetts Institute of Technology, 23 p.
- [21] Sengupta, J., Thomas, B. G., Wells, M. A. 2004. Understanding the Role Water-cooling Plays during Continuous Casting of Steel and Aluminum Alloys, MS&T Conference Proceedings, 179-193.
- [22] Thomas, B. G. 2001. Chapter 15: Continuous Casting of Steel, *Modeling for Casting and Solidification Processing*, New York: Marcel Dekker, 499-540.
- [23] W. Wang, M. Zhu, Z. Cai, S. Luo, C. Ji. 2012. Micro-Segregation Behavior of Solute Elements in the Mushy Zone of Continuous Casting Wide-Thick Slab, *steel research int.*, 83(12), 1152-1164, doi:10.1002/srin.201200102.
- [24] Jacobi, H. And Schwerdtfeger, K. 1975. Dendrite Morphology of Steady State Unidirectionally Solidified Steel, *Metallurgical Transactions A*, 7, 811-820.
- [25] Chen, W. And Zeng, J. 2015. Effect of casting speed on solidification structure and central macrosegregation during continuous casting of high-carbon rectangular billet, *La Metallurgia Italiana*, 7, 51-58.
- [26] Ludlow, V., Normanton, A., Anderson, A., Thiel, M., Ciriza, J., van der Knoop, W. 2005. Strategy to minimise central segregation in high carbon steel grades during billet casting, *Ironmaking & Steelmaking*, 32(1), 68-74, doi:10.1179/174328105X23978.

- [27] Henderson, S., Scholes, A., Clarke, B. D. 1991. Continuous casting of high-carbon steels in billet and bloom sections at sub-liquidus temperatures, Final report, Commission of the European Communities, 20-21 p.
- [28] K. Kim, T.Yeo, K.H. Oh, D.N.Lee, “Effect of Carbon and Sulfur in continuously cast strand on longitudinal surface cracks”, 1996, ISIJ International Volume 36: pp. 284-289.
- [29] Mazumdar, S. And Ray, S. K. 2001. Solidification control in continuous casting of steel, *Sādhanā*, 26(1), 179-198.
- [30] Morales-Higa, K. 2014. Physical and Mathematical Modelling in Billet Molds for Steel Quality Improvements, (PhD Thesis), Department of Mining and Materials Engineering, McGill University
- [31] Liao, Y. And Yao, Y. 2013. Applications Analysis of the Technology of Mold Electromagnetic Stirring in A Steel Mill, *Advanced Materials Research*, 721, 471-474, doi:10.4028/www.scientific.net/AMR.721.471
- [32] Deng, A. Y., Yin, X. Q., Yin, C. Q.i Wang, E. G. 2015. Effects of Electromagnetic Stirring on Cast Structure of High-Carbon High-Speed Steel. 8th International Conference on Electromagnetic Processing of Materials (EPM 2015), Cannes, France.
- [33] Bridge, M. R. And Rogers, G. D. 1984. Structural Effects and Band Segregate Formation during the Electromagnetic Stirring of Strand-Cast Steel, *Metallurgical Transactions B*, 158, 582-590.
- [34] Zhou, D., Fu, J., Wang, P. 2000. Carbon Segregation of Bearing Steel Concasting Billet, *J. Mater. Sci. Technol.* 16(3), 273-277.
- [35] Mizukami, H., Komatsu, M., Kitawaga, T., Kawakami, K. 1984. Effect of Electromagnetic Stirring at the Final Stage of Solidification of Continuously Cast Strand, *Transactions ISIJ*, 24, 923-931.

- [36] Reger, M., Vero, B., Jozsa, R. 2014. Control of Centerline Segregation in Slab Casting, *Acta Polytechnica Hungarica*, 11(4), 119-137.
- [37] Sengupta, J., Trinh, M., Currey, D., Thomas B. G. 2009. Utilization of CON1D at ArcelorMittal Dofasco's No. 2 Continuous Caster for Crater End Determination, *AISTech 2009 Steelmaking Conference Proc.*
- [38] Bode, O., Schwerdtfeger, K., Geck, H. G., Höfer, F. 2008. Influence of casting parameters on void volume and centre segregation in continuously cast 100Cr6 blooms, *Ironmaking & Steelmaking*, 35(2), 137-145, doi: 10.1179/030192307X233511.
- [39] Beguinot, J., Falce, J., Martinon, P. 1980. Microsegregation of alloying elements in structural steel plates, Final Report, Commission of the European Communities, 15 p.
- [40] Jaczak, C.F., Girardi, D. J., Rowland, E. S. 1956. On banding in steel, *Transactions of the ASM*, 48, 279-305.
- [41] Reger, M., Vero, B., Felde, I., Kardos, I. 2010. The Effect of Heat Treatment on the Stability of Centerline Segregation, *Strojniški vestnik - Journal of Mechanical Engineering* 56(2), 143-149.
- [42] Hairer, F., Karellova, A., Kremaszky, C., Werner, E., Hebesberger, T., Pichler A. 2008. Etching Techniques for the Microstructural Characterization of Complex Phase Steels by Light Microscopy Retrieved from: <http://www.mtf.stuba.sk/docs>
- [43] Vander Voort, G. F. 1999. *Metallography Principles and Practice*, ASM International, 637 p.
- [44] Poirier, D. R. and Geiger, G. H. 1994. *Transport Phenomena in Materials Processing*, Warrendale, Pa: Minerals, Metals & Materials Society, 352-355.

APPENDICES

A. SMS Concast Mould Flow Graph



Figure A-1. Actual flow rate of mould cooling water

B. Calculations of Center Carbon Segregation Indexes

Table B-1. Carbon distribution through vertical and horizontal centerline for Experiment 1

Position	0.5-1.5 cm	1.5-3 cm	3-4.5 cm	4.5-6 cm	6-7.5 cm	7.5-9 cm	9-10.5 cm	10.5-12 cm	12-13.5 cm	13.5-15 cm	15-16.5 cm	16.5-18 cm	18-19.5 cm
Vertical centerline	0.56	0.53	0.58	0.58	0.46	0.60	0.65	0.61	0.48	0.57	0.58	0.54	0.57
Horizontal centerline	0.56	0.54	0.58	0.58	0.47	0.62	0.65	0.61	0.45	0.59	0.58	0.54	0.57
Average	0.56	0.54	0.58	0.58	0.47	0.61	0.65	0.61	0.47	0.58	0.58	0.54	0.56

$$\text{Center carbon segregation index} = \frac{0.61 + 0.65 + 0.61}{3} = 1.13$$

Table B-2. Carbon distribution through vertical and horizontal centerline for Experiment 2

Position	0.5-1.5 cm	1.5-3 cm	3-4.5 cm	4.5-6 cm	6-7.5 cm	7.5-9 cm	9-10.5 cm	10.5-12 cm	12-13.5 cm	13.5-15 cm	15-16.5 cm	16.5-18 cm	18-19.5 cm
Vertical centerline	0.56	0.53	0.56	0.56	0.47	0.61	0.62	0.59	0.48	0.57	0.56	0.53	0.55
Horizontal centerline	0.55	0.53	0.56	0.55	0.48	0.60	0.62	0.61	0.46	0.56	0.56	0.53	0.55
Average	0.56	0.53	0.56	0.56	0.48	0.61	0.62	0.60	0.47	0.57	0.56	0.53	0.55

$$\text{Center carbon segregation index} = \frac{0.61 + 0.62 + 0.60}{3} = 1.11$$

Table B-3. Carbon distribution through vertical and horizontal centerline for Experiment 3

Position	0.5-1.5 cm	1.5-3 cm	3-4.5 cm	4.5-6 cm	6-7.5 cm	7.5-9 cm	9-10.5 cm	10.5-12 cm	12-13.5 cm	13.5-15 cm	15-16.5 cm	16.5-18 cm	18-19.5 cm
Vertical centerline	0.56	0.53	0.57	0.57	0.51	0.59	0.60	0.57	0.49	0.57	0.57	0.53	0.54
Horizontal centerline	0.54	0.53	0.58	0.53	0.49	0.59	0.60	0.58	0.45	0.53	0.57	0.54	0.55
Average	0.55	0.53	0.58	0.55	0.50	0.59	0.60	0.58	0.47	0.55	0.57	0.54	0.55

$$\text{Center carbon segregation index} = \frac{0.59 + 0.60 + 0.58}{3} = 1.09$$

Table B-4. Carbon distribution through vertical and horizontal centerline for Experiment 4

Position	0.5-1.5 cm	1.5-3 cm	3-4.5 cm	4.5-6 cm	6-7.5 cm	7.5-9 cm	9-10.5 cm	10.5-12 cm	12-13.5 cm	13.5-15 cm	15-16.5 cm	16.5-18 cm	18-19.5 cm
Vertical centerline	0.54	0.51	0.55	0.55	0.50	0.60	0.64	0.60	0.47	0.53	0.55	0.51	0.54
Horizontal centerline	0.53	0.51	0.55	0.54	0.50	0.59	0.64	0.60	0.51	0.53	0.55	0.50	0.54
Average	0.54	0.51	0.55	0.55	0.50	0.60	0.64	0.60	0.49	0.53	0.55	0.51	0.54

$$\text{Center carbon segregation index} = \frac{0.60 + 0.64 + 0.60}{3} = 1.14$$

Table B-5. Carbon distribution through vertical and horizontal centerline for Experiment 5

Position	0.5-1.5 cm	1.5-3 cm	3-4.5 cm	4.5-6 cm	6-7.5 cm	7.5-9 cm	9-10.5 cm	10.5-12 cm	12-13.5 cm	13.5-15 cm	15-16.5 cm	16.5-18 cm	18-19.5 cm
Vertical centerline	0.56	0.53	0.57	0.57	0.48	0.58	0.63	0.62	0.48	0.57	0.56	0.54	0.56
Horizontal centerline	0.55	0.54	0.57	0.57	0.46	0.59	0.63	0.60	0.47	0.56	0.56	0.53	0.56
Average	0.56	0.54	0.57	0.57	0.47	0.59	0.63	0.61	0.48	0.57	0.56	0.54	0.56

$$\text{Center carbon segregation index} = \frac{\frac{0.59 + 0.63 + 0.61}{3}}{0.54} = 1.13$$

Table B-6. Carbon distribution through vertical and horizontal centerline for Experiment 6

Position	0.5-1.5 cm	1.5-3 cm	3-4.5 cm	4.5-6 cm	6-7.5 cm	7.5-9 cm	9-10.5 cm	10.5-12 cm	12-13.5 cm	13.5-15 cm	15-16.5 cm	16.5-18 cm	18-19.5 cm
Vertical centerline	0.55	0.52	0.56	0.57	0.49	0.59	0.61	0.58	0.46	0.56	0.56	0.53	0.56
Horizontal centerline	0.55	0.52	0.56	0.54	0.47	0.61	0.61	0.58	0.50	0.56	0.56	0.53	0.55
Average	0.55	0.52	0.56	0.56	0.48	0.60	0.61	0.58	0.48	0.56	0.56	0.53	0.56

$$\text{Center carbon segregation index} = \frac{\frac{0.60 + 0.61 + 0.58}{3}}{0.54} = 1.10$$

Table B-7. Carbon distribution through vertical and horizontal centerline for Experiment 7

Position	0.5-1.5 cm	1.5-3 cm	3-4.5 cm	4.5-6 cm	6-7.5 cm	7.5-9 cm	9-10.5 cm	10.5-12 cm	12-13.5 cm	13.5-15 cm	15-16.5 cm	16.5-18 cm	18-19.5 cm
Vertical centerline	0.55	0.52	0.56	0.57	0.49	0.60	0.60	0.59	0.49	0.57	0.56	0.53	0.55
Horizontal centerline	0.55	0.52	0.56	0.54	0.49	0.58	0.60	0.58	0.48	0.56	0.56	0.52	0.56
Average	0.55	0.52	0.56	0.56	0.49	0.59	0.60	0.59	0.49	0.57	0.56	0.53	0.56

$$\text{Center carbon segregation index} = \frac{0.59 + 0.60 + 0.59}{3} = 1.10$$

Table B-8. Carbon distribution through vertical and horizontal centerline for Experiment 8

Position	0.5-1.5 cm	1.5-3 cm	3-4.5 cm	4.5-6 cm	6-7.5 cm	7.5-9 cm	9-10.5 cm	10.5-12 cm	12-13.5 cm	13.5-15 cm	15-16.5 cm	16.5-18 cm	18-19.5 cm
Vertical centerline	0.55	0.52	0.56	0.56	0.49	0.58	0.59	0.58	0.50	0.58	0.57	0.53	0.56
Horizontal centerline	0.55	0.53	0.56	0.56	0.49	0.58	0.59	0.58	0.50	0.55	0.56	0.52	0.55
Average	0.55	0.53	0.56	0.56	0.49	0.58	0.59	0.58	0.50	0.57	0.57	0.53	0.55

$$\text{Center carbon segregation index} = \frac{0.58 + 0.59 + 0.58}{3} = 1.08$$

Table B-9. Carbon distribution through vertical and horizontal centerline for Experiment 9

Position	0.5-1.5 cm	1.5-3 cm	3-4.5 cm	4.5-6 cm	6-7.5 cm	7.5-9 cm	9-10.5 cm	10.5-12 cm	12-13.5 cm	13.5-15 cm	15-16.5 cm	16.5-18 cm	18-19.5 cm
Vertical centerline	0.55	0.51	0.57	0.57	0.48	0.57	0.59	0.59	0.46	0.57	0.56	0.52	0.55
Horizontal centerline	0.55	0.53	0.56	0.57	0.46	0.58	0.59	0.58	0.48	0.6	0.56	0.51	0.56
Average	0.55	0.52	0.57	0.57	0.47	0.58	0.59	0.59	0.47	0.57	0.56	0.52	0.56

$$\text{Center carbon segregation index} = \frac{0.58 + 0.59 + 0.59}{3} = 1.07$$

Table B-10. Carbon distribution through vertical and horizontal centerline for Experiment 10

Position	0.5-1.5 cm	1.5-3 cm	3-4.5 cm	4.5-6 cm	6-7.5 cm	7.5-9 cm	9-10.5 cm	10.5-12 cm	12-13.5 cm	13.5-15 cm	15-16.5 cm	16.5-18 cm	18-19.5 cm
Vertical centerline	0.55	0.52	0.56	0.56	0.46	0.59	0.61	0.60	0.48	0.57	0.56	0.51	0.55
Horizontal centerline	0.54	0.51	0.55	0.56	0.50	0.60	0.61	0.58	0.47	0.55	0.55	0.52	0.55
Average	0.55	0.52	0.56	0.56	0.48	0.60	0.61	0.59	0.48	0.56	0.56	0.52	0.55

$$\text{Center carbon segregation index} = \frac{0.60 + 0.61 + 0.59}{3} = 1.11$$

Table B-11. Carbon distribution through vertical and horizontal centerline for Experiment 11

Position	0.5-1.5 cm	1.5-3 cm	3-4.5 cm	4.5-6 cm	6-7.5 cm	7.5-9 cm	9-10.5 cm	10.5-12 cm	12-13.5 cm	13.5-15 cm	15-16.5 cm	16.5-18 cm	18-19.5 cm
Vertical centerline	0.56	0.53	0.57	0.58	0.46	0.59	0.60	0.59	0.48	0.56	0.57	0.53	0.56
Horizontal centerline	0.54	0.53	0.57	0.57	0.47	0.60	0.60	0.59	0.47	0.57	0.56	0.53	0.56
Average	0.55	0.53	0.57	0.58	0.47	0.60	0.60	0.59	0.48	0.57	0.57	0.53	0.56

$$\text{Center carbon segregation index} = \frac{0.60 + 0.60 + 0.59}{3} = 1.10$$

Table B-12. Carbon distribution through vertical and horizontal centerline for Experiment 12

Position	0.5-1.5 cm	1.5-3 cm	3-4.5 cm	4.5-6 cm	6-7.5 cm	7.5-9 cm	9-10.5 cm	10.5-12 cm	12-13.5 cm	13.5-15 cm	15-16.5 cm	16.5-18 cm	18-19.5 cm
Vertical centerline	0.55	0.51	0.54	0.56	0.47	0.60	0.60	0.58	0.49	0.56	0.56	0.52	0.55
Horizontal centerline	0.54	0.51	0.56	0.55	0.47	0.58	0.60	0.58	0.47	0.56	0.57	0.51	0.54
Average	0.55	0.51	0.55	0.56	0.47	0.59	0.60	0.58	0.47	0.56	0.57	0.52	0.55

$$\text{Center carbon segregation index} = \frac{0.59 + 0.60 + 0.58}{3} = 1.09$$

Table B-13. Carbon distribution through vertical and horizontal centerline for Experiment 13

Position	0.5-1.5 cm	1.5-3 cm	3-4.5 cm	4.5-6 cm	6-7.5 cm	7.5-9 cm	9-10.5 cm	10.5-12 cm	12-13.5 cm	13.5-15 cm	15-16.5 cm	16.5-18 cm	18-19.5 cm
Vertical centerline	0.54	0.52	0.56	0.55	0.55	0.56	0.57	0.57	0.55	0.54	0.55	0.51	0.54
Horizontal centerline	0.55	0.52	0.56	0.57	0.54	0.55	0.57	0.54	0.55	0.55	0.55	0.52	0.55
Average	0.55	0.52	0.56	0.56	0.55	0.56	0.57	0.56	0.55	0.55	0.55	0.52	0.55

$$\text{Center carbon segregation index} = \frac{0.56 + 0.57 + 0.56}{3} = 1.02$$

Table B-14. Carbon distribution through vertical and horizontal centerline for Experiment 14

Position	0.5-1.5 cm	1.5-3 cm	3-4.5 cm	4.5-6 cm	6-7.5 cm	7.5-9 cm	9-10.5 cm	10.5-12 cm	12-13.5 cm	13.5-15 cm	15-16.5 cm	16.5-18 cm	18-19.5 cm
Vertical centerline	0.55	0.51	0.53	0.56	0.54	0.55	0.56	0.53	0.53	0.57	0.57	0.52	0.55
Horizontal centerline	0.56	0.52	0.56	0.57	0.54	0.56	0.56	0.57	0.53	0.56	0.56	0.52	0.55
Average	0.56	0.52	0.55	0.57	0.54	0.56	0.56	0.55	0.53	0.57	0.57	0.52	0.55

$$\text{Center carbon segregation index} = \frac{0.56 + 0.56 + 0.55}{3} = 1.01$$

Table B-15. Carbon distribution through vertical and horizontal centerline for Experiment 15

Position	0.5-1.5 cm	1.5-3 cm	3-4.5 cm	4.5-6 cm	6-7.5 cm	7.5-9 cm	9-10.5 cm	10.5-12 cm	12-13.5 cm	13.5-15 cm	15-16.5 cm	16.5-18 cm	18-19.5 cm
Vertical centerline	0.55	0.53	0.56	0.56	0.54	0.56	0.57	0.56	0.52	0.57	0.56	0.52	0.56
Horizontal centerline	0.56	0.52	0.57	0.55	0.55	0.55	0.57	0.55	0.53	0.57	0.57	0.53	0.56
Average	0.56	0.53	0.57	0.56	0.55	0.56	0.57	0.56	0.53	0.57	0.57	0.53	0.56

$$\text{Center carbon segregation index} = \frac{0.56 + 0.57 + 0.56}{3} = 1.02$$

Table B-16. Carbon distribution through vertical and horizontal centerline for Experiment 16

Position	0.5-1.5 cm	1.5-3 cm	3-4.5 cm	4.5-6 cm	6-7.5 cm	7.5-9 cm	9-10.5 cm	10.5-12 cm	12-13.5 cm	13.5-15 cm	15-16.5 cm	16.5-18 cm	18-19.5 cm
Vertical centerline	0.54	0.51	0.54	0.56	0.53	0.55	0.56	0.55	0.51	0.56	0.55	0.51	0.54
Horizontal centerline	0.54	0.51	0.54	0.53	0.50	0.55	0.56	0.54	0.52	0.55	0.55	0.50	0.53
Average	0.54	0.51	0.54	0.55	0.52	0.55	0.56	0.55	0.52	0.56	0.55	0.51	0.54

$$\text{Center carbon segregation index} = \frac{0.55 + 0.56 + 0.55}{3} = 1.02$$

Table B-17. Carbon distribution through vertical and horizontal centerline for Experiment 17

Position	0.5-1.5 cm	1.5-3 cm	3-4.5 cm	4.5-6 cm	6-7.5 cm	7.5-9 cm	9-10.5 cm	10.5-12 cm	12-13.5 cm	13.5-15 cm	15-16.5 cm	16.5-18 cm	18-19.5 cm
Vertical centerline	0.56	0.53	0.57	0.57	0.54	0.56	0.56	0.54	0.55	0.57	0.57	0.53	0.56
Horizontal centerline	0.54	0.52	0.57	0.56	0.53	0.55	0.56	0.55	0.50	0.56	0.56	0.51	0.55
Average	0.55	0.53	0.57	0.57	0.54	0.56	0.56	0.55	0.53	0.57	0.57	0.52	0.56

$$\text{Center carbon segregation index} = \frac{0.56 + 0.56 + 0.55}{3} = 1.01$$

Table B-18. Carbon distribution through vertical and horizontal centerline for Experiment 18

Position	0.5-1.5 cm	1.5-3 cm	3-4.5 cm	4.5-6 cm	6-7.5 cm	7.5-9 cm	9-10.5 cm	10.5-12 cm	12-13.5 cm	13.5-15 cm	15-16.5 cm	16.5-18 cm	18-19.5 cm
Vertical centerline	0.54	0.52	0.55	0.56	0.54	0.54	0.56	0.57	0.52	0.56	0.55	0.52	0.54
Horizontal centerline	0.54	0.51	0.55	0.57	0.56	0.55	0.56	0.55	0.53	0.53	0.55	0.51	0.54
Average	0.54	0.52	0.55	0.57	0.55	0.55	0.56	0.56	0.53	0.55	0.55	0.52	0.54

$$\text{Center carbon segregation index} = \frac{0.55 + 0.56 + 0.56}{3} = 1.01$$

C. Microstructures and Area Ratio Analyses

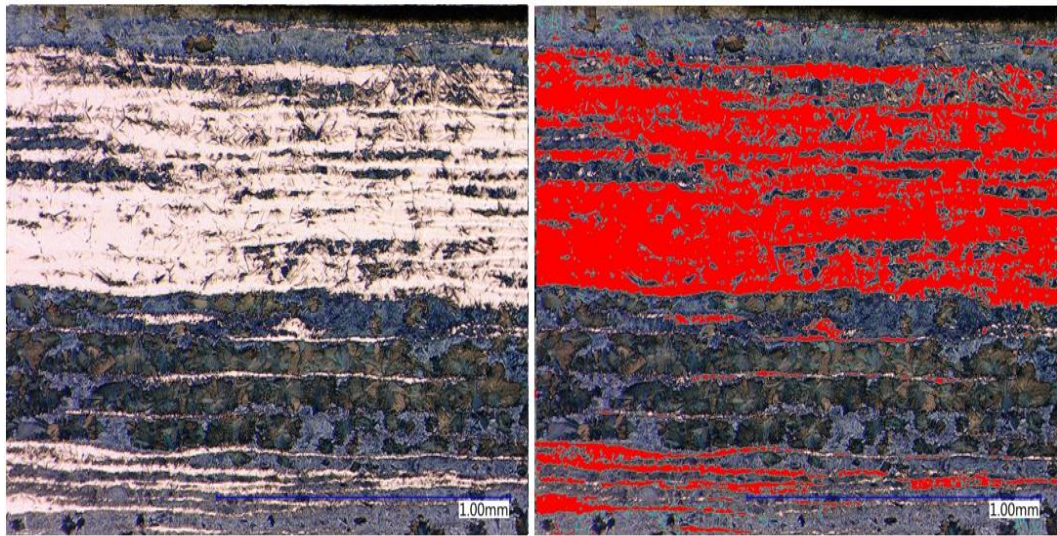


Figure C-1. Microstructure of Experiment 1 (200X, 4% Picral, 60 sec.) and area ratio analysis

Image analysis show that the area ratio of the martensite phase (red region) is 39% and bainite (black region) is 37%.

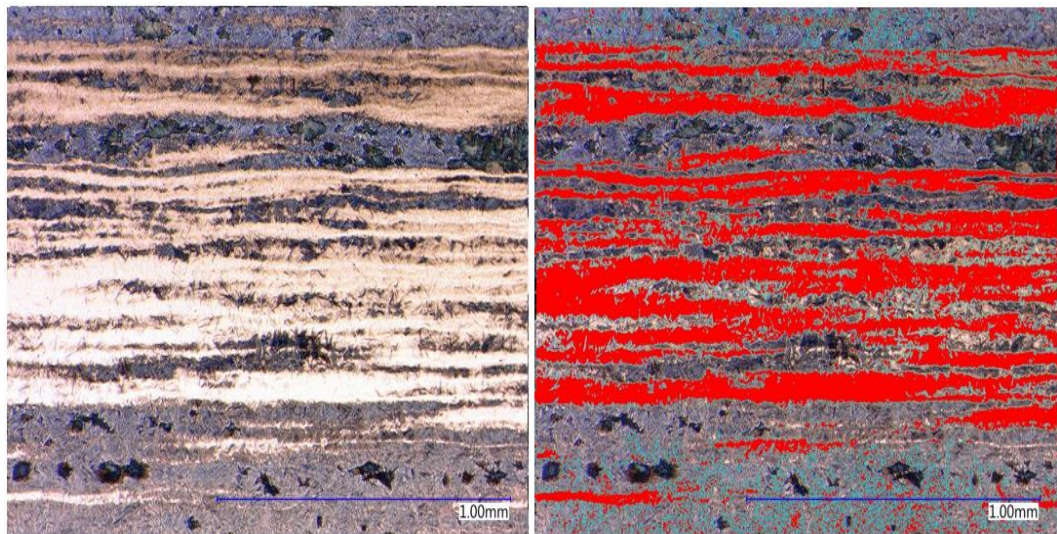


Figure C-2. Microstructure of Experiment 2 (200X, 4% Picral, 60 sec.) and area ratio analysis

Image analysis show that the area ratio of the martensite phase (red region) is 43% and bainite (black region) is 7%.

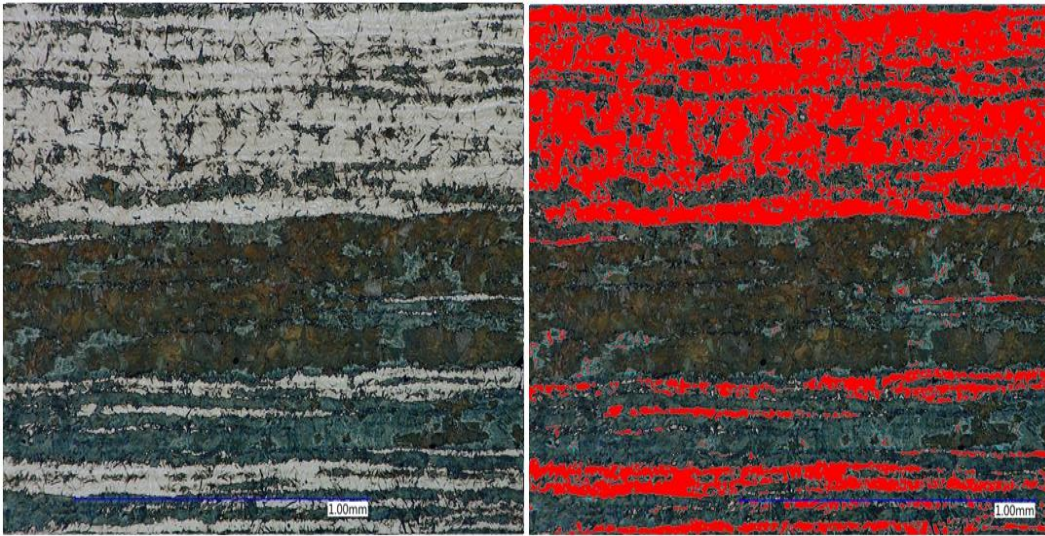


Figure C-3. Microstructure of Experiment 3 (200X, 4% Picral, 60 sec.) and area ratio analysis

Image analysis show that the area ratio of the martensite phase (red region) is 40% and bainite (black region) is 25%.

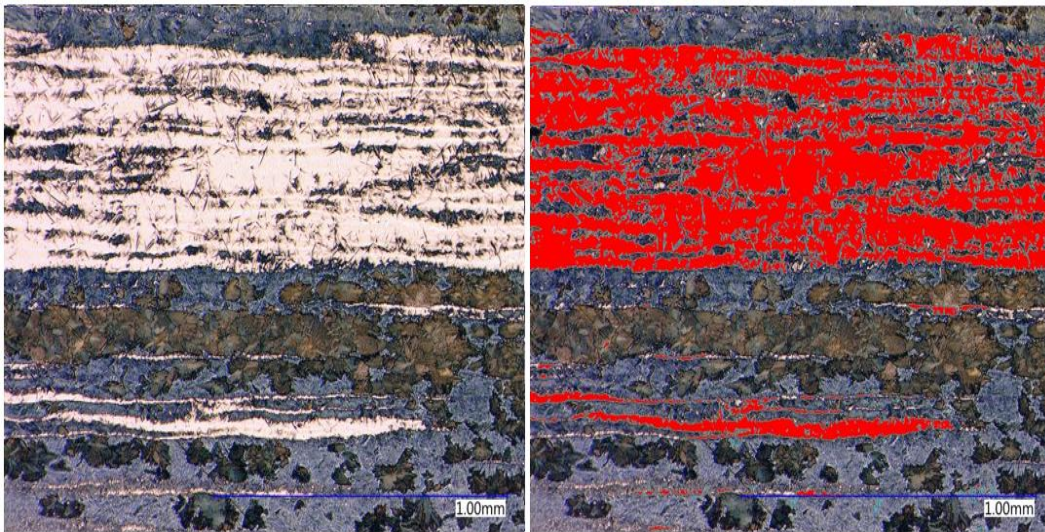


Figure C-4. Microstructure of Experiment 4 (200X, 4% Picral, 60 sec.) and area ratio analysis

Image analysis show that the area ratio of the martensite phase (red region) is 37% and bainite (black region) is 36%.

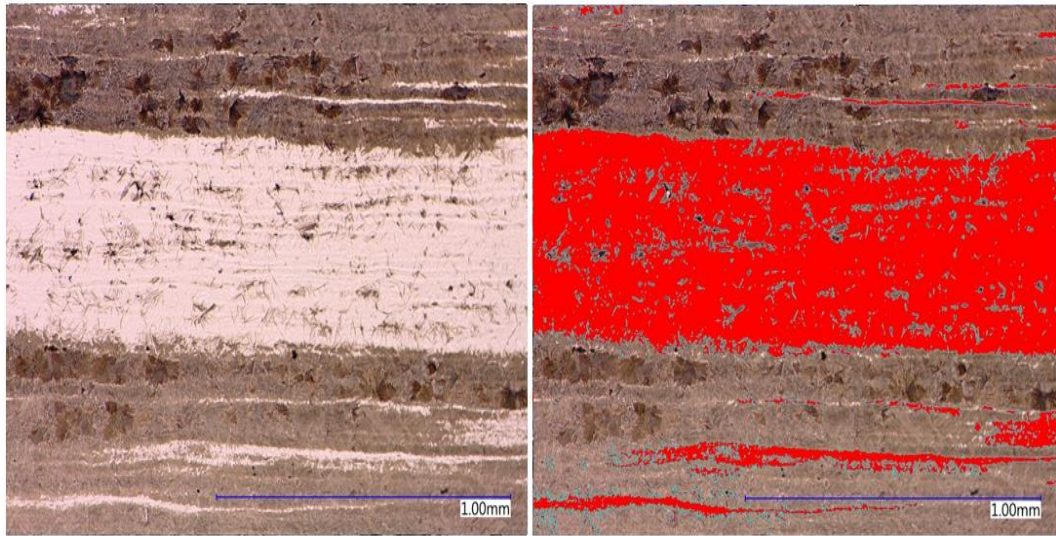


Figure C-5. Microstructure of Experiment 5 (200X, 4% Picral, 60 sec.) and area ratio analysis

Image analysis show that the area ratio of the martensite phase (red region) is 43% and bainite (black region) is 11%.

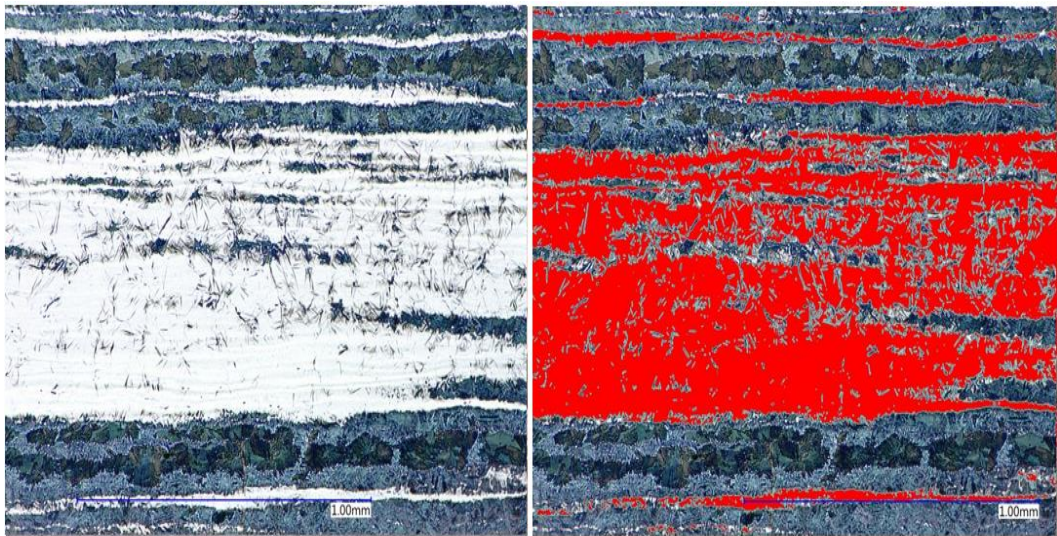


Figure C-6. Microstructure of Experiment 6 (200X, 4% Picral, 60 sec.) and area ratio analysis

Image analysis show that the area ratio of the martensite phase (red region) is 43% and bainite (black region) is 16%.

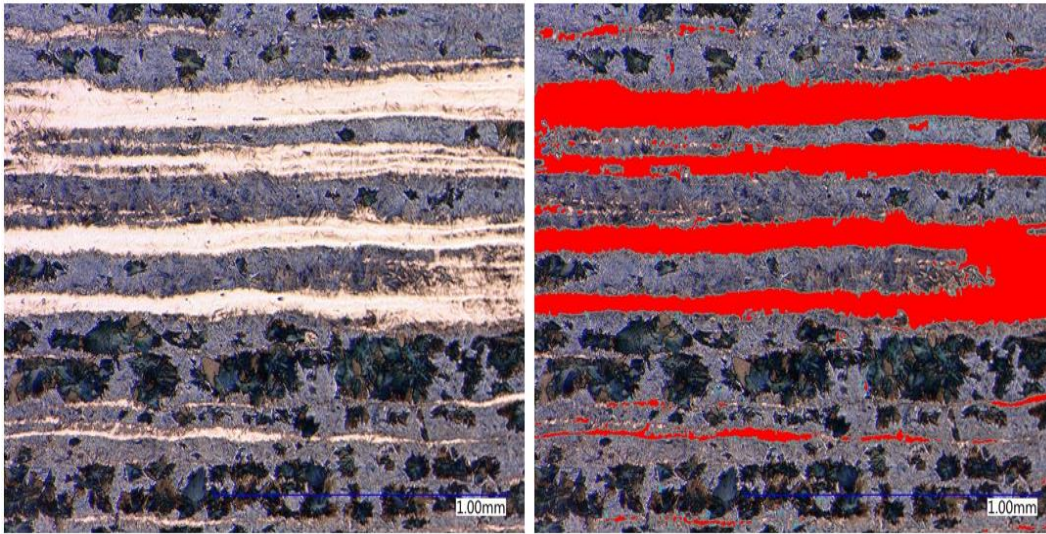


Figure C-7. Microstructure of Experiment 7 (200X, 4% Picral, 60 sec.) and area ratio analysis

Image analysis show that the area ratio of the martensite phase (red region) is 30% and bainite (black region) is 19%.

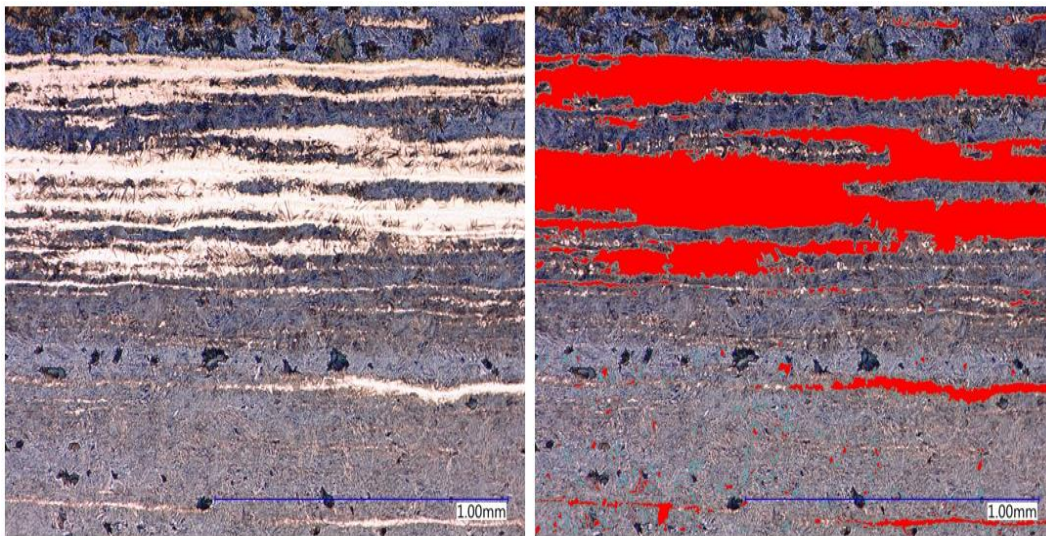


Figure C-8. Microstructure of Experiment 8 (200X, 4% Picral, 60 sec.) and area ratio analysis

Image analysis show that the area ratio of the martensite phase (red region) is 29% and bainite (black region) is 8%.

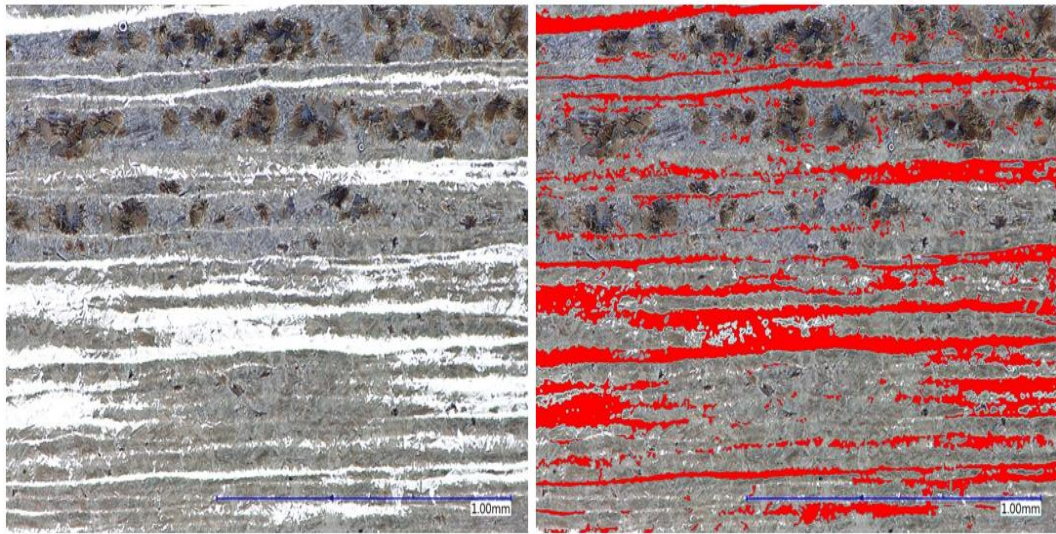


Figure C-9. Microstructure of Experiment 9 (200X, 4% Picral, 60 sec.) and area ratio analysis

Image analysis show that the area ratio of the martensite phase (red region) is 26% and bainite (black region) is 18%.

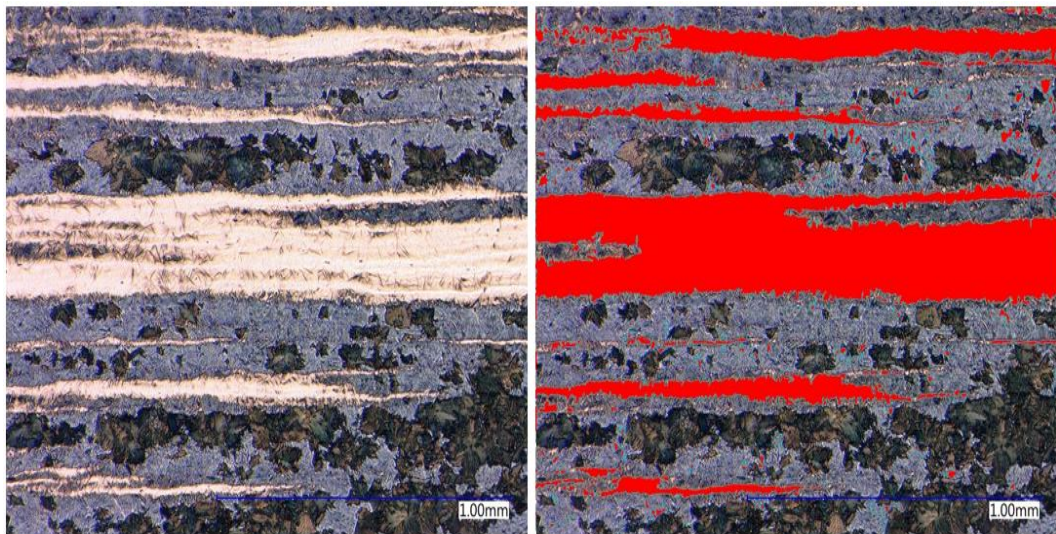


Figure C-10. Microstructure of Experiment 10 (200X, 4% Picral, 60 sec.) and area ratio analysis

Image analysis show that the area ratio of the martensite phase (red region) is 30% and bainite (black region) is 21%.

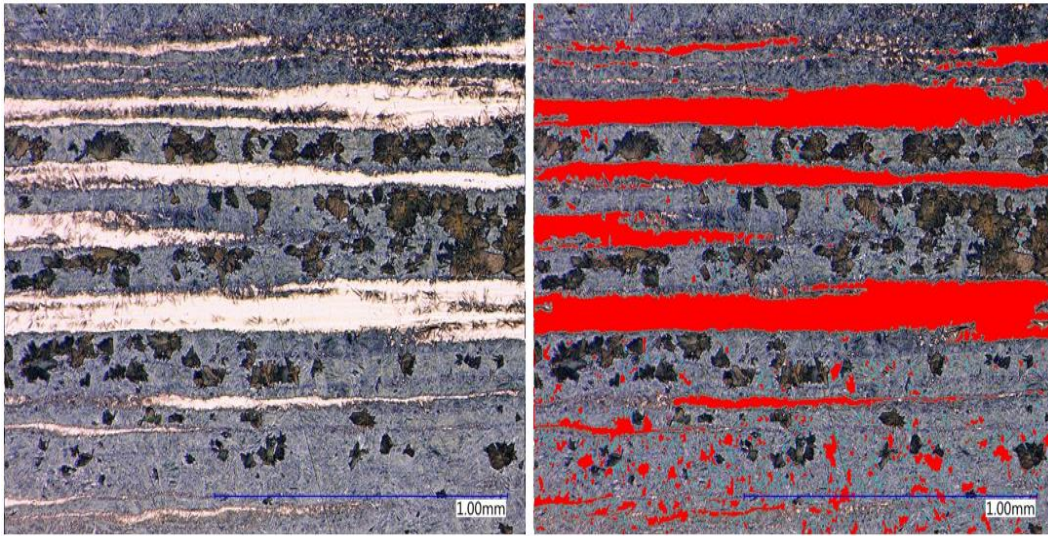


Figure C-11. Microstructure of Experiment 11 (200X, 4% Picral, 60 sec.) and area ratio analysis

Image analysis show that the area ratio of the martensite phase (red region) is 30% and bainite (black region) is 16%.

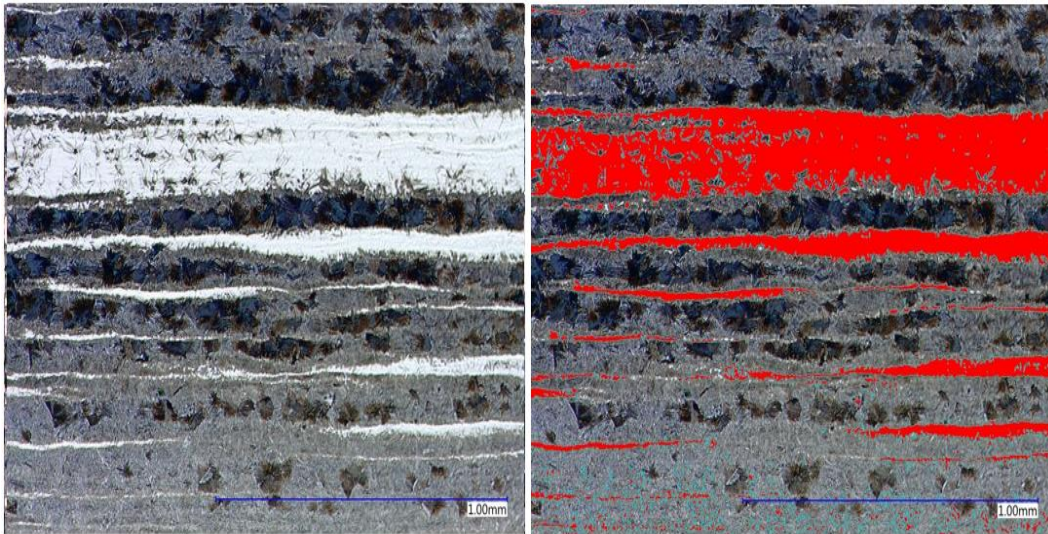


Figure C-12. Microstructure of Experiment 12 (200X, 4% Picral, 60 sec.) and area ratio analysis

Image analysis show that the area ratio of the martensite phase (red region) is 25% and bainite (black region) is 26%.

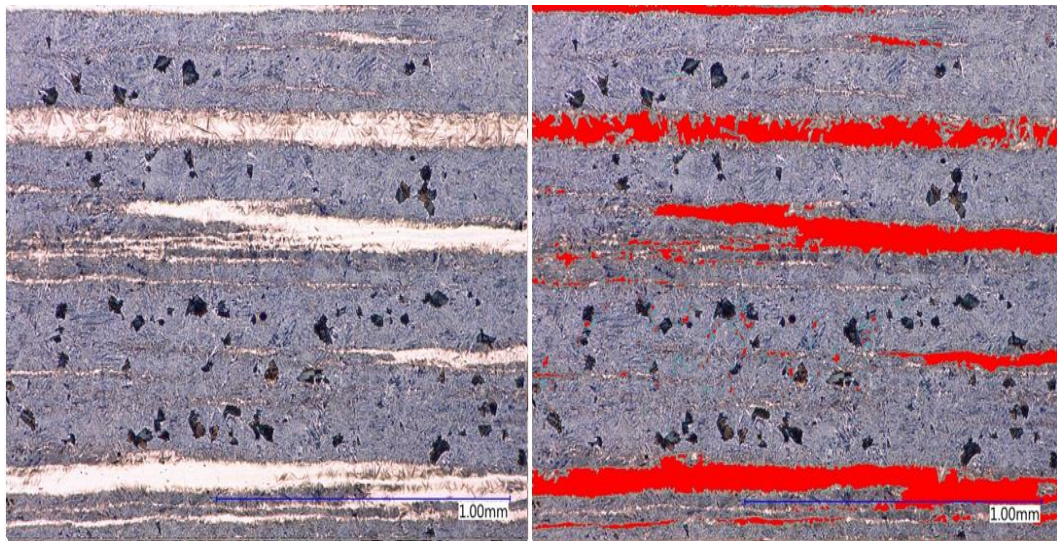


Figure C-13. Microstructure of Experiment 13 (200X, 4% Picral, 60 sec.) and area ratio analysis
Image analysis show that the area ratio of the martensite phase (red region) is 16% and bainite (black region) is 4%.

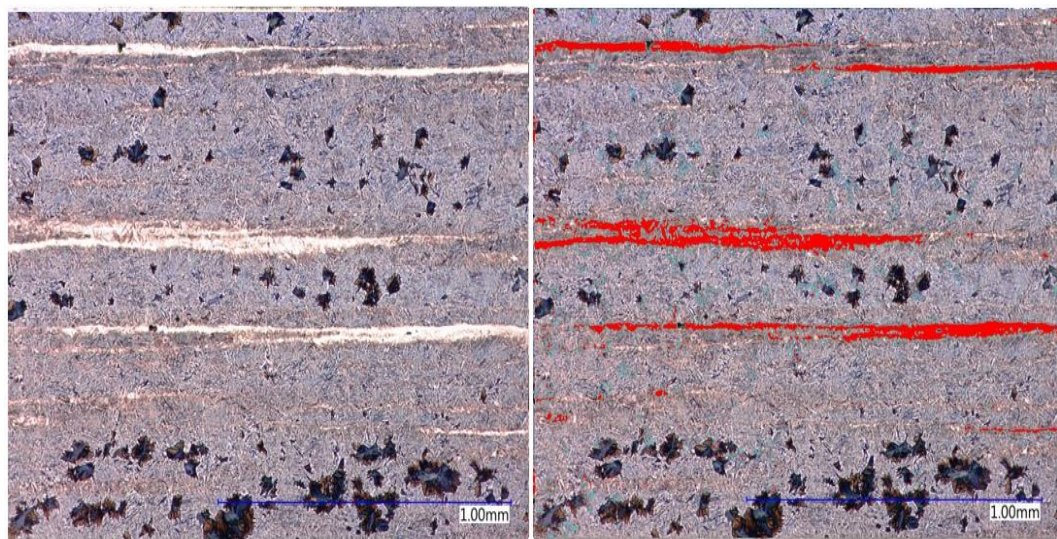


Figure C-14. Microstructure of Experiment 14 (200X, 4% Picral, 60 sec.) and area ratio analysis
Image analysis show that the area ratio of the martensite phase (red region) is 12% and bainite (black region) is 8%.

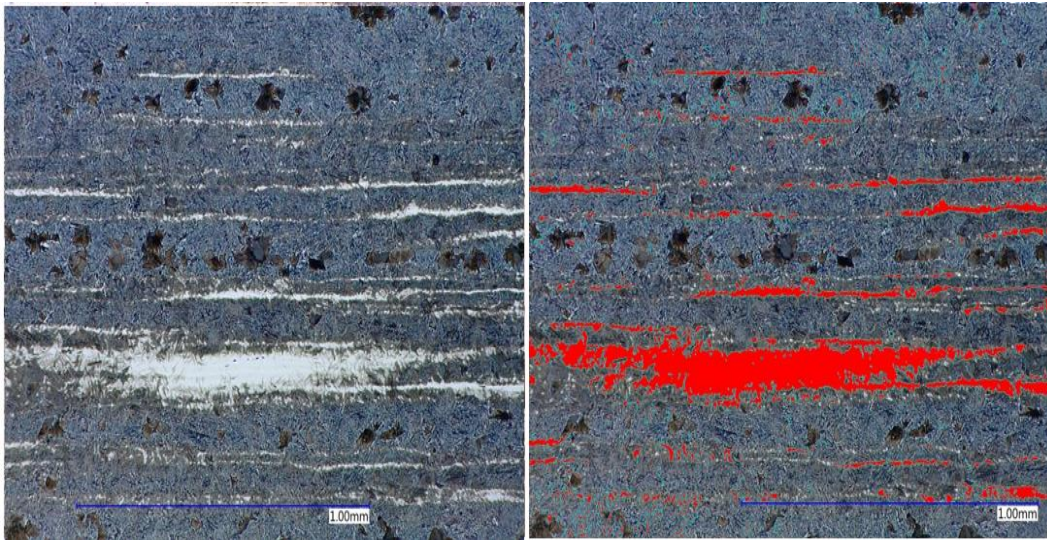


Figure C-15. Microstructure of Experiment 15 (200X, 4% Picral, 60 sec.) and area ratio analysis

Image analysis show that the area ratio of the martensite phase (red region) is 14% and bainite (black region) is 6%.

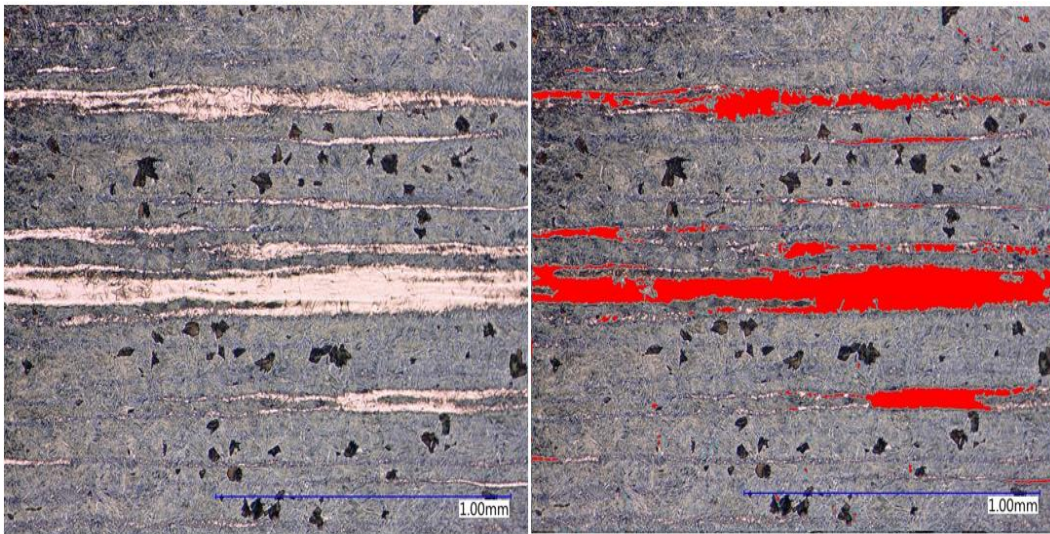


Figure C-16. Microstructure of Experiment 16 (200X, 4% Picral, 60 sec.) and area ratio analysis

Image analysis show that the area ratio of the martensite phase (red region) is 14% and bainite (black region) is 5%.

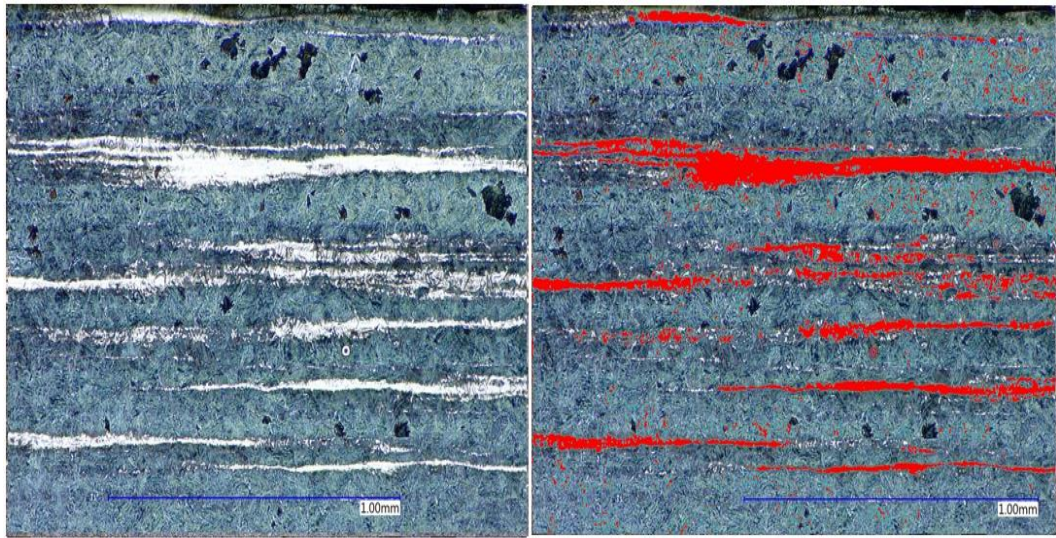


Figure C-17. Microstructure of Experiment 17 (200X, 4% Picral, 60 sec.) and area ratio analysis
Image analysis show that the area ratio of the martensite phase (red region) is 16% and bainite (black region) is 3%.

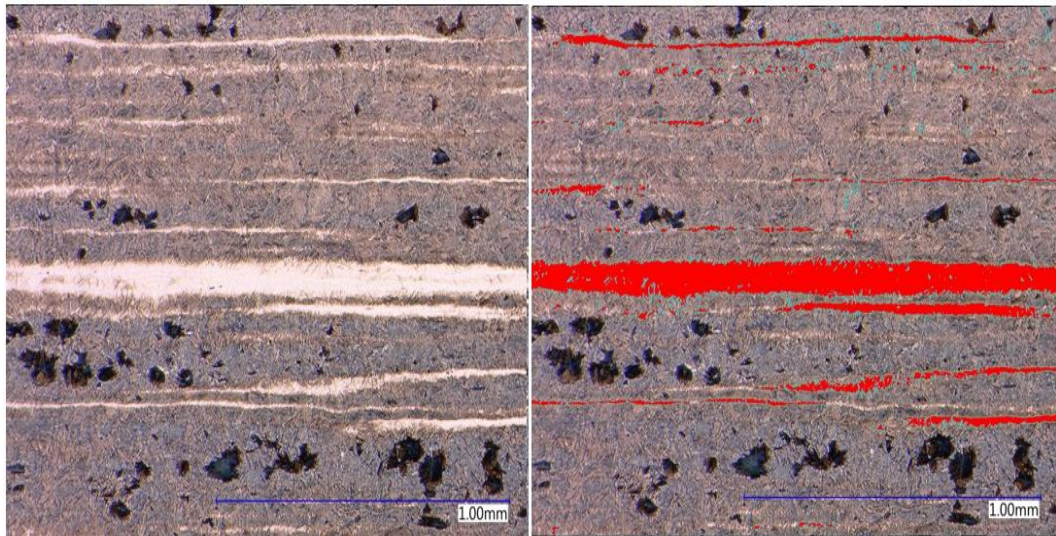


Figure C-18. Microstructure of Experiment 18 (200X, 4% Picral, 60 sec.) and area ratio analysis
Image analysis show that the area ratio of the martensite phase (red region) is 14% and bainite (black region) is 5%.